Adv Polym Sci (2013) 257: 135–202
DOI: 10.1007/12_2013_222

Published online: 7 July 2013

Phillips Cr/Silica Catalyst for Ethylene Polymerization

Ruihua Cheng, Zhen Liu, Lei Zhong, Xuelian He, Pengyuan Qiu, Minoru Terano, Moris S. Eisen, Susannah L. Scott, and Boping Liu

Abstract The Phillips Cr/silica catalyst, discovered by Hogan and Banks at the Phillips Petroleum Company in the early 1950s, is one of the most important industrial catalysts for polyethylene production. In contrast to its great commercial success during the past half-century, academic progress regarding a basic understanding of the nature of the active sites and polymerization mechanisms is lagging far behind. During the last decade, increasing research efforts have been performed on the Phillips catalyst through various approaches, including spectroscopic methods, polymerization kinetics, heterogeneous model catalysts, homogeneous model catalysts, and molecular modeling. Much deeper mechanistic understanding, together with successive catalyst innovations through modifications of the Phillips catalyst, has been achieved.

Keywords Ethylene polymerization mechanisms · Heterogeneous model catalysts · Homogeneous model catalysts · Molecular modeling · Phillips Cr/silica catalyst · Polyethylene · Polymerization kinetics

R. Cheng, Z. Liu, L. Zhong, X. He, P. Qiu, and B. Liu (✉)
State Key Laboratory of Chemical Engineering, East China University of Science and Technology, Meilong Road 130, Shanghai 200237, PR China
e-mail: boping@ecust.edu.cn

M. Terano
School of Materials Science, Japan Advanced Institute of Science and Technology, 1-1 Asahidai, Nomi, Ishikawa 923-1292, Japan

M.S. Eisen
Schulich Faculty of Chemistry, Technion-Israel Institute of Technology, Technion City, Haifa 32000, Israel

S.L. Scott
Department of Chemical Engineering, University of California, Santa Barbara, CA 93106-5080, USA

Contents

Abbreviations

AFM	Atomic force microscope
BC	Bis(triphenylsilyl) chromate
BE	Binding energy
Cp	Cyclopentadienyl
DCB-d_4	1,2-dichlorobenzene-d_4
DEAE	Diethylaluminum ethoxide
DFT	Density functional theory
DRIFTS	Diffuse reflectance infrared Fourier transform spectroscopy
DRS	Diffuse reflectance spectroscopy
DSC	Differential scanning calorimetry
EDS	Energy dispersive spectrometer
EPMA	Electron probe microanalysis
EPR	Electron paramagnetic resonance
ESR	Electron spin resonance
EXAFS	Extended X-ray absorption fine structure
FTIR	Fourier transform infrared
FWHM	Full width at half maximum
GC-MS	Gas chromatography–mass spectrometry
GPC	Gel permeation chromatography
HDPE	High density polyethylene
HMDS	Hexamethyldisilazane

LA-MS	Laser ablation–mass spectrometry
LDI-MS	Laser desorption/ionization–mass spectrometry
m/z	Mass to charge ratio
MALDI-TOF	Matrix-assisted laser desorption/ionization time of flight
MAO	Methylaluminoxane
MAS	Magic angle spin
MECP	Minimum energy crossing point
MW	Molecular weight
M_W	Weight average molecular weight
MWD	Molecular weight distribution
NMR	Nuclear magnetic resonance
ONIOM	Our own *n*-layered integrated molecular orbital and molecular mechanics
PDI	Polydispersity index
PE	Polyethylene
Ph	Phenyl
PIXE	Proton induced X-ray emission
POSS	Polyhedral oligomeric silsesquioxanes
RBS	Rutherford backscattering spectrometry
RT	Room temperature
SCB	Short-chain branch
SEM	Scanning electron microscopy
SIMS	Secondary ion mass spectroscopy
SSA	Successive self-nucleation and annealing
TCB	1,2,4-Trichlorobenzene
TEA	Triethylaluminum
TEB	Triethylborane
TEMPO	2,2,6,6-Tetramethylpiperidine-*N*-oxyl
TG-DTA	Thermogravimetry–differential thermal analysis
THF	Tetrahydrofuran
TiBA	Triisobutylaluminum
T_m	Melting temperature
TPD-MS	Temperature-programmed desorption–mass spectrometry
TPR	Temperature-programmed reduction
TPS	Triphenylsilanol
TREF	Temperature rising elution fractionation
UV-vis	Ultraviolet–visible
XANES	X-ray absorption near edge structure
XAS	X-ray absorption spectroscopy
XPS	X-ray photoelectron spectroscopy
XRD	X-ray diffraction

1 Introduction

The discovery of Ziegler–Natta catalysts for olefin polymerization in 1953 was one of the most important achievements in the field of synthetic polymer chemistry during the past 60 years. Parallel to the discovery, another important catalyst for polyethylene production, SiO_2-supported inorganic chromium oxide, known as Phillips catalyst, was also discovered and commercially applied on a large scale [1–4]. Nowadays, this catalyst is used to produce over 10 million tons of high-density polyethylene (HDPE), accounting for about half of the world's market. Compared with the Ziegler–Natta and metallocene catalysts, the Phillips catalyst exhibits unique polymerization behaviors and can produce PE with distinctive polymer chain microstructures. The catalyst is known to be highly active for ethylene polymerization with or without using organometallic cocatalysts or a preliminary activation step using organometallic cocatalysts or any other reducing agents (such as CO or H_2). Its HDPE products feature an ultrabroad molecular weight distribution (MWD; the typical polydispersity index is larger than 10), small amount of long chain branches and a vinyl end-group for each PE chain. The products show high melt strength and are especially applicable for blow molding products like hollow containers. In the last few decades, the applications for exclusive Phillips HDPE products, including gasoline tanks for the automobile industry and ultralarge plastic containers and pipes, have experienced a successively increasing market demand.

Compared with the great success in commercial applications, academic progress on the Phillips catalyst is lagging far behind, in spite of numerous research efforts during the past 60 years. Aspects of the Phillips catalyst concerning the formation, structure, oxidation state of active sites, and polymerization mechanisms, especially the initiation mechanism, are still mysterious. The difficulties for basic studies on this important industrial catalyst system are mainly derived from the low percentage of active Cr species, the complexity of heterogeneous catalyst systems, the multiple valence states of Cr, the instant encapsulation of active sites by produced polymer, and the ultrafast polymerization rate.

Application of the Phillips catalyst in ethylene polymerization includes two important processes: catalyst preparation and catalyst activation through reduction. The catalyst is usually prepared by impregnation of an aqueous solution of chromium compound, such as chromate acetate, on porous amorphous silica gel, and subsequent calcination at high temperatures between 300 and 900°C in oxygen or dry air. It is generally accepted that chromate acetate first decomposes and is oxidized into bulk CrO_3. This is followed by a reaction with surface hydroxyl groups on silica gel during the calcination process, through which chromium compound could be highly dispersed and stabilized as surface hexavalent chromate species, i.e., monochromate, dichromate, and sometimes even polychromate, as illustrated in Scheme 1 [2, 5–9]. As for the reductive activation process for ethylene polymerization, the hexavalent chromate species is transferred into a lower oxidation state, i.e., divalent Cr(II) species, as the final active precursor for ethylene polymerization by ethylene monomer (C_2H_4), carbon monoxide (CO), Al-alkyl cocatalysts (e.g., TEA), or even other reducing agents.

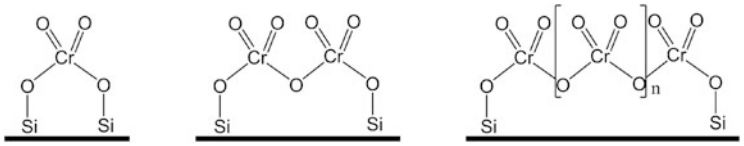

Scheme 1 Plausible structures of surface-stabilized hexavalent chromate species $Cr(VI)O_{x,surf}$ on the silica surface of the Phillips Cr/silica catalyst ($n \geq 1$)

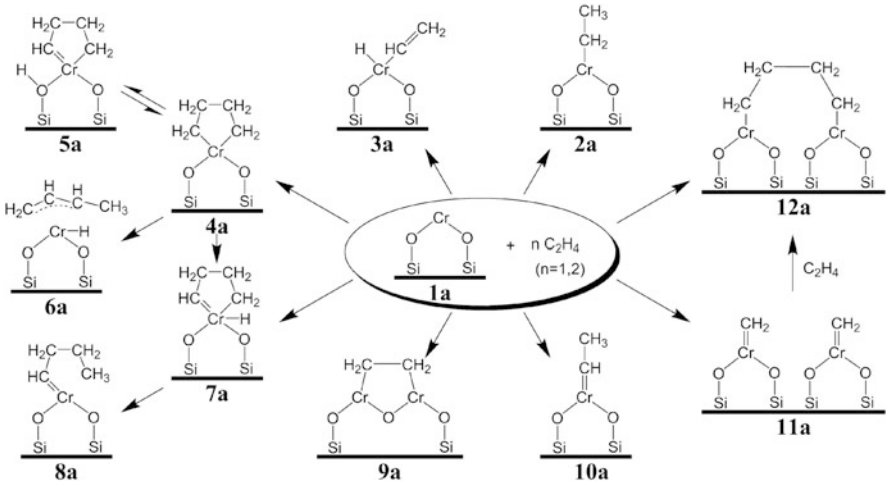

Scheme 2 Various initiation mechanisms proposed in the literature for ethylene polymerization over the pre-reduced Phillips $Cr(II)O_x/SiO_2$ catalyst

Because the Phillips catalyst is unique for its metal-alkyl-free feature in both the catalyst preparation and subsequent polymerization processes, ethylene monomer could play a key role in the activation through reduction of the hexavalent chromate species into surface-stabilized Cr(II) species [$Cr(II)O_{x,surf}$] as the final active precursor, followed by initiation of ethylene polymerization through alkylation of the Cr(II) center during the initial stage, in which an induction period is usually observed after the introduction of ethylene monomer at usual operating temperatures (lower than 150°C) [2, 6, 10]. The initiation mechanism in terms of an alkylation of the Cr(II) center by ethylene monomer, followed by the propagation of the first polyethylene chain is the most interesting and important academic question awaiting further exploration [2, 11]. Scheme 2 shows various initiation mechanisms that have been proposed on the basis of either pure speculation or controversial evidence:

1. Arguments on Cr-alkylidene species (Cr-carbene) [12, 13] and contradictory IR band assignments of the C–H bond vibration in a possible Cr-alkylidene species [14, 15] are still continuing. Therefore, the active sites concerned with Cr-alkylidene species (**5a**, **7a**, **8a**, **10a**, **11a**) [12, 14, 16, 17] under a supposed modified Ivin–Rooney–Green chain propagation [13, 18] still lack conclusive evidence.

2. The low IR detectability of any possible methyl end groups in the initial growing polymer chains [17, 19–21] on the active sites also sheds great doubts on those proposed active sites relating to metallacyclic species (**4a**, **9a**, **12a**) [16–18, 22, 23].
3. The models (**2a**, **3a**, **6a**) [24] involving a proposed Cossee–Arlman chain propagation [25], with either Cr–C or Cr–H as active sites similar to conventional Ziegler–Natta catalysts, still hold the most popularity [2, 11], although the origin of the first hydride scrambling is still obscure (e.g., for **2a**). These models are mainly speculated from the chain configuration of Phillips polyethylene chains featuring one vinyl and one methyl group on each chain end. The vinyl chain end is thought to be derived from chain transfer through β-hydride elimination during a Cossee–Arlman chain propagation.

In the polyolefin industry, there exists a strong driving force for development of new catalysts with better performance and improvements in the structures and properties of PE products through successive catalyst innovations of the traditional Phillips catalyst [2–4, 11]. During the past 60 years, several modified Phillips catalysts have been successfully developed and commercialized through surface modification of the silica support and catalyst with Ti, F, Al, or B compounds, more or less based on the progress in the academic field, although innovation regarding this catalyst is very limited. Another important commercial silica-supported Cr-based HDPE catalyst is Union Carbide's silyl chromate S-2 catalyst, which is solely applied in the gas phase UNIPOL polymerization processes [26]. This catalyst is usually prepared by chemisorption of bis (triphenylsilyl) chromate (BC) on partially dehydrated silica gel at around 600°C. Due to its similar structure and performance compared with the Phillips catalyst, in our opinion it could be considered as a heterogeneous model of the Phillips catalyst. Due to the presence of an electron-donating triphenylsilyl ligand, a much longer induction period exists without using any organometallic cocatalyst for ethylene polymerization. This catalyst combined with Al-alkyl cocatalyst usually produces polyethylene with broader MWD at both ends of the high and low molecular weight fractions than the Phillips catalyst without using cocatalyst [26]. Almost no improvement of this silica-supported silyl chromate S-2 catalyst has been reported, apart from a modified preparation procedure through transformation from Phillips catalyst by addition of triphenylsilanol (TPS) to avoid the use of highly toxic and expensive BC compound [27, 28]. Another Union Carbide Cr-based polymerization catalyst, formed upon treating partially dehydrated silica with chromocene (Cp_2Cr) and named S-9 catalyst, is not used industrially at present [29]. It is a supported metallocene catalyst featuring very poor ability of α-olefin incorporation in copolymerization with ethylene and produces polyethylenes with narrow MWD. It is very clear that further catalyst innovations through modifications of the traditional Cr-based industrial catalysts are still highly demanded [30].

During the last decade, increasing research efforts have been performed on Phillips catalysts through various approaches including spectroscopic methods, polymerization kinetics, heterogeneous model catalysts, homogeneous model

catalysts, and molecular modeling. Much deeper mechanistic understanding, together with successive catalyst innovations through modifications of the Phillips catalyst, has been achieved. The advances in the field of Phillips catalysts during the past half-century have been reviewed in depth by McDaniel in 1985 [2], Zecchina and coworkers in 2005 [11], and McDaniel in 2008 and 2010 [3, 4]. This present contribution aims at an overview of the achievements of the last decade, unraveling the mechanistic aspects of the activation, the nature of the active chromium species, and the polymerization mechanisms through both experimental and computational approaches, as well as catalyst innovation through modification of the Phillips catalyst with particular emphasis on the studies undertaken in the authors' laboratory.

2 Approaches Using Spectroscopic Methods

The state of surface Cr species, which is closely related to the molecular structure, texture, and orientation of the chromium oxide on the catalyst surface, is crucial for a deeper understanding of the Phillips catalyst. Many modern analytical methods [8, 11, 31], such as oxygen chemisorptions [32], magnetic susceptibility measurement [33], XRD [5, 34–36], EPR [33, 37–41], SIMS [42], Raman [35, 43–50], UV-vis DRS [33, 39, 43, 50], XAS (EXAFS-XANES) [48, 51–55], PIXE [56], TPR [36, 39], SEM/EDS [57], FTIR [11, 22, 50, 54, 55, 58–63], XPS [6, 8, 56, 64–71], NMR [41, 71, 72], AFM [73], EPMA [8], TPD-MS [67], TG-DTA [10], RBS [74], LA-MS, and LDI-MS [75], have been used separately or jointly to characterize the physico-chemical state of Cr species on Phillips catalysts [11, 31]. These approaches attempt to provide direct or indirect evidence for the anchoring of chromate species at the surface during activation and the ability of the catalyst to polymerize ethylene, especially at the early stage of polymer chain formation. For example, based on the combination of the FTIR, Raman, and UV-vis spectroscopic results, monochromate species were identified anchored on the surface of the Cr/silica catalyst at low chromium loadings [47]. The monochromate structure on a highly diluted $Cr/SiO_2/Si(100)$ system was also confirmed by EXAFS results [53]. In the polymerization mechanism study, the in-situ FTIR spectroscopy suggested that the initiation mechanism followed a metallacycle route [23]. Very recently, Groppo and coworkers [76, 77] reviewed the spectroscopic investigations into the Phillips catalyst. However, the lower concentration of the Cr species, diversity of the amorphous silica gel surface, and high sensitivity to moisture and air are major obstacles for exploring the structure of Cr species in relation to polymerization activities. At the same time, these obstacles have led to difficulty in combining different experimental findings from different groups into one unifying picture. Although a definite explanation of the nature of the active site relating to the polymerization mechanism has not yet been achieved, it will be demonstrated in the following sections that valuable understanding has been

achieved through various spectroscopic methods concerning thermal activation of the Phillips catalyst, activation of the Phillips catalyst by CO or Al-alkyl cocatalysts, activation of the Phillips catalyst by ethylene monomer, and modification of the Phillips catalyst by Ti.

2.1 Thermal Activation of the Phillips Catalyst

During the preparation of Phillips catalyst, thermal activation is a crucial stage in which the chromium oxide is anchored into surface-stabilized chromate species. In this calcination process, a highly dispersed state of surface-stabilized chromate species, including mono-, di-, and polychromate, can be achieved through the redispersion cycles of sublimation, volatilization, spreading, deposition, and stabilization of bulk CrO_3 on a silica support surface [2]. By measurement of molar ratios of Δ[OH]/[Cr], McDaniel [5] suggested that the initial bonding was monochromate at 200°C (Δ[OH]/[Cr] = 2), but that the dichromate became dominant at 500°C (Δ[OH]/[Cr] = 1), while polychromates might be formed above 800°C (Δ[OH]/[Cr] < 1). On the basis of DRIFTS and DRS results, Panchenko et al. [78] confirmed that the reactions of CrO_3 with the silica calcined at 250°C, 400°C, and 800°C dominantly yield monochromates, dichromates, and polychromates, respectively. However, two unfavorable problems might occur during the thermal activation process: the calcination-induced reduction of surface-stabilized Cr(VI) species into lower valence state (+5, +4, or +3) and the creation of aggregated Cr_2O_3 (usually in crystallized form) even in an oxidizing atmosphere (O_2 or dry air). These affect to a great extent the physico-chemical state of the surface Cr species and thus the properties and performance of the catalyst. High resolution XPS, which has been demonstrated to be a very powerful method for a better understanding of the physico-chemical nature of surface chromium species through monitoring their transformation on Phillips catalysts calcined at various conditions, has benefitted the investigation of the origins of these two problems [8, 67, 68, 70, 79, 80].

For the Phillips catalyst calcined in dry air at 800°C for 20 h with 0.4 Cr nm^{-2} loading, two oxidation states were found in the XPS measurement [8]. The first, with a binding energy (BE) of 581.81 eV and a full width at half maximum (FWHM) of 9.62 eV, was assigned as the surface-stabilized chromate $Cr(VI)O_{x,surf}$ species with an oxidation state of +6 (atomic concentration 70.4%). The second, with a BE of 577.21 eV and a FWHM of 4.43 eV, was assigned as an oxidation state of +3 (atomic concentration 29.6%), which was quite different from the typical values of the bulk Cr_2O_3, strongly suggesting a surface-stabilized and highly dispersed characteristic of trivalent Cr species chemically bonded to silica surface [$Cr(III)O_{x,surf}$]. Compared with bulk Cr_2O_3, the higher BE of $Cr(III)O_{x,surf}$ species might result from the stabilizing effect of the silica as well as the environmental effect of neighboring chromate species. The larger FWHM value could be ascribed to its variety in molecule structure and the heterogeneity of the silica surface. The

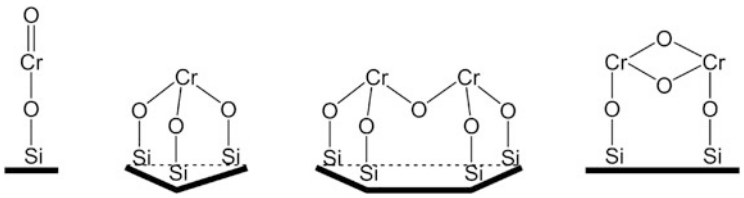

Scheme 3 Plausible structures of surface-stabilized trivalent chromium species $Cr(III)O_{x,surf}$ on the silica surface of the Phillips Cr/silica catalyst

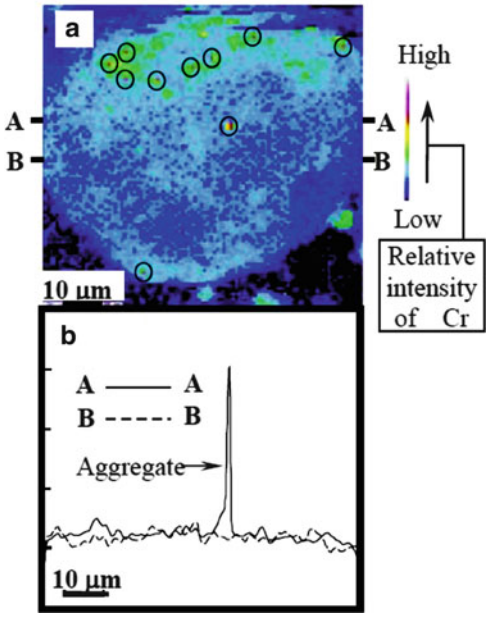

Fig. 1 EPMA map (**a**) and line curves (**b**) of the chromium distribution on the Phillips Cr/silica catalyst. The line curves of *A–A* and *B–B* in (**b**) correspond to the chromium distribution at the straight-line positions of *A–A* and *B–B* in (**a**), respectively. The *red patches* marked in *circles* in (**a**) correspond to small aggregates of surface Cr species

surface-stabilized $Cr(III)O_{x,surf}$ species on Phillips catalysts have been frequently reported by other researchers [33, 81]. Although its specific molecular structure still remains ambiguous, four plausible structure models (illustrated in Scheme 3) have been proposed. The formation of this $Cr(III)O_{x,surf}$ species was thought to originate from calcination-induced reduction of the chromate $Cr(VI)O_{x,surf}$ species and to increase with calcination temperature and time.

Figure 1 shows typical results of an electron probe microanalysis (EPMA) map and line curves of the Cr distribution on the calcined catalyst [8]. As can be seen, the Cr species mostly dispersed uniformly on the surface of each catalyst particle. However, the heterogeneity of Cr distribution on individual catalyst particles

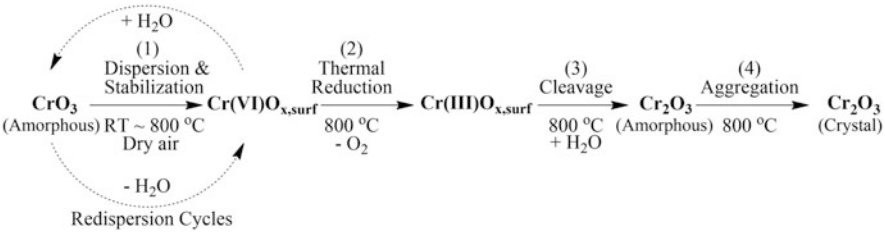

Scheme 4 Plausible mechanism of formation of aggregated Cr_2O_3 on the Phillips catalyst with 0.4 Cr nm^{-2} loading during calcination in the preparation process

revealed local aggregates of Cr species sized 200–300 nm. These aggregates, corresponding to the red patches in the map image (marked in circles) in Fig. 1a and to a sharp peak in the line curves in Fig. 1b, were suggested to be microcrystal particles of Cr_2O_3.

The irreversible formation of chromium oxide clusters, in the form of α-Cr_2O_3, is a well-known phenomenon occurring on the Cr/silica catalyst for Cr loadings higher than 1 wt% and/or in the presence of water poisoning. According to previous reports [33, 56, 64, 82], the formation of aggregated Cr_2O_3 on catalysts with a low level of Cr loading usually occurred in the later stage of calcination, followed by the full stabilization of bulk CrO_3 as chromate species and a consequent calcination-induced reduction into $Cr(III)O_{x,surf}$ species. Previously, the formation of aggregated Cr_2O_3 was usually thought to be related to the thermal decomposition (or reduction) of bulk CrO_3, as illustrated in (1). The XPS measurement [8] showed that the purposely introduced moisture induced the transformation of all the $Cr(III)O_{x,surf}$ species and one-seventh of the $Cr(VI)O_{x,surf}$ species into aggregates of Cr_2O_3 at high temperature, regardless of the oxidizing or inert atmosphere. Considering the traces of moisture from the simultaneous dehydroxylation of residual hydroxyl groups on the silica surface, the formation of aggregated Cr_2O_3 microcrystals might be induced by traces of moisture through cleavage of the $Cr(III)O_{x,surf}$ species during the calcination. The mechanism is illustrated in (2):

$$Cr(VI)O_{x,surf} + H_2O \underset{\text{dry air}}{\overset{800^\circ C}{\rightleftharpoons}} CrO_3 \xrightarrow[\text{dry air}]{800^\circ C} Cr_2O_3 + O_2 \quad (1)$$

$$Cr(III)O_{x,surf} + H_2O \xrightarrow[\text{dry air}]{800^\circ C} Cr_2O_3 \quad (2)$$

Thus, a plausible mechanism concerning the formation of Cr_2O_3 microcrystals during calcination in the preparation of Phillips catalyst was speculated (Scheme 4). At the first stage, the bulk CrO_3 was dispersed and stabilized as surface chromate species through the reaction with the hydroxyl groups on silica during the calcination process from room temperature (RT) to 800°C in dry air. Gradually, a highly dispersed state of chromate species can be achieved through many redispersion cycles of sublimation, volatilization, spreading, deposition, and stabilization of bulk CrO_3, as well as hydrolysis, re-spreading, re-deposition, and re-stabilization

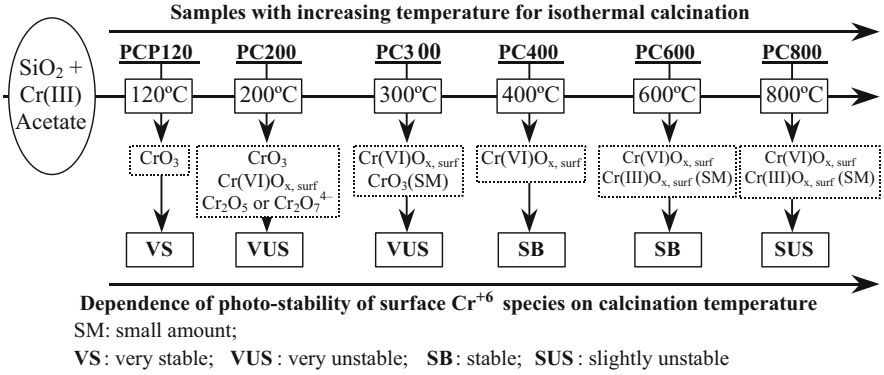

Fig. 2 Dependence of surface components of various Phillips catalyst samples on calcination temperature under isothermal conditions. *SM* small amount, *VS* very stable, *VUS* very unstable, *SB* stable, *SUS* slightly unstable

of chromate species on the support surface. These cycles may be facilitated in the presence of traces of moisture generating from the successive dehydroxylation of silica in the early stage of dispersion and support of bulk CrO_3 during calcination. During this period, the thermal decomposition of bulk CrO_3 can also be sufficiently inhibited by the presence of oxidizing gas (dry air or O_2). At the same time, the dehydroxylation also results in increasing strain in surface siloxane groups and in increasing reduction potential of the surface chromate species. At a certain critical point, the calcination-induced reduction of chromate species into $Cr(III)O_{x,surf}$ species would be expected (Scheme 4, reaction 2). Thereafter, traces of low moisture from dehydroxylation might split some $Cr(III)O_{x,surf}$ species, leading to the formation of Cr_2O_3 microcrystals (Scheme 4, reactions 3 and 4). Higher temperature, longer duration, and higher content of moisture in the last stage of the calcination process can lead to more serious aggregation of surface Cr species.

In order to further understand the specific transformation procedure of surface chromium species during the thermal activation process, Phillips catalysts isothermally calcined at various temperatures were prepared and characterized by XPS. The substantial dependence of surface Cr components of Phillips catalysts in terms of the calcination temperature in isothermal preparation is summarized in Fig. 2 [68, 70]. These catalysts (with Cr 1.0 wt% loading) isothermally calcined at 200°C, 300°C, 400°C, 600°C, and 800°C were designated PCX, where X is the calcination temperature. PCP120 was the silica support impregnated with chromium acetate and subsequently dried at 120°C, and all the other PCX catalysts were derived from PCP120. The specific surface Cr components of various catalyst samples versus calcination temperatures were clarified. The bulky CrO_3 started to be transformed into supported chromate species at 200°C and could be completely stabilized on silica gel surface as chromate species at 400°C. Partial thermal decomposition of bulky CrO_3 into bulky pentavalent Cr oxide [e.g., Cr_2O_5 or $(Cr_2O_7)^{4-}$] was only observed on samples calcined at 200°C due to the incomplete stabilization of bulky CrO_3 into chromate species. Only a slight thermally induced partial reduction of chromate species into $Cr(III)O_{x,surf}$ was observed at high temperatures (600–800°C).

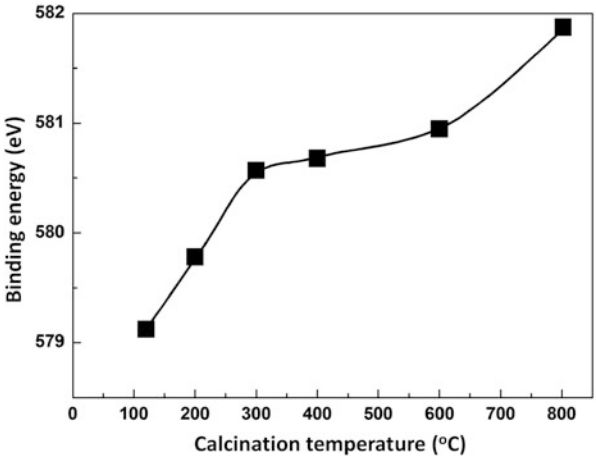

Fig. 3 Dependence of binding energy [Cr 2p (3/2)] of surface Cr^{6+} species of various Phillips catalysts on calcination temperature for preparation of the catalysts from PCP120 precursor

The successive increase in BE values of hexavalent chromium species with increasing calcination temperature from PCP120 to PC800 is plotted in Fig. 3. The chromate species [$Cr(VI)O_{x,surf}$] on the catalyst became more and more electron deficient with increased calcination temperatures from 200°C to 800°C. This correlates well with the typical polymerization behavior of Phillips catalysts, i.e., that the polymerization activity increases with an increase in calcination temperature. The dominant supporting of bulky CrO_3 on a silica gel surface and simultaneous dehydroxylation of the silica gel surface at 120–300°C account for the drastic increase in BE values of hexavalent chromate species in this temperature range for isothermal calcination. The slowly increasing of BE values of chromate species from 300°C to 600°C was solely derived from dehydroxylating residual surface hydroxyl groups. Another enhancement of the increase in BE values of chromate species from 600°C to 800°C might come from further dehydroxylation of residual hydroxyl groups, as well as enhancement of surface tension from easier relaxation of surface siloxane groups induced by high temperature.

The dependence of BE values on the XPS acquisition time during the XPS measurement indicated that further increasing the XPS acquisition from 10 to 30 or 120 min may lead to the catalyst being reduced by the soft X-ray irradiation during the XPS measurement, which provides a good method for evaluation of the photostability of Phillips catalysts prepared under different conditions. The photostability of surface chromate species on Phillips catalysts was found to be significantly dependent on the calcination temperature used for catalyst preparation (see Fig. 2); the sample calcined at moderate temperatures (400–600°C) showed the highest photostability [70].

2.2 Activation of Phillips Catalysts by CO or Al-alkyl Cocatalysts

The reduction of Cr(VI) to lower oxidation state is the first step in the induction period in the ethylene polymerization process. Active site precursors for polymerization can be formed after reduction of the chromate species by CO (usually at 350°C) or Al-alkyl cocatalyst (e.g., TEA) in a separated pre-activation step, or by ethylene monomer itself during the initial stage of polymerization [2]. Activation by ethylene monomer is most frequently used in the commercial processes. The use of CO or Al-alkyl cocatalyst as reduction agent may shorten or remove the induction period, which is frequently used at the laboratory scale. The effect of activation using different reducing agents for the Phillips catalyst was systematically investigated by XPS characterization.

Phillips catalyst reduced by CO at 350°C can exhibit instantaneous polymerization activity upon contact with ethylene [2] and is generally considered as an ideal catalyst system in spectroscopic investigations of the early stages of ethylene polymerization [11]. Comparison of the oxidation states of surface Cr species on PC600 (calcined) and PC600/CO (PC600 pre-reduced by CO at 350°C for 1 h) catalysts measured by XPS method suggested that about 63% of surface Cr species were reduced into surface-stabilized Cr(II) species by CO, leaving a certain amount of residual chromate species on PC600/CO [80]. The DRS results [83] showed that the Cr active sites could be fully available for reduction at higher reduction temperature (600°C).

The activation of the Phillips catalyst by Al-alkyl cocatalyst was also systematically studied by XPS and solid state NMR [69, 84]. XPS quantified the existence of four oxidation states, including +2, +3, +5, and +6, of surface Cr species on TEA-modified catalysts. It was found that the relative concentration of active sites was around 14.4–24.9 mol% Cr for the TEA-modified Phillips catalysts depending on the calcination temperature and Al/Cr molar ratio. The correlation of polymerization activities as well as the oxidation states of surface chromium species with the molar ratio of Al/Cr is shown in Fig. 4. It seemed that only the surface chromium species in oxidation states of +2 and +6 were possibly related with the activity of the ethylene polymerization catalysts. The correlation suggested that the active precursor of the chromium cluster can be named as a $Cr^{2+}{\cdot}2Cr^{6+}$ cluster composed of one $Cr(II)O_{x,surf}$ species and two $Cr(VI)O_{x,surf}$ species, in which the $Cr(II)O_{x,surf}$ species act as the real center of active chromium precursor and the residual $Cr(VI)O_{x,surf}$ species are also necessary components acting as the neighboring ligand environment with electronic and steric effects. Three plausible chemical structural models of the $Cr^{2+}{\cdot}2Cr^{6+}$ cluster are proposed in Scheme 5, based on the correlation between XPS and polymerization results and our previous understanding of the surface chemical nature of calcined Phillips $Cr(VI)O_x/SiO_2$ catalysts and pre-reduced $Cr(II)O_x/SiO_2$ catalysts.

The ^{1}H and ^{27}Al MAS solid state NMR spectra clearly demonstrated that the existing states of surface Al species in the TEA-modified Phillips catalysts strongly

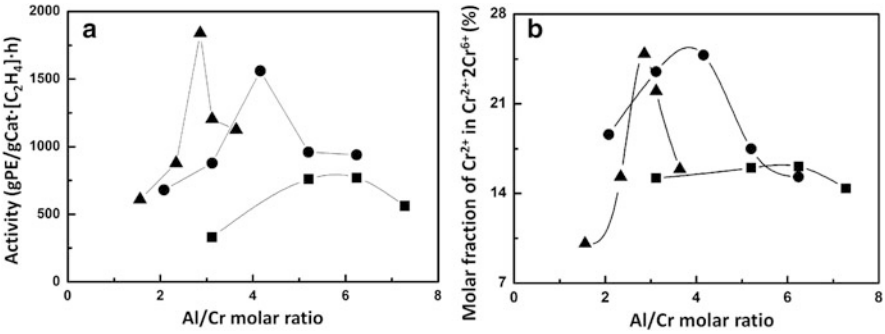

Fig. 4 Al/Cr molar ratios versus polymerization activity (**a**) and the molar fraction of Cr^{2+} (**b**) in $Cr^{2+}{\cdot}2Cr^{6+}$ cluster on the TEA-modified Phillips catalyst calcined at 400°C (*filled squares*), 600°C (*filled circles*), and 800°C (*filled triangles*)

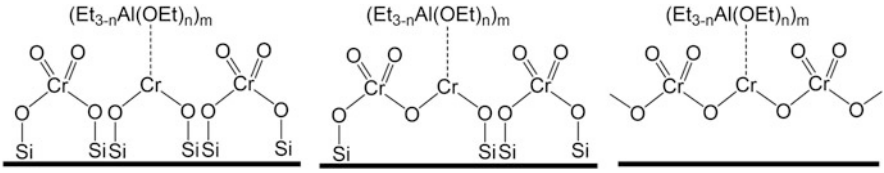

Scheme 5 Three plausible structure models of the active Cr^{2+} precursors existing as a $Cr^{2+}{\cdot}2Cr^{6+}$ cluster on the TEA-modified Phillips catalyst; $n = 1$ or 2; $m = 1$ or 2

depended on the concentration of TEA and the calcination temperature used during the catalyst preparation process [84]. In Fig. 5, three kinds of Al species with 6-, 5-, and 4-coordination states are distinguished for the PC400, PC600, and PC800 catalysts modified by TEA at various Al/Cr molar ratios. For PC400/TEA catalysts, the profiles were only slightly changed with various Al/Cr molar ratios, and the 6-coordinated Al species was dominant. For the PC600/TEA, the peak intensity of the 4-coordinated Al species significantly increased with increasing Al/Cr molar ratios, resulting in a dramatic change in the relative amounts of 6-, 5-, and 4-coordinated Al species. For higher Al/Cr molar ratios, the spectra completely changed, and the 5- and 4-coordination states of the surface Al species could not be clearly distinguished and the 6-coordinated Al species became dominant again. For PC800/TEA, it was observed that the 6-coordinated Al species was still predominant in a narrow range of Al/Cr molar ratio, except the sharp and strong peak of 4-coordianted Al species at the Al/Cr ratio of 2.34.

A relationship between the Al/Cr molar ratio and relative amount of 4-coordinated Al species on the PC400/TEA, PC600/TEA, and PC800/TEA catalysts is illustrated in Fig. 6 [84]. For PC400/TEA catalysts, the relative amounts of 4-coordinated Al species increased only slightly with the increase in Al/Cr ratios. For PC600/TEA and PC800/TEA catalysts, the relative amounts of 4-coordinated Al species firstly increased with an increase in Al/Cr ratios then reached a

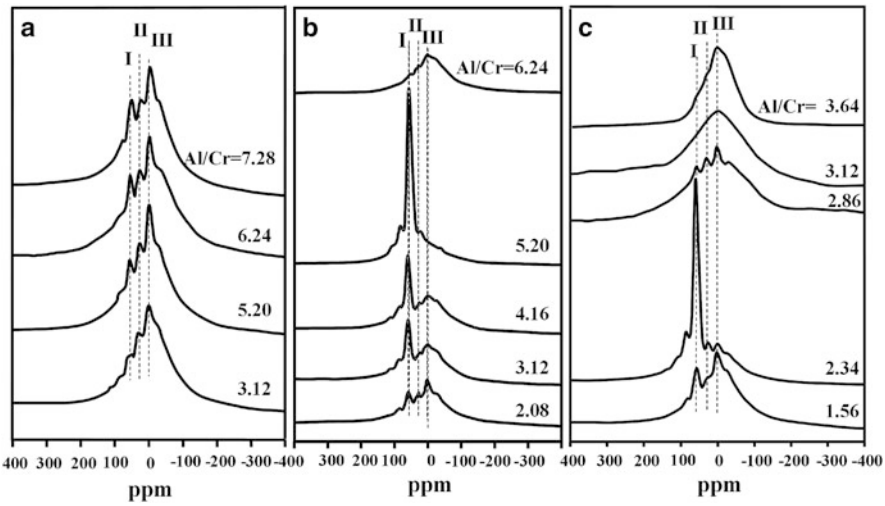

Fig. 5 ^{27}Al MAS NMR spectra of (**a**) PC400, (**b**) PC600, and (**c**) PC800 catalysts modified by TEA at the Al/Cr molar ratios listed; *I* 4-coordinated Al, *II* 5-coordinated Al, *III* 6-coordinated Al

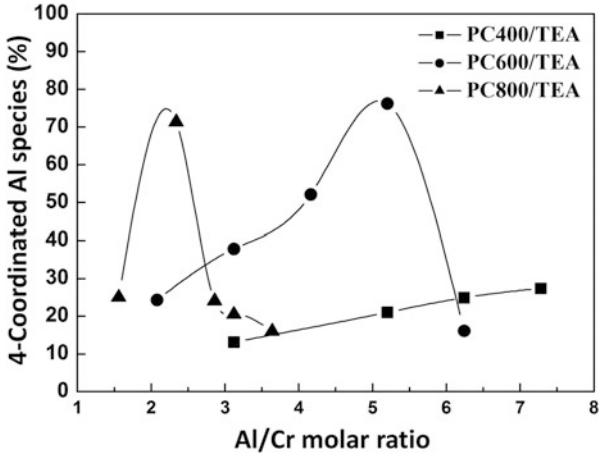

Fig. 6 Correlation between the Al/Cr molar ratio and the relative amount of 4-coordinated Al species on the PC400/TEA, PC600/TEA, and PC800/TEA catalysts

maximum value. With the further increase in Al/Cr ratios, the 4-coordinated Al species decreased. It was interesting to find that with an increase in Al/Cr molar ratio, the activities of the three types of catalysts (PC400/TEA, PC600/TEA, and PC800/TEA) first increased to a maximum value then decreased as shown in Fig. 4. The similar trend in Figs. 4 and 6 inspired us to consider that only the 4-coordinated Al species on the surface of the TEA-modified Phillips catalyst was directly related to the active Cr sites for ethylene polymerization.

Table 1 Evolution of alkenes and formaldehyde from the ethylene-treated Phillips catalyst under various conditions

	HCHO	C_2H_4	C_3H_6	C_4H_8	C_5H_{10}	C_6H_{12}	C_7H_{14}
	m/z						
Samples	30	28	42	56	70	84	98
RT/2 h	+	+	+	+	−	−	−
RT/5 h	+	+	+	+	−	−	−
RT/10 h	+	+	+	+	−	−	−
50°C/2 h	+	+	+	+	−	−	−
100°C/0.5 h	+	+	+	+	+	−	−
100°C/1 h[a]	+	+	+	+	+	+	+
150°C/0.5 h[a]	+	+	+	+	+	+	+

+, detected; −, not detected

[a]Polyethylene was confirmed by IR

2.3 Activation of the Phillips Catalyst by Ethylene Monomer

Activation of the Phillips catalyst directly by ethylene monomer was further investigated by XPS and TPD-MS methods in order to shed some light on the reaction mechanisms during the induction period. Deconvolution of the XPS spectra for industrial Phillips Cr/silica catalysts treated in ethylene atmosphere at RT for 2 h revealed that surface chromium species presented in three oxidation states: surface chromate $Cr(VI)O_{x,surf}$ species; surface-stabilized trivalent Cr(III) species; and surface-stabilized Cr(II) species. Compared to the original catalyst before ethylene treatment, about one-third of chromate $Cr(VI)O_{x,surf}$ species (i.e., ca. 22.6% of the whole surface Cr) was reduced to Cr species in lower oxidation states during the ethylene treatment, even under ambient conditions [67].

TPD-MS characterization of the calcined Phillips catalyst before and after treatment within ethylene atmosphere for 2 h under ambient conditions confirmed the evolution of three species: formaldehyde ($m/z = 30$); olefins with an odd number of carbon atoms, i.e., propylene ($m/z = 42$); and olefins with an even number of carbon atoms, i.e., butene ($m/z = 56$) [79]. As shown in Table 1, various new olefin species with pentene ($m/z = 70$), hexene ($m/z = 84$), and heptene ($m/z = 98$) also appeared under various catalyst treatment conditions in ethylene atmosphere [85]. Higher temperature led to the formation of olefins with higher carbon number. Moreover, the formation of polyethylene was also confirmed by IR characterization over catalyst samples treated at 100°C/1 h or 150°C/0.5 h in ethylene.

Formaldehyde is a by-product of the redox reaction between ethylene and hexavalent chromate species, resulting in the formation of divalent chromium species. Subsequently, the Cr(II) species coordinated with formaldehyde might act as the active precursor at lower temperatures to produce the new short olefins with both odd and even numbers of carbon atom. The experimental evidence obtained from the early stage of ethylene polymerization cannot be rationalized

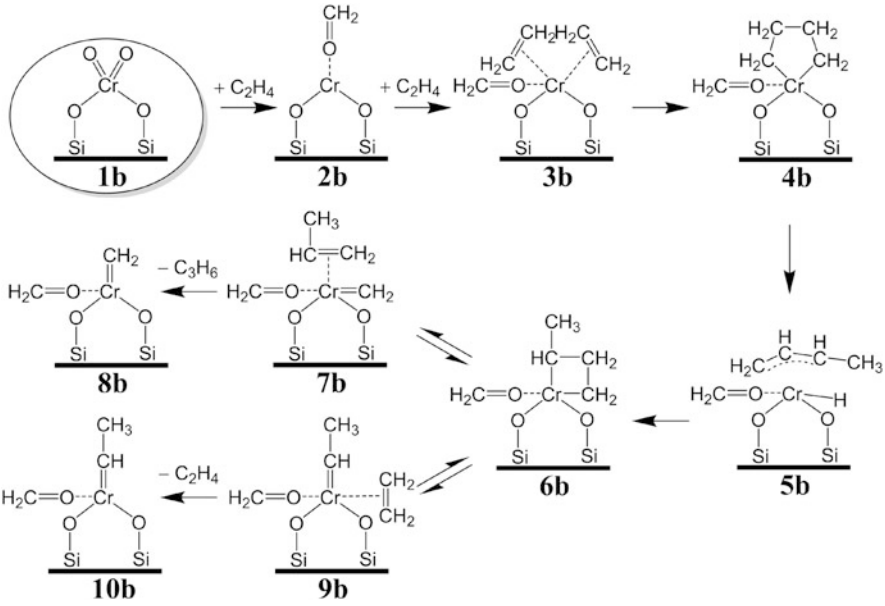

Scheme 6 Plausible mechanistic routes for the formation of the first hydrocarbon species, propylene, during the induction period over the non-pre-reduced Phillips Cr/silica catalyst through interaction with ethylene under various conditions

by the Cossee–Arlman mechanism [25]. It should be mentioned that the conversion of ethylene into higher olefins with both odd and even numbers of carbon atoms is a well-established phenomenon that was believed to proceed by metathesis over metal alkylidene species [86]. This indicated that the coordination of formaldehyde on surface-stabilized divalent chromium species results in the formation of active precursor for olefin metathesis rather than polymerization. The active sites in heterogeneous transition metal-catalyzed olefin metathesis are generally thought to be a transition metal alkylidene species, as for their well-defined homogeneous analogues [87]. In our work, the signal for Cr-alkylidene species for the sample treated at 100°C for 0.5 h was firstly observed in XPS measurement [85]. At the same time, the evolution of the Cr-metallacyclic species can be considered to be prior to that of the Cr-alkylidene species after gradual increase in ethylene treatment time. Thus, a metathesis initiation mechanism based on the experiment was speculated and is shown in Scheme 6. The π-allyl Cr(II)-hydride species **5b**, which formed through the metallacyclopentane **4b**, was converted into metallacyclobutane **6b** [88]. The metallacyclobutane species (**6b**) was subsequently subjected to metathesis, generating either Cr(IV)-methylidene **7b** and the first hydrocarbon species propylene or Cr(IV)-ethylidene **9b** and a new ethylene monomer [87]. The subsequent metathesis of the first hydrocarbon species propylene on Cr(IV)-ethylidene **8b** and/or Cr(IV)-methylidene **10b** led to the formation of the second hydrocarbon species butene during the induction period [86, 87, 89].

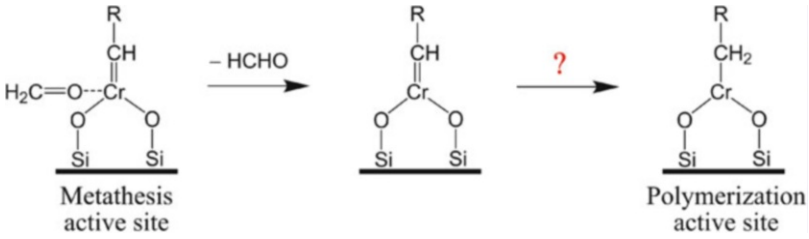

Scheme 7 Plausible transformation of metathesis site into polymerization site from induction period to polymerization period on the Phillips catalyst

It is made clear that the Cr(II) species adsorbed with formaldehyde during the induction period could serve as active site precursor for ethylene metathesis, and the gradual desorption of formaldehyde at higher temperatures transforms the ethylene metathesis site into an ethylene polymerization site resulting in accelerating-type kinetics (as shown in Scheme 7). The question is how the ethylene polymerization reaction occurred starting from the Cr-carbene species formed during the induction period. Scott and coworkers reported the SiO_2-supported Cr-alkylidene catalyst to be highly active for ethylene polymerization, producing HDPE with similar chain conformation as that produced by Phillips catalyst [90–94]. The analyzing of the microstructures of two polyethylenes obtained by industrial Phillips catalysts might give some clues. Firstly, two ethylene homopolymers from both calcined and Al-alkyl pre-reduced Phillips catalysts were analyzed. The ^{13}C NMR spectra showed that the peak intensity of methyl branches was always strongest in the methyl, ethyl, and butyl branches [85], suggesting that propylene was the first and dominant olefin formed from ethylene metathesis. The generated propylene subsequently inserted into growing polyethylene chains to form methyl braches. Due to the coexistence of ethylene metathesis active sites with polymerization sites, the formation of short chain branches (SCBs) over the Phillips catalyst during ethylene homopolymerization can be rationalized well by the in-situ formation of various short olefins with both even and odd number of carbon atoms from ethylene metathesis sites and subsequent in-situ copolymerization with ethylene monomer over the ethylene polymerization sites.

Another example came from the polymer produced by copolymerization of ethylene and cyclopentene over Phillips catalyst [95]. As shown in Fig. 7, the 1,2-insertion and 1,3-insertion of cyclopentene into the polyethylene chain were confirmed. The absence of any internal double bond (C=C) in the copolymer ruled out the ring-opening metathesis polymerization mechanism. This evidence strongly implied that Cr=C might not be an active site for polymerization. Cr–C active sites under the Cossee–Arlman mechanism should be responsible for the chain propagation. From analysis of the structure of the polymer produced by copolymerization of the isotope-labeled monomer, McGuinness et al. also provided unambiguous support for chain growth via a Cossee–Arlman process on Phillips catalyst [96]. Based on the above-mentioned experimental evidence, during the induction period the

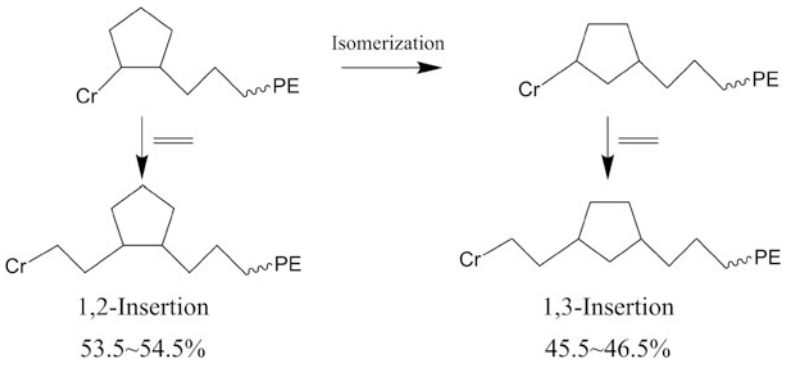

Fig. 7 Mechanisms of 1,2-insertion and 1,3-insertion of cyclopentene into the polyethylene main chain during ethylene and cyclopentene copolymerization over Phillips catalyst

Cr=C species (metathesis active sites) should be transformed into Cr–C species (polymerization active sites) in a mysterious way, as illustrated in Scheme 7. Such mysterious phenomenon of interconversion between catalysis of olefin metathesis and olefin polymerization with other types of catalysts has been previously reported [97, 98] and needs further investigation in the future.

2.4 Titanium Modification of the Phillips Catalyst

The Ti-modified Phillips catalyst is a very important industrial catalyst that is widely used in ethylene polymerization for promotion of polymerization activity and regulation of the microstructure of the polymer chains, but the mechanism of its action still remains mysterious. We characterized several industrial Ti-modified Phillips catalysts calcined at 650°C and 820°C using ^{1}H MAS solid state NMR and XPS. As shown in Fig. 8, the ^{1}H MAS solid-state NMR spectra provided the first direct evidence of surface residual Ti–OH groups on the Ti-modified Phillips catalysts. In Fig. 9, the high-resolution XPS studies on these industrial catalysts clearly demonstrated that the BE value of surface chromate species slightly increased with increased Ti loading of the catalysts, indicating the increased electron-deficiency of surface chromate species due to modification by Ti [71]. The slight increase in the FWHM values also indicated the broadening of the distribution of surface chromate species. Calcination temperatures of 650–820°C showed a similar effect to that of Ti loading in terms of the increased electron-deficiency of surface chromate species, which could be rationalized by the removal of more electron-donating surface hydroxyl groups and the increase in surface tension due to dehydroxylation of surface residual hydroxyl groups at higher calcination temperatures.

In summary, it has been demonstrated that much deeper understanding of the thermal activation during catalyst preparation, activation by CO or Al-alkyl

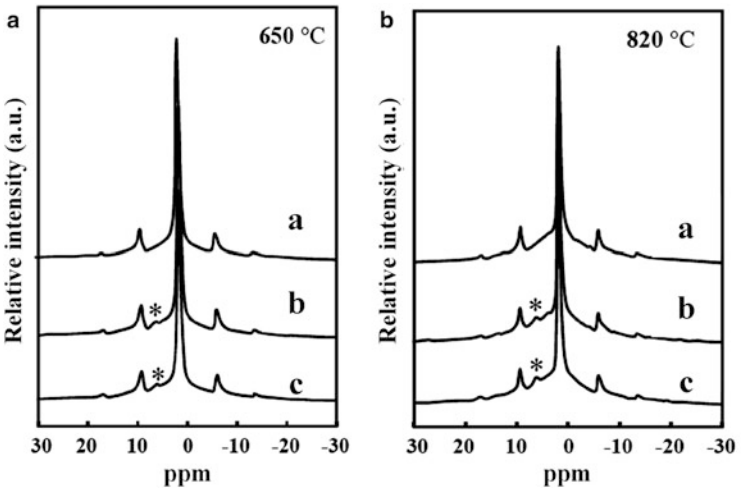

Fig. 8 ^{1}H MAS solid state NMR spectra for various Phillips catalysts calcined at (**a**) 650°C and (**b**) 820°C: Ti-free (*curve a*), modified by 2.38 wt% Ti (*curve b*), and modified by 3.45 wt% Ti (*curve c*). *Asterisks* indicate peak corresponding to surface Ti-OH groups

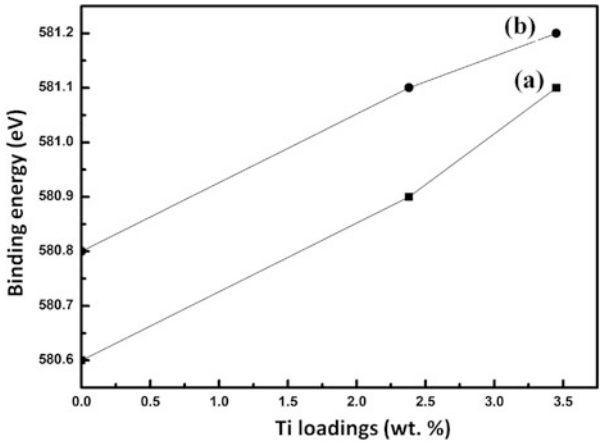

Fig. 9 Dependence of binding energy [Cr 2p (3/2)] of surface Cr^{6+} species of various Phillips catalysts on Ti content of the Phillips catalyst calcined at (*a*) 650°C and (*b*) 820°C

cocatalysts, activation by ethylene monomer during the induction period, and the effect of Ti-modification of Phillips catalysts has been achieved through various spectroscopic methods, in particular through combined multiple methodologies. Further development can be expected with the development of the spectroscopic techniques and the emergence of new techniques such as time- and temperature-resolved FTIR spectroscopy [62], pressure- and temperature-resolved FTIR spectroscopy under in-situ or operando conditions [63, 77], in-situ XAS

spectroscopy [99], LA-MS, and LDI-MS [75], which were frequently involved in recent studies of the Phillips catalyst. The characterization under close to actual commercial conditions is also a challenge as well as an opportunity to cast some light on the related mechanisms. At the same time, the combination of modern spectroscopic methods with other methodologies such as polymerization kinetic, model catalyst, and molecular modeling techniques as well as with analysis of the microstructures of polymer chains will play more and more important roles in the future and will be partially outlined in the following sections.

3 Approaches Using Polymerization Kinetics

Kinetic investigation through either polymerization experiments or mathematic modeling both for slurry and gas phase polymerization is one of the most important ways to investigate catalytic mechanisms and to provide basic data for polymerization reactor and process design. Mathematic modeling of ethylene polymerization kinetics over Phillips catalysts has been demonstrated as a powerful tool for the precise evaluation of the basic kinetic parameters and to establish equations for structure–property regulation through control of process parameters [100–103]. The polymerization kinetics of Phillips catalysts could be significantly affected by the reductive activation process for ethylene polymerization using different activators such as ethylene, CO, Al-alkyl cocatalysts (e.g., TEA), or even other reducing agents. The polymerization kinetics of Phillips catalysts using ethylene monomer itself as activator for ethylene polymerization has been systematically investigated [2]. Typically, a linearly built-up type of kinetic curve would be presented, with an induction period dependent on the polymerization temperature and ethylene pressure. Reductive activation by CO only diminishes the induction period without changing the character of the built-up type of kinetic curve. In recent years, activation of the Phillips catalyst by Al-alkyl cocatalysts is becoming one of the most important ways to improve the catalyst performance and the microstructure and properties of the polyethylene (PE) products. As is well known, Al-alkyl cocatalyst is an indispensable component for most of the olefin polymerization catalysts such as Ziegler–Natta and metallocene catalysts. The Al-alkyl cocatalyst could act as reducing agent, alkylation agent, poison scavenger, and have a marked impact on the polymer microstructure by control of the chain transfer and stereospecificity. Also, excess amount of Al-alkyl cocatalyst could deactivate the catalyst through over-reduction of the active Cr species. Ethylene polymerization with Phillips catalyst without using any organometal cocatalyst is taken as the most important evidence to support the monometallic active site mechanism. Therefore, Al-alkyl cocatalyst could be excluded as the active site former for Phillips catalysts.

During the last few decades, experimental reports about the combination of Al-alkyl cocatalyst with the Phillips catalyst have been very limited. Spitz et al. [104] reported the significant effect of TEA on Phillips catalyst for the activity,

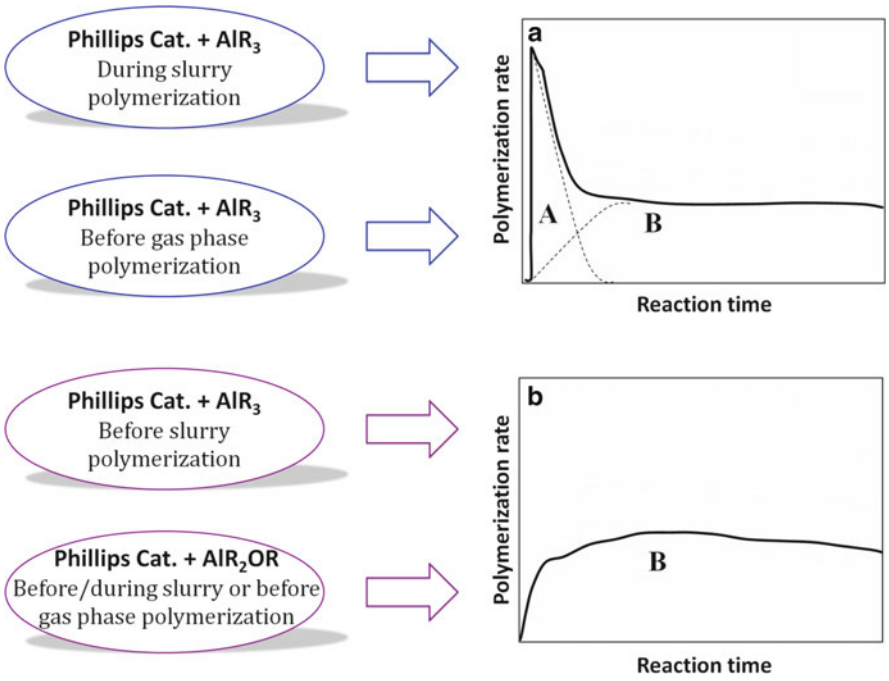

Fig. 10 Two types of kinetic curve for ethylene polymerization over Phillips-type catalysts. (**a**) Hybrid of two typical types of kinetic curve: fast activation followed by fast decay (*A*) and slow activation followed by slow decay (*B*). (**b**) Single-type curve with slow activation followed by slow decay (*B*)

kinetics and 1-hexene incorporation for ethylene/1-hexene copolymerization in liquid 1-hexene. McDaniel and Johnson [105, 106] studied the effects of TEB on the polymerization kinetics of the Phillips catalyst with different supports ($AlPO_4$, SiO_2, Al_2O_3). Tait and coauthors [107] studied the effects of TiBA on kinetics and polymer morphology with Phillips catalyst. Our series of studies on the Phillips catalyst combined with Al-alkyl cocatalyst revealed that the polymerization kinetics could be significantly affected by the type of Al-alkyl cocatalyst as well as by the timing of its introduction for both slurry and gas phase ethylene polymerization (see Fig. 10) [69, 80, 84, 95, 108–110]. For the same Al-alkyl cocatalyst, catalyst activation by the cocatalyst before polymerization (in catalyst preparation) or during polymerization with simultaneous interaction of catalyst with Al–alkyl cocatalyst and monomer would make a significant difference in the polymerization kinetics. As shown in Fig. 10a, the kinetic curve (type a) follows hybrid-type kinetics and can be deconvoluted into two basic types of typical kinetic curves: one type with fast activation followed by fast decay and the other type with slow activation followed by slow decay. They should be derived from two different types of active sites. The kinetic curve of type b (shown in Fig. 10b) follows only one single type of kinetics, with slow activation followed by slow decay. Sections 3.1

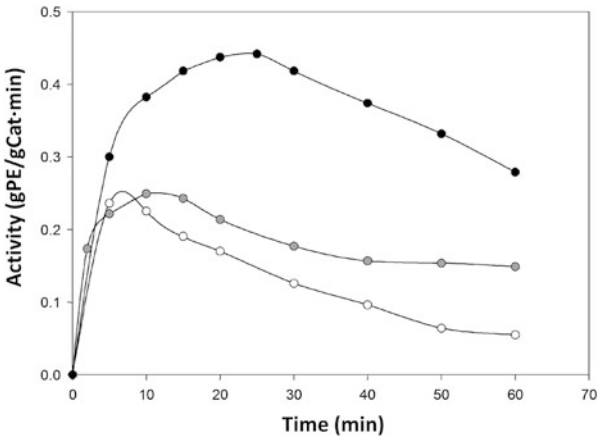

Fig. 11 Kinetic curves of the TEA-modified Phillips catalyst (PC600/TEA) at Al/Cr molar ratios of 2.08 (*white symbols*), 3.12 (*grey symbols*), and 4.16 (*black symbols*), before ethylene slurry polymerization. Polymerization conditions: catalyst amount, 100 mg; polymerization temperature, 60°C; ethylene pressure, 0.15 MPa; solvent heptane, 20 mL

and 3.2 will discuss how the type of cocatalyst (AlR_3 or AlR_2OR), the timing of introduction of cocatalyst (before or during polymerization), and the type of polymerization (slurry or gas phase), can dramatically affect the polymerization kinetics as shown in Fig. 10.

3.1 Activation by Al-alkyl Cocatalyst Before Polymerization

In the previous sections, a combined XPS and solid state NMR spectroscopic investigation of Phillips catalysts (PC400/TEA, PC600/TEA, and PC800/TEA) calcined at 400°C, 600°C, and 800°C, respectively, followed by activation with TEA cocatalyst before slurry polymerization showed that 4-coordinated Al species, rather than the 5- or 6-coordinated Al species, were directly related with the polymerization-active Cr species. Figure 11 shows the polymerization kinetics for the PC600/TEA catalyst at different Al/Cr molar ratios of 2.08, 3.12, and 4.16 [69]. Kinetic curves of type b (Fig. 10b) show a gradual built-up of polymerization rate from zero to a maximum followed by gradual decrease to a stationary rate, which was found to be the same typical form of kinetics as for $TiCl_3$/TEA and metallocene/MAO catalysts. This type of kinetics for TEA-modified Phillips catalysts was consistent with those reported by Spitz et al. [104] and McDaniel and Johnson [105, 106] using Cr/silica/TEA and Cr/$AlPO_4$/TEB catalysts, respectively.

The Phillips catalyst is mostly applied in ethylene slurry polymerization using loop reactors. It is also now being commercially used in gas phase ethylene polymerization processes. However, it is very difficult to find reports about ethylene gas phase polymerization using Phillips catalysts in the literature because it is a great challenge to perform gas phase polymerization on a laboratory scale. Recently, we carried out gas phase ethylene polymerization over silica-supported

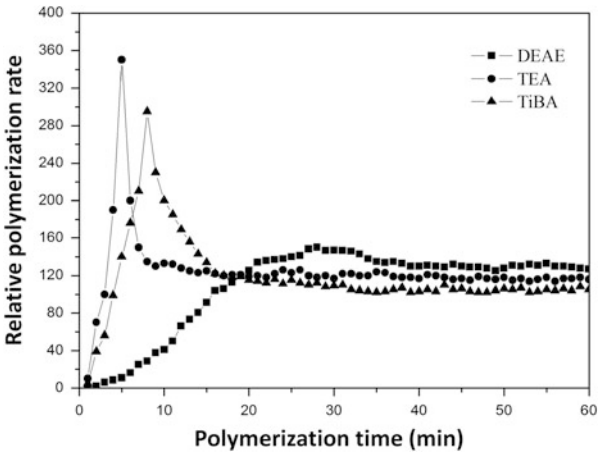

Fig. 12 Kinetic curves of ethylene polymerization of S-2 catalysts modified with various cocatalysts before gas phase polymerization. Polymerization conditions: catalyst amount, 200 mg; polymerization temperature, 92°C; ethylene pressure, 1.2 MPa

silyl chromate S-2 catalysts pre-reduced by three Al-alkyl cocatalysts in a specially designed gas phase high-speed stirred-autoclave reactor [109]. The catalyst was pre-activated by TEA, TiBA, or DEAE before the gas phase ethylene polymerization during the catalyst preparation step. As shown in Fig. 12, the gas phase ethylene homopolymerization kinetic curves over the TEA- or TiBA-modified S-2 catalysts belonged to type a (Fig. 10a), which is a hybrid type of kinetics composed of two basic types of typical kinetic curve: one type with fast activation followed by fast decay and the other type with slow activation followed by slow decay. Such type of polymerization kinetics might not be suitable for application in large-scale gas phase olefin polymerization processes because reactor fouling and agglomeration can easily occur. In the case of the DEAE-modified S-2 catalyst, the gas phase ethylene homopolymerization kinetic curve is type b (Fig. 10b), which is a simple type of polymerization kinetics with slow activation followed by slow decay. Although the polymerization activity for the DEAE-modified S-2 catalyst is slightly lower than the TEA- or TiBA-modified catalysts, its polymerization kinetics would be of benefit for the heat transfer within the gas phase polymerization fluidized bed reactor [111]. The differences in the structure and in the reducing and alkylation capabilities of AlR_3 (TEA and TiBA) and AlR_2OR (DEAE) cocatalysts might be responsible for their totally different ethylene polymerization kinetics, but the mechanism is still not known and awaits further exploration.

3.2 Activation by Al-alkyl Cocatalyst During Polymerization

The Al-alkyl cocatalyst could also be introduced during the polymerization stage, with simultaneous interaction of catalyst with Al–alkyl cocatalyst and monomer within the polymerization reactor. Ethylene homopolymerization using Phillips catalyst PC600 calcined at 600°C followed by activation with TEA cocatalyst

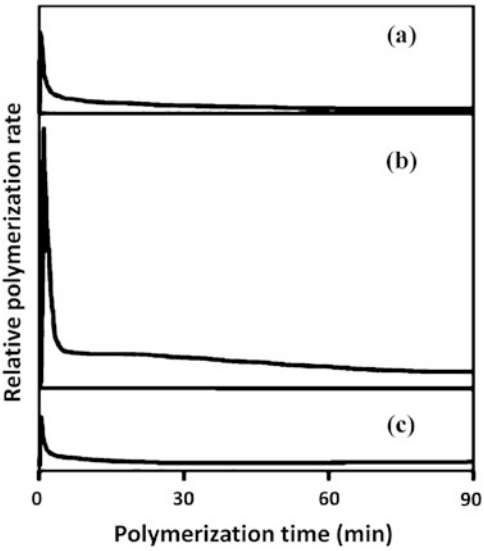

Fig. 13 Kinetic curves of ethylene polymerization using Phillips catalyst PC600 activated by TEA during slurry polymerization with Al/Cr molar ratio: (**a**) 7.5; (**b**) 15.0; (**c**) 22.5. Polymerization conditions: catalyst amount, 100 mg; polymerization temperature, 60°C; ethylene pressure, 0.13 MPa; solvent heptane, 20 mL; cocatalyst TEA in heptane, 1 M

during the slurry polymerization process was carried out with Al/Cr molar ratios of 7.5, 15.0, and 22.5 [84]. As shown in Fig. 13, the catalyst showed type a (Fig. 10a) ethylene polymerization kinetics, which is a hybrid type of kinetics composed of two basic types of typical kinetic curves. Such hybrid-type polymerization kinetics must originate from two different types of active sites (here named Site-**A** and Site-**B**). Our previous reports have described a mechanistic speculation of the origin of the two types of active sites for ethylene polymerization as well as their plausible transformation during activation of the Phillips catalyst either by Al-alkyl cocatalyst or by ethylene monomer and CO, which is illustrated in Scheme 8. Under the simultaneous interaction of TEA and ethylene monomer with PC600 catalyst, some chromate Cr(VI) species were reduced to Cr(II) species by ethylene monomer with formaldehyde as byproduct. The coordination of formaldehyde with Cr(II) species (named as Site-**C1** in Scheme 8) could occur, which could lead to the formation of Site-**A** through the desorption of formaldehyde by TEA or ethylene monomor. Due to the very exposed feature, Site-**A** could easily coordinate with ethylene monomer and could also easily be over-reduced by TEA cocatalyst. Therefore, Site-**A** showed high activity but fast decay. On the other hand, some chromate Cr(VI) species were reduced by TEA and then coordinated with Al-alkoxy resulting in Site-**B**, with slow activation and slow decay. Within Site-**B**, the Cr(II) center was strongly coordinated with Al-alkoxy byproduct, which may hinder the coordination of ethylene monomer but avoid further over-reduction by TEA. Therefore, Site-**B** had lower activity and higher stability compared with Site-**A**. The ^{13}C NMR spectra of the homopolymers obtained from this catalyst system showed the signal of the branching carbons of methyl, ethyl, propyl, and *n*-butyl. Site-**C1** was a metathesis site and could produce propylene, 1-butene, and 1-pentene, which was consistent with the ^{13}C NMR spectroscopic evidence of the ethylene

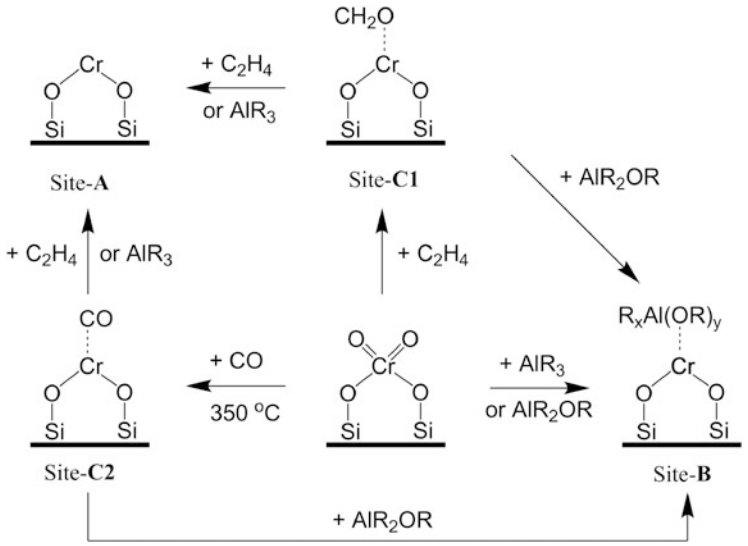

Scheme 8 Plausible mechanism for the formation of two kinds of ethylene polymerization active sites (Site-**A** and Site-**B**) and metathesis active sites (Site-**C1** and Site-**C2**) on Phillips-type catalysts under various conditions; $x = 1$ or 2; $y = 1$ or 2

homopolymers obtained from this catalyst system showing the signals of the branching carbons of methyl, ethyl, and propyl. With increase in the Al/Cr molar ratios in the polymerization, the relative amount of SCBs of polymers from the catalyst system also decreased, because the competition between ethylene monomer and TEA reduced the chromate Cr(VI) species into Cr(II) sites and accelerated the conversion of metathesis active site-**C1** to polymerization active Site-**B** with more TEA.

Ethylene homopolymerization using Phillips catalyst PC600 calcined at 600°C followed by activation with DEAE cocatalyst during the slurry polymerization process was carried out with Al/Cr molar ratios of 7.5, 15.0, and 22.5 [84]. As shown in Fig. 14, a typical single-type polymerization kinetics corresponding to type b in Fig. 10b was observed, which was completely different from the kinetics with the same catalyst activated by TEA at the same conditions (as shown in Fig. 13). This type of polymerization kinetics could be ascribed to one type of active site (Site-**B**) formed in two ways. One was similar with the PC600 activated by TEA: some chromate Cr(VI) species were reduced to Cr(II) species by ethylene monomer and coordinated with formaldehyde, then formaldehyde-coordinated Cr(II) sites were transformed to DEAE-coordinated Cr(II) sites by substitution, as shown in Scheme 8. On the other hand, some chromate Cr(VI) species were reduced by DEAE, and then the Al-alkoxy product coordinated with the Cr(II) sites. Site-**B** had relatively low activity and high stability. Based on the microstructure analysis, the relative amount of SCBs of polymers obtained from the DEAE systems was even more than that from TEA catalyst systems. This can be explained as follows. Firstly, the reduction ability of DEAE was weaker than that of TEA. More Cr(VI) species

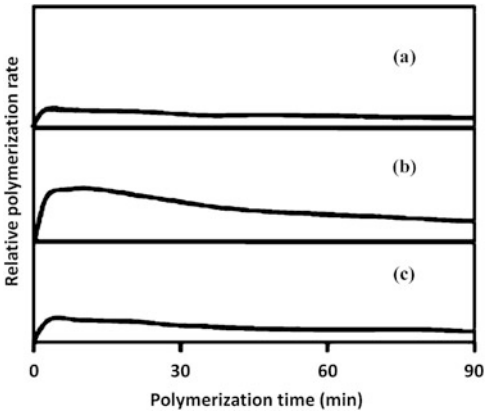

Fig. 14 Kinetic curves of ethylene polymerization using Phillips catalyst PC600 activated by DEAE during slurry polymerization with Al/Cr molar ratio: (*a*) 7.5; (*b*) 15.0; (*c*) 22.5. Polymerization conditions: catalyst amount, 100 mg; polymerization temperature, 60°C; ethylene pressure, 0.13 MPa; solvent heptane, 20 mL; cocatalyst DEAE in heptane, 1 M

could be reduced by ethylene and coordinated with formaldehyde to form Site-**C1**. Secondly, DEAE needed a longer time for the conversion of metathesis active sites into polymerization active sites. More α-olefin will be formed from metathesis active sites to insert into the polymer chains. Thirdly, different Al-alkoxyl byproducts of the reaction between TEA/DEAE and chromate species, subsequently coordinated with the chromium active site, will also affect the incorporation rate of α-olefin comonomers.

Ethylene homopolymerization or 1-hexene/ethylene copolymerization, using Phillips catalyst PC600/CO calcined at 600°C treated with activation by CO at 350°C followed by TEA cocatalyst activation during the slurry polymerization process, was carried out with Al/Cr molar ratios of 7.5, 15.0, and 22.5 [80, 110]. For this catalyst system, it was expected that N_2 could not remove all adsorbed CO from the Cr(II) due to the similar electron characteristics of CO and formaldehyde and due to the high coordinative unsaturation of the Cr(II) center. According to XPS results (Fig. 4), it was found that almost one-third of the chromate(VI) species still existed after the normal CO pre-reduction procedure. Under these complex conditions, a hybrid-type polymerization kinetics (corresponding to type a in Fig. 10a) was still found for both homo- and copolymerization, as shown in Fig. 15. One of the types with instant activation and fast decay originated from the active site (Site-**A** in Scheme 8), formed through desorption of formaldehyde (Site-**C1**) or CO (Site-**C2**) from the Cr(II) site by TEA or ethylene monomer. The other type with slow activation and slow decay was from the Site-**B**, formed from the reduction of residual chromate(VI) species by TEA. The formed Al-alkoxyl can strongly coordinate with the Cr(II) site and thus protect the Cr(II) center from further over-reduction by TEA. The first peaks of the copolymerization kinetic curves from Site-**A** became broader in comparison with those of homopolymerization, suggesting either that the decay of Site-**A** became slower in the presence of comonomer or that the transformation of metathesis

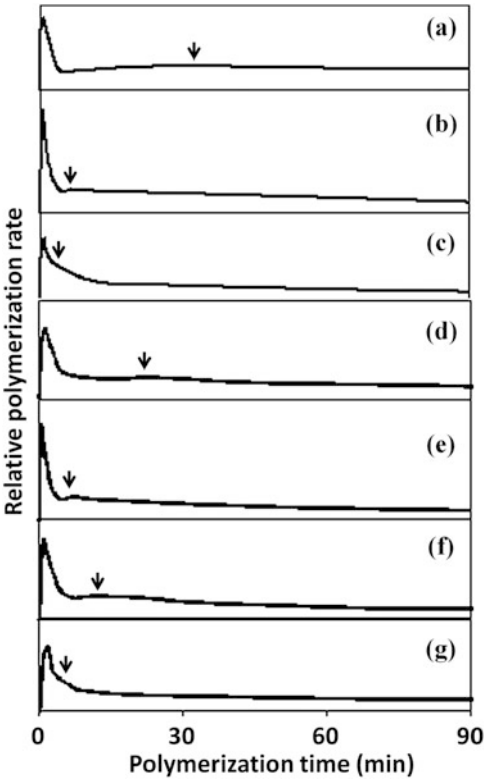

Fig. 15 (*a–c*) Kinetic curves of ethylene homopolymerization using Phillips catalyst PC600/CO activated by TEA during slurry polymerization with Al/Cr mole ratio of (*a*) 7.5, (*b*) 15.0,and (**c**) 22.5. (*d–g*) Kinetic curves of ethylene/1-hexene copolymerization under (*d*) Al/Cr ratio of 7.5 with 10 vol% of 1-hexene, (*e*) Al/Cr ratio of 15.0 with 5 vol% of 1-hexene, (*f*) Al/Cr ratio of 15.0 with 10 vol% of 1-hexene, and (*g*) Al/Cr ratio of 22.5 with 10 vol% of 1-hexene. The *arrow* indicates the maximum activity on Site-**B**. Polymerization conditions: catalyst amount, 100 mg; polymerization temperature, 60°C; ethylene pressure, 0.13 MPa; solvent, heptane, 20 mL; cocatalyst TEA in heptane, 1 M

Site-**C1** and/or Site-**C2** into polymerization Site-**A** was slowed down due to the stronger reduction of 1-hexene than of ethylene. With increasing Al/Cr mole ratio from 7.5 to 22.5, the time to reach maximum activity from Site-**B** in copolymerization became shortened from 25 to 5 min (Fig. 15, arrows). All the obtained homo- and copolymers were characterized by ^{13}C NMR. The peaks assigned to the branching carbons of methyl and butyl branches in the copolymers and methyl branches in the homopolymers were found, which could rationalize well the existence of Site-**C1** and/or Site-**C2** for ethylene metathesis to form propylene as a comonomer for the in-situ copolymerization. Similar polymerization kinetics were also observed in copolymerization of ethylene with cyclopentene using Phillips catalyst PC600 calcined at 600°C followed by TEA cocatalyst activation during the slurry polymerization process [95]. The only difference was that cyclopentene played the role of 1-hexene during the active site formation and transformation process. Besides the 1,2- and 1,3-insertion of cyclopentene into the polyethylene main chain (Fig. 7), the in-situ copolymerization of propylene, 1-butene, and 1-pentene in the same system was also confirmed by ^{13}C NMR, indicating the existence of ethylene metathesis active site (Site-**C1** and/or Site-**C2**) during the formation of the polymerization sites [95].

In summary, investigation of the polymerization kinetics over Phillips-type catalysts could provide deep mechanistic understanding and valuable information to guide the design and optimization of the polymerization processes. It has been demonstrated that the polymerization kinetics could be drastically affected by the types of cocatalysts, the timing of introduction of the cocatalyst, and the types of polymerization. From the industrial point of view, the direct activation of Phillips-type catalysts by AlR_3-type cocatalysts during the polymerization process within the polymerization reactor should be avoided in ethylene slurry polymerization. As for gas phase ethylene polymerization, activation of Phillips-type catalysts by AlR_3 during catalyst preparation before polymerization should also be forbidden. We could expect that more efforts should be devoted to the investigation of gas phase polymerization kinetics, combination of experiments with kinetic modeling and microkinetic modeling based on first principle calculations in the near future.

4 Approaches Using Heterogeneous Model Catalysts

The surface complexity of the traditional Phillips Cr/silica catalyst derives from the following aspects: the coexistence of mono-, di-, and polychromate species, the inevitable formation of Cr_2O_3 microcrystals [8, 11], the formation of surface chromium species in lower oxidation states due to thermally induced reduction of surface chromate species at high temperature, the low fraction of active Cr species in the total Cr loading [4, 11], the ambiguous and complicated reactions for the formation of the first chromium–carbon bond between ethylene monomer and surface chromate species. These factors greatly contribute to the surface complexity of the industrial Phillips catalyst and thus hinder academic progress in basic understanding of the nature of active sites and polymerization mechanisms for this important commercial polyolefin catalyst. During the last decades, various heterogeneous models with more uniform and well-defined structure of surface chromium species have been designed to facilitate the fundamental investigations in this field. Typical reported heterogeneous models for Phillips catalysts are listed in Scheme 9. These models can be generally divided into two groups: surface hexavalent chromate species (models **1c**, **2c**, **6c**, **9c**, and **10c**) and surface chromium species with lower oxidation states (models **3c**, **4c**, **5c**, **7c**, and **8c**).

S-2 catalyst prepared by wet impregnation of BC into thermally pretreated silica gel could be considered as a commercial heterogeneous model (**1c**) for Phillips catalysts [26, 112]. The S-2 catalyst shows an increased activity after supporting on silica gel compared with BC and produces HDPEs with even broader molecular weight distribution than that produced by the Phillips catalyst. Model **2c** was firstly prepared by McDaniel [113] via mild grafting (at 200°C) of CrO_2Cl_2 onto thermally pretreated silica. The CrO_2Cl_2 grafted onto silica pretreated at 400°C showed similar surface chromate structure and polymerization activity to the Phillips catalyst. Recently, Scott and colleagues [54, 114] prepared similar catalysts via ambient anhydrous grafting of CrO_2Cl_2 onto silica pretreated at 200°C, 450°C and

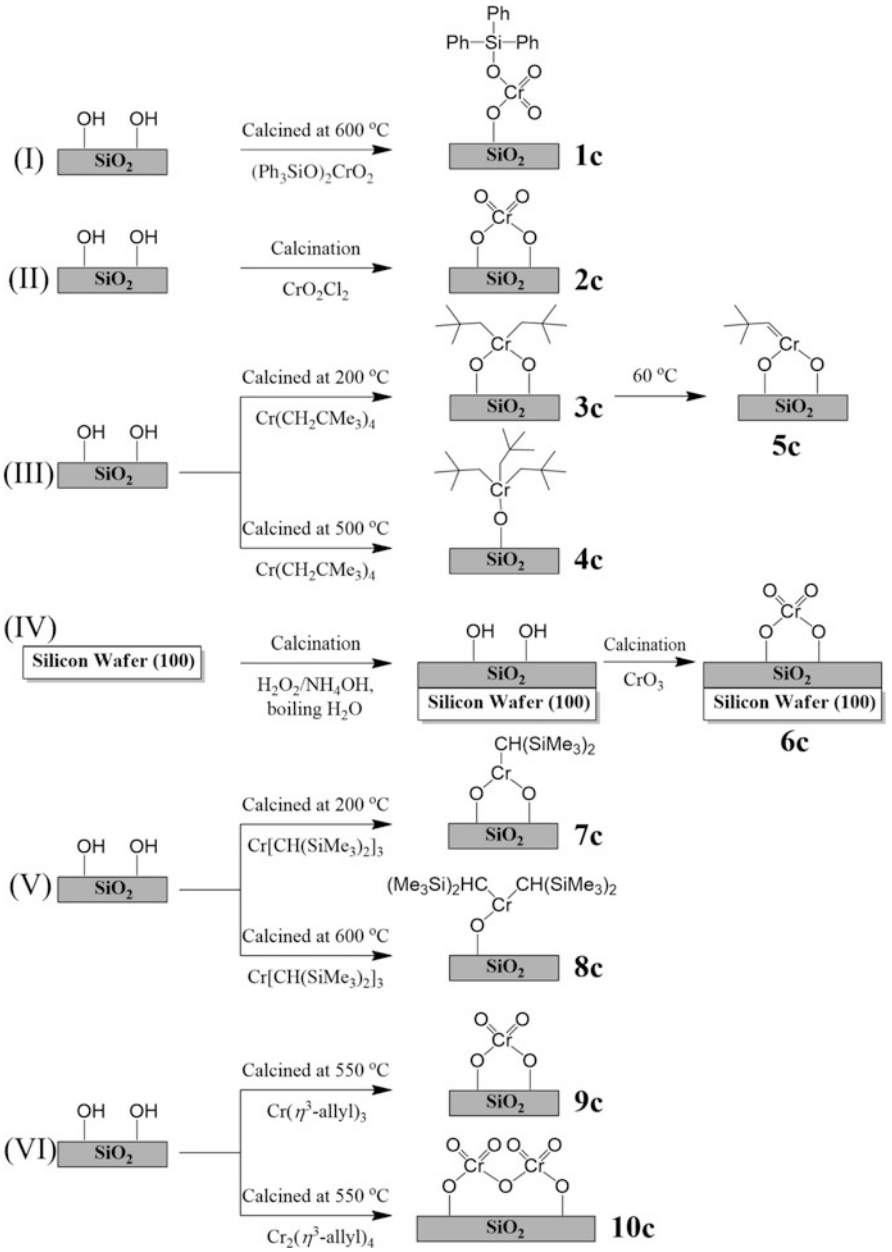

Scheme 9 Heterogeneous models reported in the literature for the Phillips Cr/silica catalyst

800°C. By combination of IR, XANES, and EXAFS, they explained that the higher polymerization activity over CrO_2Cl_2 grafted onto silica pretreated at 800°C was related to the more strained six-membered chromasiloxane rings. Thüne et al. [115]

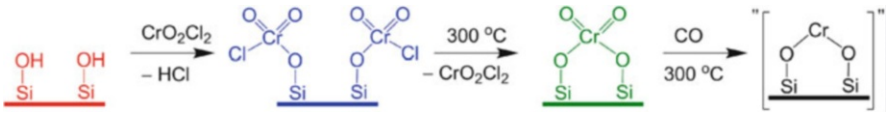

Scheme 10 Preparation procedure for the heterogeneous divalent model Phillips catalysts

reported a flat surface model catalyst by impregnating aqueous CrO_3 on a flat Si (100) substrate covered by an amorphous silica layer, shown as model **6c**. This flat catalyst covered with monochromate showed ethylene polymerization activity at 160°C, whereas the pre-reduced surface Cr(II) species failed to polymerize ethylene due to its extreme sensitivity to air and moisture [53]. Recently, Terano and colleagues [116] chose different starting materials [Cr(η^3-allyl)$_3$ and Cr_2(η^3-allyl)$_4$] to vary the surface structures of the catalysts (monochromate and dichromate, shown as models **9c** and **10c**, respectively). It was found that the surface dichromate model catalyst **10c** produced more methyl branching in its PE products. Models **3c**, **4c**, and **5c** were reported by Scott and coworkers [90–94, 117] via grafting of tetravalent Cr[$CH_2C(CH_3)_3]_4$ onto silica pretreated at 200°C (**3c**) or 500°C (**4c**). Upon mild heating at 60°C, a supported Cr-alkylidene complex **5c** was formed on silica pretreated at 200°C, which showed instant ethylene polymerization activity without using any cocatalyst. Monoi and coworkers [118, 119] reported a trivalent model catalyst by the supporting of Cr[$CH(SiMe_3)_2]_3$ on silica pretreated at 200 or 600°C. When the pretreating temperature was 200°C, Cr species were supported on silica through two Si–O–Cr bonds, shown as model **7c**, whereas for the case of 600°C, the grafting took place via only one Si–O–Cr bond to silica to form model **8c**. Compared to the Phillips catalyst, these catalysts showed high ethylene polymerization activity without using any cocatalyst and displayed very similar performance except for increased sensitivity of the hydrogen response. In addition, further reaction over **8c** with excess Cr[$CH(SiMe_3)_2]_3$ was likely to lead to the formation of new active sites for ethylene trimerization [119]. Although the above-mentioned heterogeneous model catalysts displayed representative polymerization activity at certain temperatures with or without the cocatalyst and offered the opportunity for further understanding of Phillips catalysts, no direct evidence on the real active sites and polymerization mechanisms has yet been achieved.

Very recently, we performed further studies over extremely air-sensitive divalent model Phillips catalysts via CO reduction (at 300°C) of model **2c** [55]. Two heterogeneous divalent model Phillips catalysts were prepared via ambient anhydrous grafting of CrO_2Cl_2 onto silica pretreated at 500 and 800°C, followed by heating and CO reduction at 300°C, as shown in Scheme 10. As shown in Fig. 16, the obtained Cr(II)/S948-800 [Cr(II) supported on silica pretreated at 800°C] catalyst showed higher ethylene polymerization activity than that of Cr(II)/S948-500 [Cr(II) supported on silica pretreated at 500°C] catalyst without any induction period at RT. Further characterizations were performed to explore the origin of the different activities of the two catalysts. From the CO stretching region in the IR spectra, two obvious peaks (ca. 2,190 and 2,180 cm^{-1}) were shown for Cr(II)/S948-500 catalyst,

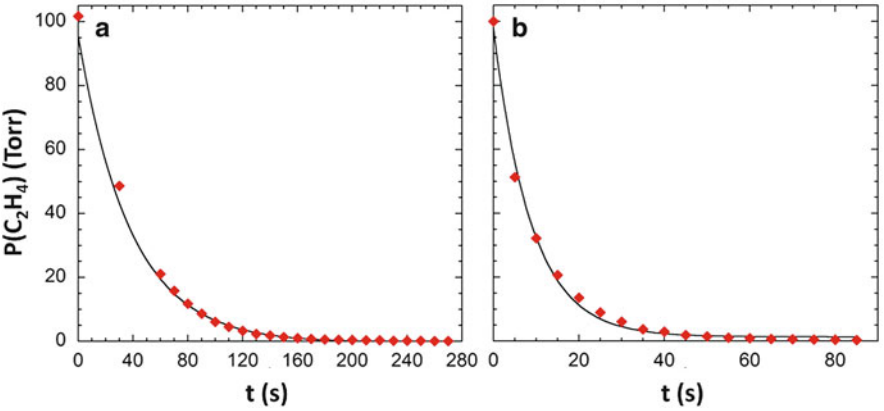

Fig. 16 Ethylene uptake profiles (*symbols*) in a batch reactor at 23°C, over (**a**) Cr(II) grafted on S948-500 (102.7 mg, 1.71 wt% Cr, 34.5 μmol Cr); and (**b**) Cr(II) grafted on S948-800 (314.3 mg, 0.62 wt% Cr, 38.1 μmol Cr). The *lines* are three-parameter fits to the first-order integrated kinetic rate equation

and three for Cr(II)/S948-800 (ca. 2,190, 2,187, and 2,180 cm^{-1}), shown in Fig. 17. After deconvolution of the IR spectrum of Cr(II)/S948-500 catalyst, a third peak at 2,187 cm^{-1} was also observed. Furthermore, the results of the IR deconvolution showed that the area ratio of the peaks at ca. 2,190 and 2,180 cm^{-1} was constant at 2.0 for both catalysts, which was not related to the variations in the pretreating temperature for silica or the evacuation time of adsorbed CO. We assumed that these two peaks (ca. 2,190 and 2,180 cm^{-1}) can be attributed to the symmetric and asymmetric stretching of the dicarbonyl species $(\equiv SiO)_2Cr(CO)_2$ while the other peak at ca. 2,187 cm^{-1} was assigned to the monocarbonyl species $(\equiv SiO)_2Cr(CO)$.

The speculated presence of dicarbonyl and monocarbonyl species on the silica surface was further confirmed by ONIOM calculations. The model cut from the (100) face of β-cristobalite was applied to mimic the local structures of the silica surface. Two different molecular models with replaceable and irreplaceable siloxane ligand were built for the dicarbonyl and monocarbonyl species, respectively, as shown in Fig. 18. The calculated relative shifting for the symmetric and asymmetric CO stretching was 11 cm^{-1}, very close to the experimental value of 12 cm^{-1}, which revealed information on the local coordination environment of the Cr(II) site (see structures **5e** and **6e** in Scheme 11).

For more direct evidence, an EXAFS analysis was performed for the model catalysts. Figure 19 shows that the fitting in *k* and *R* space was quite good, and the detailed structural parameters of the model for this fitting are presented in Scheme 11. The main difference between the catalysts was that the coordination numbers for the first shell of Cr(II) were four for Cr(II)/S948-500 and three for Cr (II)/S948-800, varying in the coordination number of siloxane ligand from the silica surface. A smaller average number of coordinated siloxane ligands, resulting in a great difference in the bonding of the two silanolate ligands, might be the key to the

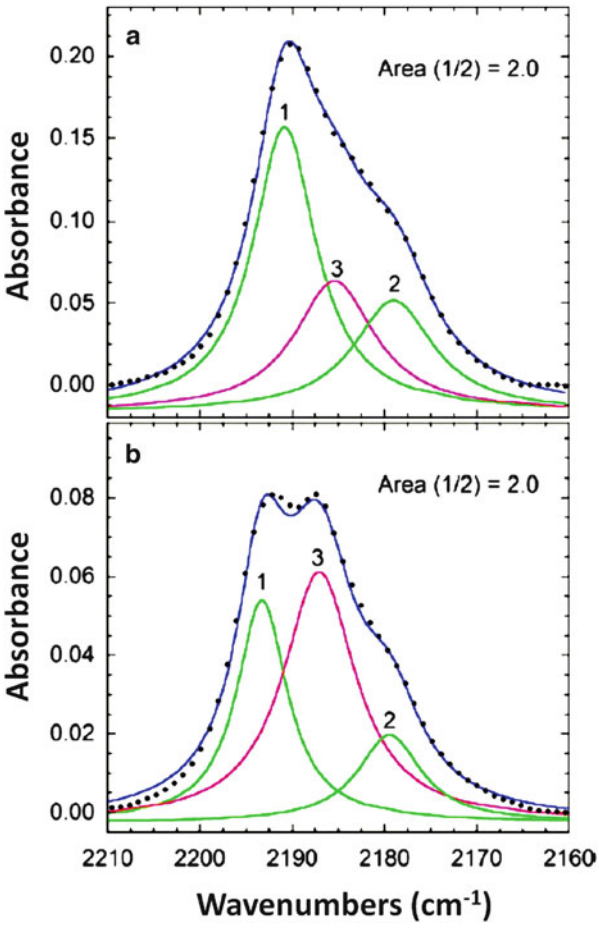

Fig. 17 Deconvolution of experimental IR spectra in the CO stretching region (*symbols*) into three Lorentzian components (*lines 1*, *2*, and *3*) for (**a**) Cr(II)/S948-500 and (**b**) Cr(II)/S948-800. The spectra predicted by the deconvoluted components is also shown

much higher ethylene polymerization activity of the model catalyst Cr(II)/S948-800 since its silica bears an irreplaceable siloxane ligand to keep the coordination number of Cr(II) at three when contacting with ethylene (as shown in Scheme 12). For model catalyst Cr(II)/S948-500, the more abundant species was the Cr(II) with coordination number of four, binding to two replaceable siloxane ligands.

In summary, it was made clear that the coordination of the divalent active site precursor with the siloxane ligands present on the silica support surface in terms of the catalyst calcination temperature was crucial for determination of the precise microstructures and coordination environment of the active Cr species and thus the performance of the Phillips catalyst. Multiple spectroscopic methods including FTIR and XAS (EXAFS/XANS) combined with molecular modeling and polymerization experiments probing into the heterogeneous Phillips model catalysts proved to be very effective. Spectroscopic investigation of the contact of ethylene with these two divalent heterogeneous model catalysts at low temperature is still in

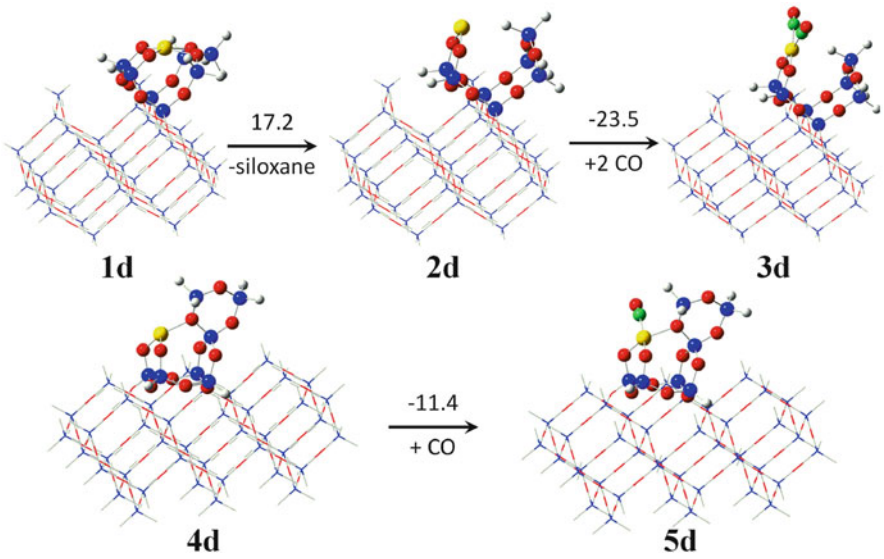

Fig. 18 Computational models for grafted "$(\equiv SiO)_2Cr$" sites, differing in total Cr coordination number, are shown without (**1d** and **4d**) and with (**3d** and **5d**) coordinated CO. The *numbers over* the *arrows* denote binding energies in kcal mol^{-1}, relative to the CO-free Cr(II) clusters (**2d** and **4d**) and free ligands (CO or siloxane). Color key: Cr (*yellow*), O (*red*), Si (*blue*), C (*green*), H (*white*). Inner layer: *ball-stick*; outer layer: *wireframe*

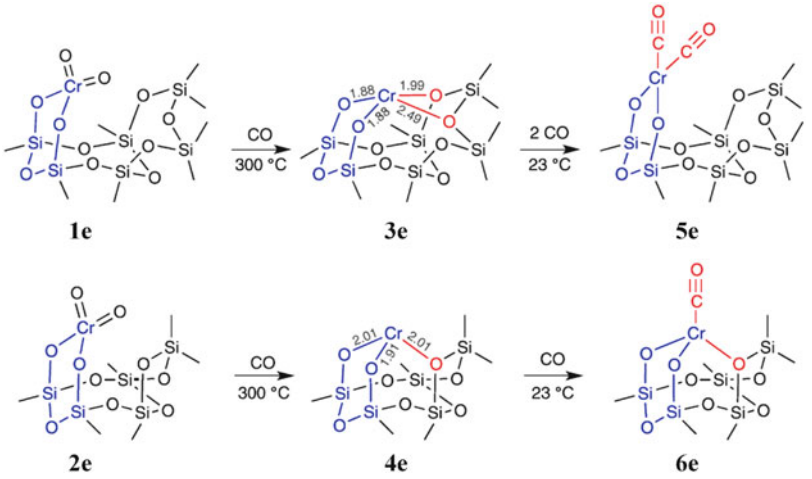

Scheme 11 Proposed structures for chromate sites (**1e**, **2e**) embedded in six-membered chromasiloxane rings (*blue*) on highly dehydroxylated amorphous silica; the corresponding Cr (II) sites, Cr(II)/S948-500 (**3e**) and Cr(II)/S948-800 (**4e**) formed upon reduction, (showing the distances obtained by EXAFS curve fitting); and their corresponding carbonyl complexes (**5e**, **6e**). Additional siloxane and carbonyl ligands are shown in *red*. Bond length is in Å

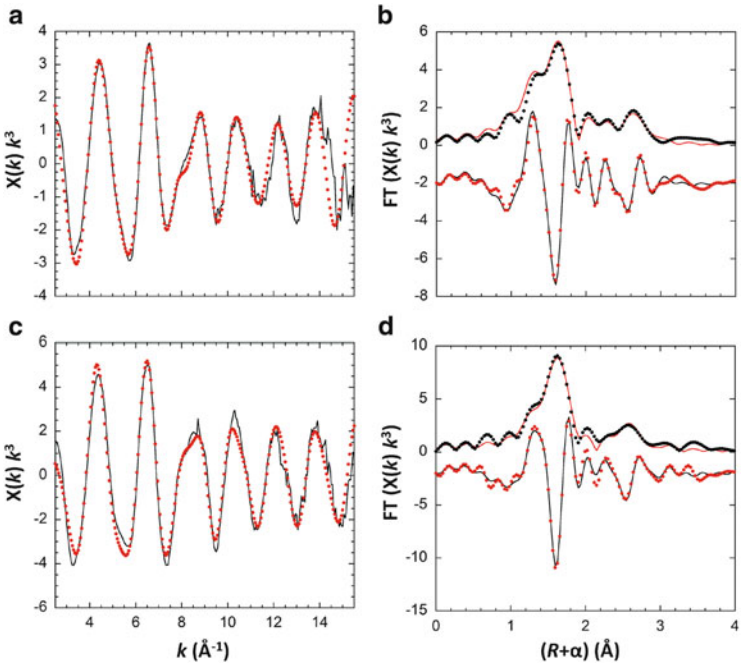

Fig. 19 Single-scattering refinements of the EXAFS for Cr(II) supported on S948-500 (**a**, **b**) and S948-800 (**c**, **d**). Frames (**a**) and (**c**) show the data (*dotted lines*) and curve fits (*solid lines*) in k^3-weighted *k*-space. Frames (**b**) and (**d**) show the FT magnitudes (*upper dotted lines*), imaginary components (*lower dotted lines*) and curve fits (*solid lines*) in *R* space

progress by our group via in-situ techniques in order to figure out the formation of the first Cr–C bond and the initiation mechanism of ethylene polymerization. A step forward in the interpretation of the nature of the active sites and polymerization mechanisms (especially the initiation mechanism of the first polyethylene chain) requires the combination of heterogeneous model catalyst systems with more advanced and multiple characterization techniques, especially in-situ/operando techniques as well as molecular modeling. The rational design and utilization of new heterogeneous model Phillips catalysts is expected to allow further progress in better understanding of the real and complex catalyst system.

5 Approaches Using Homogeneous Model Catalysts

In the previous section, investigations on heterogeneous model catalysts with more uniform and well-defined structure of surface chromium species supported on silica gel had been demonstrated as a powerful strategy for the basic study of Phillips catalysts. However, the complexity is still derived from the heterogeneity of the

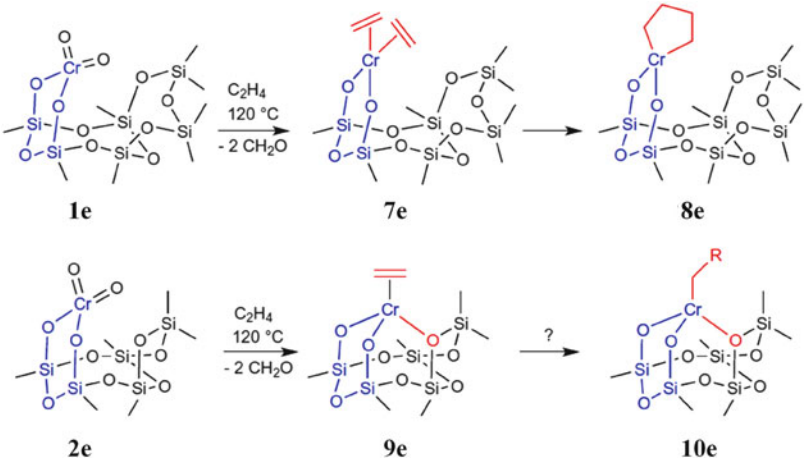

Scheme 12 Two different possible routes for ethylene reduction/activation of silica-supported chromates (**1e**, **2e**) embedded in six-membered chromasiloxane rings (*blue*). In the absence of coordinated siloxane ligands, the bis(ethylene) complex **7e** is transformed readily to the polymerization-inactive chromacyclopentane **8e** [120], while a non-displaceable siloxane ligand in the mono(ethylene) complex **9e** prevents metallacycle formation and therefore opens an alternate, as-yet unknown, path to a monoalkylchromium(III) site capable of polymerizing ethylene. Additional siloxane, ethylene monomer and subsequent formed bonds are shown in red

amorphous silica support as well as the fact that more than 99% of the active sites exist within the micro- and mesopores in the inner surface of the silica support. During the last few decades, various homogeneous model catalysts have been developed in order to simplify such complexity of the traditional Phillips catalyst originating from the silica support [121]. Some typical homogeneous model catalysts are listed in Scheme 13, including the $Cr(II)OH^+$ and $Cr(III)O^+$ cations (models **1f** and **2f**) [122, 123], bistriphenylsilyl chromate (BC) (model **3f**) [111], a POSS-supported Cr catalyst (model **4f**) [124, 125], siloxane chromate ester (model **5f**) [126], spirocyclic chromium(II) siloxane (model **6f**) [127], 1,3,5-triazacyclohexane complexes of chromium(III) (model **7f**) [128], cationic alkyl complexes of chromium (III) (model **8f**) [121, 129–131], and $[(Ph_3SiO)Cr \cdot (THF)]_2(\mu\text{-}OSiPh_3)_2$ (model **9f**) [40, 41]. Some recently reported novel homogeneous Cr-based complexes based on low-valence chromium species for ethylene polymerization or oligomerization, such as imido, β-diketiminates and reduced Schiff base [N, O] chelate derivatives, which are far from the character of the Phillips catalyst, will not be considered here [132–137].

Hanmura et al. [122, 123] found two simple chromium cations $Cr(II)OH^+$ and $Cr(III)O^+$ (models **1f** and **2f**) that could dimerize ethylene into 1-butene without using any organometallic cocatalyst, and proposed that they could be treated as simple homogenous cluster models for the Phillips catalyst. Baker and Carrick [111] reported ethylene polymerization over BC (model **3f**), a hexavalent chromate compound bearing two triphenylsilyl ligands, at elevated temperatures ($\geq$130°C)

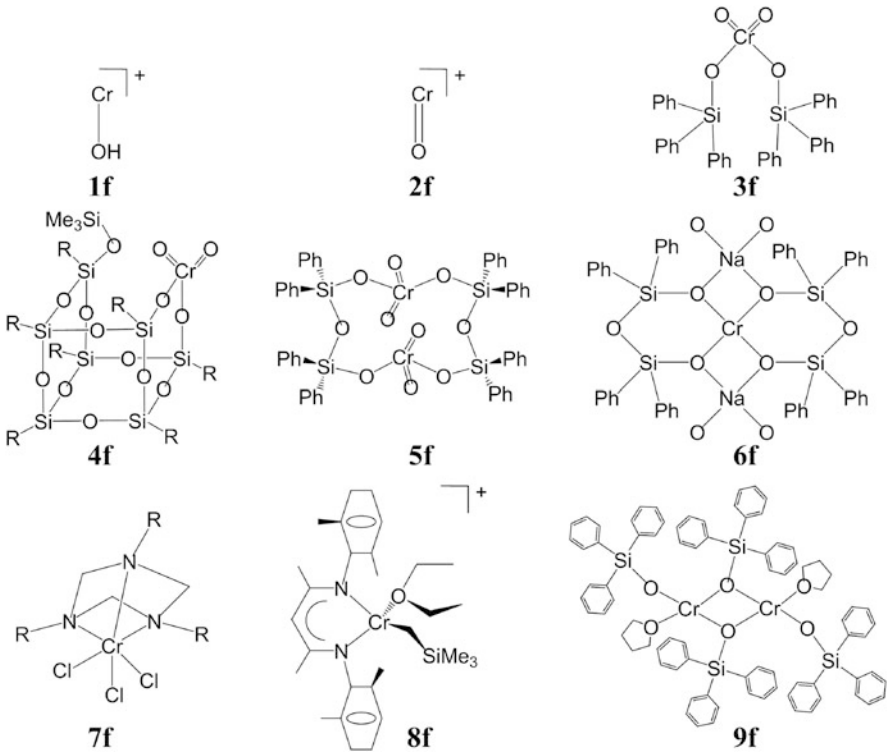

Scheme 13 Homogeneous models reported in the literature for the Phillips Cr/silica catalyst

and ethylene pressures (≥350 atm) in cyclohexane solution without adding any cocatalyst. In our opinion, BC could be taken as a homogeneous model for the Phillips catalyst and should be more extensively studied. A POSS-supported Cr complex $[(c\text{-}C_6H_{11})_7Si_7O_{11}(OSiMe_3)]CrO_2$ (model **4f**) developed by Feher and Blanski seemed to be a more realistic homogeneous model of the Phillips catalyst [124, 125]. Abbenhuis reported a homogeneous 12-membered inorganic heterocycle Cr(VI) model catalyst (model **5f**) that was active for ethylene polymerization [126]. Sullivan and coworkers reported a homogeneous spirocyclic Cr(II) siloxane model catalyst (model **6f**) for ethylene polymerization [127]. This catalyst showed no activity without Al-alkyl cocatalyst and poor activity in the presence of $AlMe_3$ cocatalyst, which was rationalized by the authors as being due to the partial deactivation of this homogeneous divalent model catalyst because of its ultrahigh sensitivity to air and moisture. The homogeneous triazacyclohexane Cr(III) complex (model **7f**) reported by Köhn et al. showed a high ethylene polymerization activity and resembled the Phillips catalyst in many important properties, such as the high dependence of MW on the polymerization temperature and the presence of methyl and vinyl end groups in each PE chain. However, a considerable amount of MAO was needed to activate the catalyst, presenting single-site catalyst characters

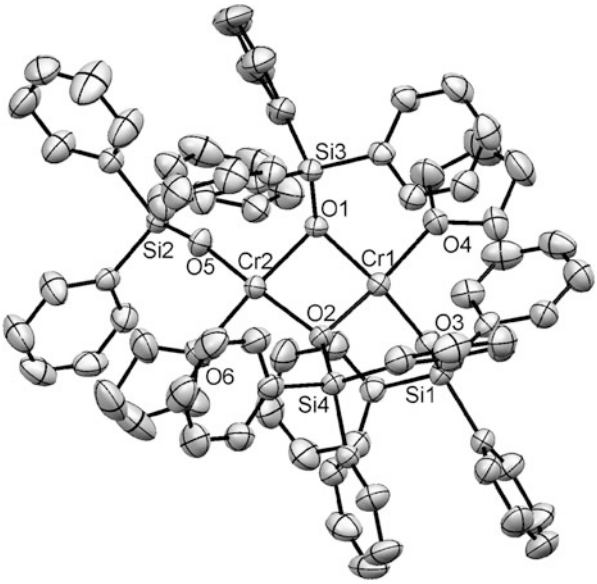

Fig. 20 Crystal structure of $[(Ph_3SiO)Cr \cdot (THF)]_2(\mu\text{-}OSiPh_3)_2$ (**9f**) with ellipsoids at the 50% probability level and hydrogen atoms omitted for clarity. Selected bond distances (Å) and angles (°): Cr(1)–O(3), 1.928(2); Cr(1)–O(2), 2.014(2); Cr(1)–O(1), 2.023(2); Cr(1)–O(4), 2.066(2); Cr(1)–Cr-(2), 2.880(1); O(3)–Cr(1)-O(2), 97.70(8); O(3)–Cr(1)–O(1), 167.00(8); O(2)–Cr(1)–O(1), 81.03(8); O(3)–Cr(1)–O(4), 90.51(8); O(2)–Cr(1)–O(4), 169.47(8); O(1)–Cr(1)–O(4), 92.43(8)

with a MWD of 2–4 for its PE products [128]. Theopold and coworkers [121, 129–131] reported a series of cationic alkyl Cr(III) catalysts for ethylene polymerization and claimed that these catalysts bearing β-diiminates ligand could mimic the hard coordination environment of the silica surface and thus could be taken as models of the Phillips catalyst (model **8f** shows one example). However, these catalysts showed ethylene living polymerization behavior, which was far from the character of the Phillips catalyst. It is still a great challenge to find ideal homogeneous model catalyst systems to mimic the polymerization behaviors of the industrial Phillips catalyst.

Recently, a novel homogeneous triphenylsiloxy complex of chromium(II) model catalyst $[(Ph_3SiO)Cr \cdot (THF)]_2(\mu\text{-}OSiPh_3)_2$ (model **9f**) was successfully synthesized and structurally characterized. Its ethylene polymerization performance was systematically investigated in a comparison with that of BC (model **3f**) [40, 41]. Model **9f** catalyst was prepared by a simple reaction of $CrCl_2$ with TPS and NaH (1:2:2) in THF. Figure 20 shows its crystal structure as a dinuclear Cr(II) complex bearing two bridging siloxy ligands in a tetrahedrally distorted square planar coordination geometry. Another example of such dinuclear Cr(II) complex bearing two bridging siloxo ligands in a similar tetrahedrally distorted square planar coordination geometry is $\{Cr[^{Me_3Ph}NSi(Me_2)N'Si(Me_2)O](THF)\}_2$ [138], which was not considered as a catalyst for ethylene polymerization. Model **9f** was found to be inactive for ethylene polymerization in the absence of Al-alkyl cocatalysts under 20 atm. and RT, even after increasing the temperature to 100°C for 16 h, which might be due to the existence of two strongly coordinated THF molecules within model **9f**. Therefore, an Al-alkyl cocatalyst such as MAO or TiBA was used for the ethylene slurry polymerization over the two model catalysts (**3f** and **9f**).

Table 2 Results of ethylene polymerization/oligomerization runs using BC (**3f**) and [$(Ph_3SiO)Cr \cdot (THF)]_2$ (μ-$OSiPh_3)_2$ (**9f**) with Al-alkyl cocatalysts[a]

Entry[b]	Cocatalyst	Al/Cr	PE (g)	M_w (g mol^{-1})	PDI	T_m (°C)	Activity[c]	Oligomer[d] (g)	Vinyl[e] (mol%)
1	MAO	100	1.20	191,000	2.6	134.7	152	0	–
2[f]	MAO	200	0.81	240,000; 5,400	2.1; 1.1	131.7	103	0	–
3[f]	MAO	500	0.64	254,000; 3,000	2.1; 1.6	129.8	386	2.4	90.3
4[f]	MAO	1,000	0.43	295,000; 1,900	2.8; 1.2	129.2	690	5.0	81.6
5[f]	MAO	1,500	0.55	313,000; 1,500	2.8; 1.4	127.4	413	2.7	84.6
6	TiBA	4	1.58	69,000	3.0	132.8	201	0	–
7	TiBA	10	0.71	158,000	2.4	132.9	90	0	–
8	TiBA	500	Traces[g]	–	–	–	–	–	–
9	MAO	50	1.67	185,000	5.2	134.5	226	0	–
10	MAO	100	1.44	223,000	4.1	122.1	195	0	–
11	MAO	200	0.43	141,000	2.9	120.4	709	4.8	92.6
12	MAO	500	0.31	64,000	2.2	N/A	743	5.2	84.2
13	MAO	1,000	0.34	49,000	2.3	N/A	827	5.8	89.1
14	TiBA	4	0.21	196,000	5.2	135.1	28	0	–
15	TiBA	10	0.16	136,000	4.6	134.4	22	0	–
16	TiBA	500	Traces[g]	–	–	–	–	0	–

[a]Standard conditions: $T = 22°C$, $V = 10$ mL, $P = 20$ atm., catalyst = 10 mg, time = 30 min
[b]Entries 1–8 for BC catalyst, entries 9–16 for $[(Ph_3SiO)Cr \cdot (THF)]_2$ (μ-$OSiPh_3)_2$ catalyst
[c]Activity in g $(mmol_{Cr})^{-1}$ h^{-1} by adding polymerization activity to oligomerization activity
[d]By integration of the NMR olefinic resonances with respect to the Me of the toluene solvent
[e]By integration of the NMR olefinic resonances
[f]Bimodal distribution from GPC analyses
[g]Less than 0.05 g

The ethylene polymerization results are summarized in Tables 2 and 3. Solid PE was obtained by using model **9f** with MAO at low Al/Cr molar ratios (Al/Cr $\leq$ 100) (Table 2, entries 9, 10). With a further increase in Al/Cr molar ratios (Al/Cr $\geq$ 200) (Tables 2 and 3, entries 11–13), liquid oligomers were surprisingly obtained together with a small amount of PE. ^{1}H NMR results revealed liquid oligomers with high contents of terminal vinyl groups (>84%), mostly linear α-olefins, thereby the predominant chain transfer mechanism could be β-H elimination in this model catalyst system. It is shown in Table 2 that the activities of entries 11–13 (average 760 g $mmol_{Cr}^{-1}$ h^{-1}) were much higher than the activities of entries 9 and 10 (average 210.5 g $mmol_{Cr}^{-1}$ h^{-1}). It was very interesting to find that a transformation of ethylene polymerization into ethylene nonselective oligomerization occurred over model **9f** catalyst using MAO as cocatalyst when the Al/Cr ratio was increased from 50 to 1,000. A similar transformation phenomenon was also discovered over BC (model **3f**) combined with MAO as cocatalyst (see entries 1–5 in Tables 2 and 3). The only difference was that the critical point of Al/Cr molar

Table 3 Distributions of ethylene oligomerization products over BC (**3f**) and $[(Ph_3SiO)Cr \cdot (THF)]_2$ (μ-$OSiPh_3)_2$ (**9f**) with Al-alkyl cocatalysts[a]

				Oligomer distribution[d] (%)						
Entry[b]	Cocatalyst	Al/Cr	Oligomer[c] (g)	C_6	C_8	C_{10}	C_{12}	C_{14}	C_{16}	Vinyl[e] (mol%)
3[f]	MAO	500	2.4	12.5	25.7	26.8	18.3	9.5	4.3	90.3
4[f]	MAO	1,000	5.0	9.5	19.2	18.4	25.3	14.6	7.3	81.6
5[f]	MAO	1,500	2.7	10.5	23.5	11.4	26.2	15.1	8.0	84.6
11	MAO	200	4.8	13.5	16.1	21.8	21.5	14.9	7.2	92.6
12	MAO	500	5.2	10.1	35.6	11.5	18.9	11.1	6.2	84.2
13	MAO	1,000	5.8	12.3	31.6	16.1	11.0	9.1	9.0	89.1

[a]Standard conditions: $T = 22°C$, $V = 10$ mL, $P = 20$ atm., catalyst = 10 mg, time = 30 min
[b]Entries 1–8 for BC catalyst, entries 9–16 for $[(Ph_3SiO)Cr \cdot (THF)]_2$ (μ-$OSiPh_3)_2$ catalyst
[c]By integration of the NMR olefinic resonances with respect to the Me of the toluene solvent
[d]By GC-MS, values of C_4 are not given due to volatility, remainder is C_4 and C_{18+}
[e]By integration of the NMR olefinic resonances
[f]Bimodal distribution from GPC analyses

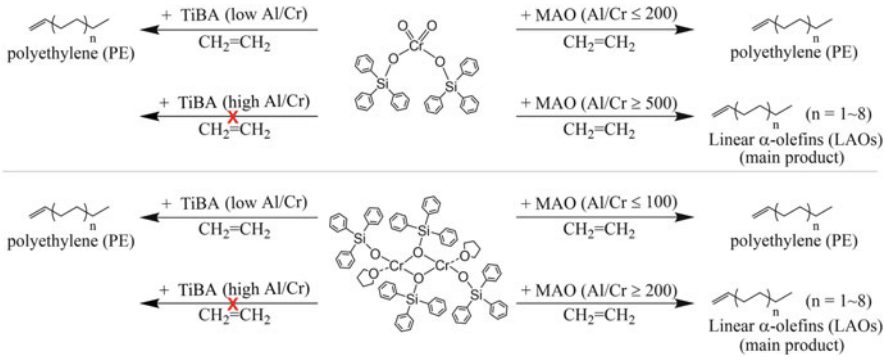

Scheme 14 Transformation of ethylene polymerization to ethylene nonselective oligomerization over BC (**3f**, *upper*) and $[(Ph_3SiO)Cr \cdot (THF)]_2$($\mu$-$OSiPh_3)_2$ (**9f**, *lower*) complexes

ratio for the transformation of model **3f** was much higher than that of model **9f**, which can be rationalized by assuming that reduction of the hexavalent chromate model **3f** into a lower valence state should consume more MAO. It was noteworthy that only a small amount of PE but no liquid oligomer was produced in the case of TiBA as cocatalyst for both model catalysts. Larger amounts of TiBA only completely deactivated the two model catalysts, probably due to its much stronger reducing power than MAO.

The transformation from ethylene polymerization to ethylene nonselective oligomerization over the two model catalysts (**3f** and **9f**) in the presence of Al-alkyl cocatalyst MAO with the increase in Al/Cr molar ratio is shown in Scheme 14. Such interesting transformation phenomenon could not be found using the same catalysts combined with TiBA. Similar polymerization/oligomerization transformation behavior has also been reported recently on Cr-based ethylene trimerization

catalysts by changing the cocatalyst from $[(^{i}Bu)_2Al]_2O$ to MAO [139]. Comprehensive theoretical molecular modeling focusing on such interesting polymerization/oligomerization transformation mechanisms is still in progress.

In order to shed some light on the nature of active sites relating to the transformation between ethylene polymerization and nonselective oligomerization over the two model catalyst systems, several spectroscopic methods including NMR, ESR, and MALDI-TOF MS were applied. For the case of the model **3f**/MAO system, a very characteristic isotropic, hyperfine structure multiplet assigned to a cationic $[Cr(\eta^6\text{-arene})_2]^+$ sandwich complex was observed from the ESR spectrum, indicating that part of the complex was reduced to a $Cr(I)^+$ species, which was coordinated by two molecules of toluene (or arenes from the dissociated Ph_3SiO groups) to yield the cationic $(\eta^6\text{-arene})_2$ complex. Similar ESR results for the same cationic $[Cr(\eta^6\text{-arene})_2]^+$ sandwich species were also obtained in the model **9f**/MAO catalyst system at different Al/Cr molar ratios.

In the ^{29}Si NMR spectrum of the model **9f** catalyst activated by MAO, aluminum species containing the Ph_3SiO group were observed. Thus, the Cr–C bond was likely to be produced by transferring the methyl group from MAO to the chromium center during the activation. Correspondingly, the Ph_3SiO group was transferred from the Cr center to the aluminum of MAO to produce the aluminum species containing a Ph_3SiO group, accompanied by the formation of a cationic $[Cr(\eta^6\text{-arene})_2]^+$ sandwich complex.

The alkyl radical is known to be an important intermediate during the activation reaction between transition metal-based polyolefin catalysts and metal alkyl cocatalysts. However, it is difficult to characterize by spectroscopic methods due to its high reactivity and short lifetime. An investigation to confirm the generation of alkyl radicals during the activation of model **3f** with TiBA by fullerene radical trapping combined with ESR as well as MALDI-TOF MS was performed. A new ESR signal (Fig. 21b) of the multiple addition paramagnetic adducts of butyl radicals to fullerene was successfully observed compared with the ESR signal without fullerene, and the addition of butyl radicals to fullerene was confirmed by MALDI-TOF MS analysis (Fig. 21a). The butyl radical intermediate could be considered to be generated during the reduction and alkylation of BC with TiBA. Similar ethyl and methyl radical formation has been previously reported during the activation reaction in other olefin polymerization catalyst systems [140, 141].

In order to understand the identity (active or inactive) of the cationic $[Cr(\eta^6\text{-arene})_2]^+$ species in model **3f**/TiBA catalyst system, a temperature-dependent ESR experiment (220–350 K) was performed to monitor ethylene polymerization (in the NMR tube). In Fig. 22, it can be seen that the multiplet ($g = 1.995$) of the cationic $[Cr(\eta^6\text{-arene})_2]^+$ species remained unchanged, indicating that this kind of species was not active at these reaction conditions. No other ESR signals were observed during the temperature raising process (220–350 K), although the solid PE had been observed at 290 K. This result indicated that the active species for ethylene polymerization cannot be observed by ESR spectroscopy. Therefore, the valence state of the active species in model **3f**/TiBA catalyst system might be Cr(II), which was always ESR silent. However, Cr(III) cannot be excluded on the basis of the

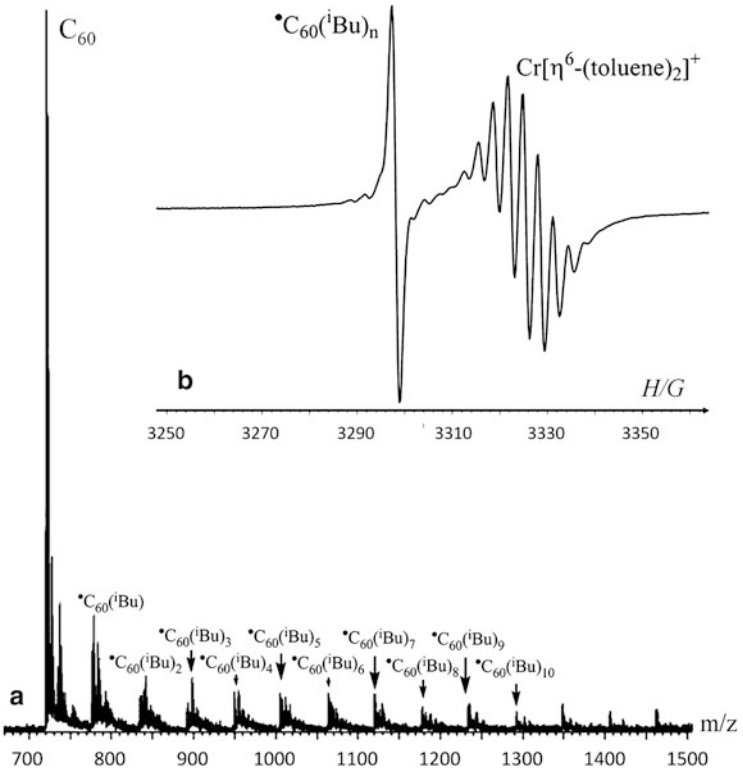

Fig. 21 ESR and MALDI-TOF monitoring of the mixture of BC (**3f**) with fullerene C60 activated by TiBA (Al/Cr = 4): (**a**) MALDI-TOF MS spectrum; (**b**) ESR spectrum at 290 K in toluene

limited experimental results, because it was generally observed by ESR spectroscopy at very low temperatures up to 77 K. Further mechanistic study through combined experimental and theoretical modeling is now still in progress in order to clarify the nature of the active sites and their transformation behavior.

In summary, two homogeneous model catalysts with triphenylsiloxy ligands of chromium(II) and chromium(VI) (models **3f** and **9f**) were systematically studied for ethylene polymerization in the presence of Al-alkyl cocatalyst. Similar transformation phenomenon from ethylene polymerization to nonselective oligomerization was discovered over both model catalysts using MAO as a cocatalyst depending on the Al/Cr molar ratios. A cationic $[Cr(I)(\eta^6\text{-arene})_2]^+$ sandwich complex was observed for both catalyst systems combined with MAO or TiBA and was excluded as being the active site for ethylene polymerization. Further mechanistic investigations on these model catalyst systems as well as their relevance to the Phillips catalyst are still in progress in order to elucidate the mechanisms of such interesting phenomena. The well-defined molecular structure of homogeneous catalysts provide good basis for their investigation with molecular modeling as well as other spectroscopic methods, especially in-situ or operando techniques. The

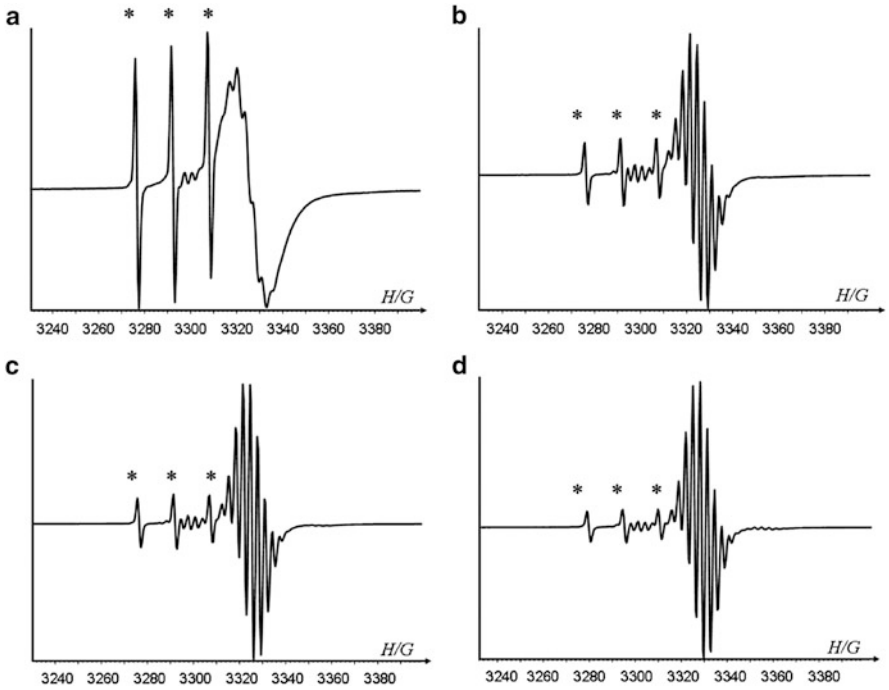

Fig. 22 Monitoring of ethylene polymerization over **3f**/TiBA (Al/Cr = 4) by in-situ ESR spectroscopy (from 220 to 350 K): (**a**) 220 K, (**b**) 270 K, (**c**) 290 K, and (**d**) 350 K. For determination of the *g* factor spectrum recorded with TEMPO ($g = 2.0058$), the three lines of TEMPO are marked with *asterisks*

development and utilization of novel and more realistic homogeneous Phillips catalysts are still great challenges and are expected for further progress in this important field in the near future.

6 Approaches Using Molecular Modeling

Although numerous experiments and spectroscopic characterizations have been conducted on the Phillips catalyst, the precise structure of the active site on the silica surface, reduction of the surface chromate species during the induction period, the formation of the first chromium–carbon bond, and the mechanism for ethylene polymerization still need to be further clarified [11]. In order to achieve more specific information, molecular modeling approaches could provide a useful complement to the experiments and enable us to study these obscure mechanistic problems directly at the atomic and molecular level. In the last decade, very precise mechanistic pictures of the Cr-based polymerization catalysts have been obtained using different theoretical methods, especially through a combination of the experimental findings with theoretical calculations.

6.1 Molecular Models

To understand the behavior of the heterogeneous catalyst, a molecular model must be first built to mimic the active sites anchored on the support. Regarding the Phillips catalyst, the hexavalent chromate species on a silica surface is believed to be reduced to lower valence states, usually Cr(II), resulting in a mononuclear or dinuclear Cr(II) site, which is bound to the silica surface through two oxygen linkages. During the last decade, various molecular models have been built for the active sites of the Phillips catalyst, as graphically shown in Fig. 23.

As early as 2004, we employed hexavalent chromic acid (**1g**) as a simple molecular model for simulating the coordination of ethylene on the pre-reduced monochromate site of the Phillips catalyst [142]. Soon after that, a more realistic silsesquioxane-supported cluster model **2g** was built for theoretical investigation in order to elucidate the effects of silica gel and its surface fluorination on the properties of the Phillips catalyst [143, 144]. Meanwhile, Hanmura et al. [122, 123] found that two simple chromium cations [$Cr(II)OH^+$ and $Cr(III)O^+$, as shown in **1f** and **2f**] could possibly dimerize ethylene into 1-butene without using any organometallic cocatalyst. Because the chromium centers in these two kinds of cations were directly bonded to an oxygen atom, and the Phillips catalyst was composed of chromium supported on silica gel through oxygen linkages, the authors claimed that **1f** and **2f** could be treated as homogenous cluster models for the Phillips catalyst.

A group of cluster models **3g**–**10g** created by Espelid and Børve in a series of systematic DFT investigations on the active sites of the Phillips catalyst are shown in Fig. 23 [120, 145–149]. Clusters **3g**–**6g** were four kinds of mononuclear Cr(II) sites varying in –O–Cr–O– angles. **4g** was a pseudo-tetrahedral cluster. **6g** was a pseudo-octahedral cluster, and the other two clusters were built with different bond angles to represent the heterogeneity of the silica surface. Cluster **3g** was a four-membered chromasiloxane ring with a much higher ring strain and thermodynamically unfavorable formation requiring a heat of 24.6 kcal mol^{-1}. For clusters **4g** and **5g**, the heats of Cr anchoring reaction decreased with the increasing ring size. Compared to the experimental frequencies of 986 ± 46 cm^{-1} for a dehydrated silica-supported chromium oxide catalyst [83], the two computed harmonic Cr=O stretching frequencies were 1,016 and 1,054 cm^{-1} for the cluster **4g**. Furthermore, the computed *d*–*d* transition of $^5A'$-$^5A''$ at a vertical transition energy of 10,400 cm^{-1} also agreed with the experimental observation of *d*–*d* transition in Cr^{2+} ions conducted by Weckhuysen and Wachs [150]. Therefore, the six-membered chromasiloxane ring **4g** was chosen by Espelid and Børve as a key model for a series of DFT studies on the Phillips catalyst. The cluster **6g** with geometry constraint to reserve D_{3h} symmetry was only used in chromium *d*–*d* transition study for comparison with clusters **4g** and **5g** [145]. The hydrogen transfer was also evaluated by means of DFT studies using a large cluster **7g** [147]. Two dinuclear clusters, **8g** and **9g**, represented the silica-supported dichromate species sited on narrow and wide sites [146]. The cluster **10g** was a trivalent

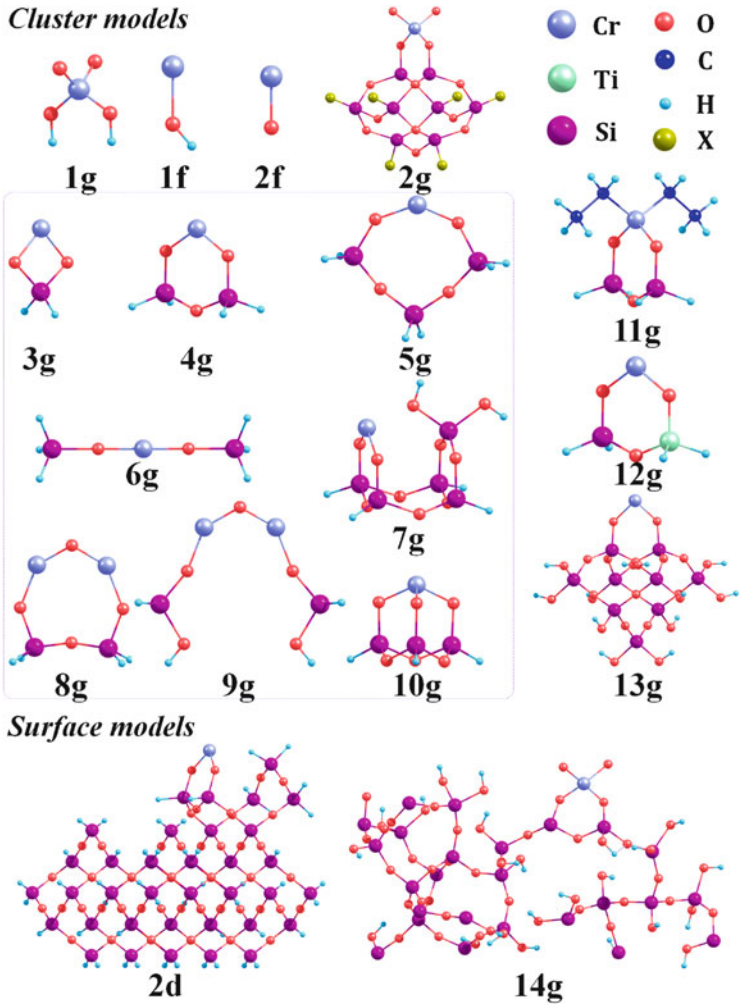

Fig. 23 Various molecular models for the Phillips Cr/silica catalyst that have been reported in the literatures

cluster model for modeling the properties of Cr(III) species on the silica surface of the Phillips catalyst [145].

The six-membered chromasiloxane(II) ring was also adopted and confirmed as a model of active Cr species in many theoretical investigations [54, 71, 146, 151, 152]. In a parallel study, Schmid and Ziegler [153] reported a theoretical calculation on the surface-supported Cr(IV) species (**11g**) for ethylene polymerization. A low barrier for chain propagation was found through a transformation from neutral chromium-alkylidene (Cr-carbene) complex to cationic chromium-alkyl complex in the early stage of ethylene polymerization. Demmelmaier et al. further confirmed the validity of the six-membered chromasiloxane ring **4g** as an ideal model rather

than the larger ring **5g** for the Phillips catalyst through a combination of experiments and theoretical calculations [54, 114]. Recently, Zecchina et al. reported the adsorption of probe molecules (CO, N_2) on the six-membered chromasiloxane(II) ring **4g** and found a good agreement between the calculated vibrational frequencies and the experimental observations by increasing the percentage of Hartree−Fock exchange in the hybrid density functional B3LYP [151]. Alternatively, we [71] studied the effects of Ti-modification of the Phillips catalyst using the modified six-membered chromasiloxane ring **12g**. Combined with the experimental findings, a reasonable mechanistic understanding has been made for the effects of Ti-modification of Phillips catalysts, such as promotion of the polymerization activity, extension of MWD to the low molecular weight region, and improvement of the distribution of inserted comonomers. Moreover, we [154] studied the reduction of the hexavalent chromate species by ethylene during the induction period and unraveled the behavior of Cr(II) active sites (**4g**) with or without coordination of formaldehyde, which was generated through the reduction of chromate species by ethylene. Recently, Tonosaki et al. [152] found that the calculated activation energies for both ethylene insertion and chain transfer were in good agreement using the six-membered chromasiloxane ring **4g** and a slightly larger cluster **13g**. It was pointed out that the intrinsic origin of the broad MWD of the polyethylene produced by Phillips catalysts might be derived from the multiple coordination environments around the active Cr site on the silica surface.

It has long been recognized that the silica support is not an inert component of the catalyst that simply directs polymer particle morphology. The neglect of the real silica surface could introduce some artificial effects and provide an unrealistic environment for the adsorption of monomer on active chromium centers [155]. Nowadays, with the improvement in computing resources and the development of quantum methodologies, full quantum calculations using a large surface-supported model or a periodic model of silica gel surface can be performed. Very recently, we developed a surface model **2d** containing 37 Si atoms through supporting of a six-membered chromasiloxane ring onto a silica surface cutting from the β-cristobalite crystal structure, whose surface was proposed to resemble that of amorphous silica [55]. The results were in good agreement with the experimental spectra as discussed in Sect. 4. Guesmi and Tielens [156] reported an amorphous silica surface slab containing 120 atoms ($Si_{27}O_{54}{\cdot}13H_2O$) that represented the amorphous character of the hydroxylated silica surface involving different silanol types. Through a periodic DFT calculation, a higher stability of mono-oxo and di-oxo chromium species was confirmed in comparison with chromium-hydroxyl species. The main conclusion of their study was a strong support of the six-membered chromasiloxane ring on the amorphous silica surface as a valuable molecular model for the Phillips catalyst. Thus far, all the related theoretical calculations mentioned above agree that the six-membered chromasiloxane ring **4g** could serve as a reasonable cluster model for the Phillips catalyst, but that the effects of the silica support should be considered as well.

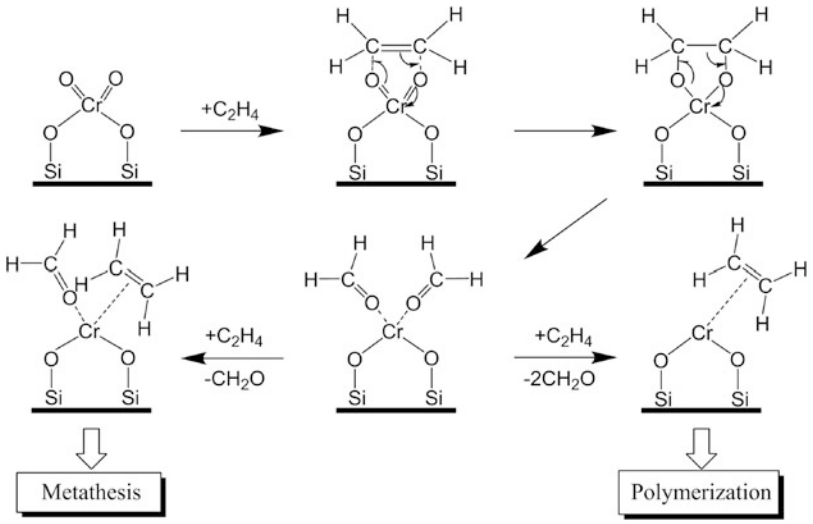

Scheme 15 Plausible monomer reaction mechanism between ethylene and monochromate site on the Phillips Cr/silica catalyst during the induction period of ethylene polymerization

6.2 Reaction Mechanism During the Induction Period

In the absence of organometallic cocatalyst, the hexavalent chromate species on the Phillips catalyst is first reduced to a lower valence state by ethylene monomers. Experimentally, we found that the exposure of ethylene to Phillips catalyst during the induction period at RT led to the reduction of $Cr(VI)O_{x,surf}$ precursors to $Cr(II)O_{x,surf}$ species with the simultaneous formation of formaldehyde and unsaturated hydrocarbon species, such as propylene and butene. The proposed reaction mechanisms during the induction period are shown in Scheme 15 [79].

In order to elucidate the proposed reaction mechanism for the Phillips catalyst during the induction period, we recently performed a theoretical investigation to study the role of formaldehyde [154]. Through extensive calculations on all the possible configurations, three kinds of stationary complexes were located and are referred to as **4g** for a complex without any formaldehyde, **4g-1** for a complex with one adsorbed formaldehyde, and **4g-2** with two adsorbed formaldehydes. The optimized geometries are graphically shown in Fig. 24.

There were three kinds of Cr(II) sites generated after the reduction of hexavalent chromate species by ethylene monomers. **4g** represented the naked cluster model for the Cr(II) site of the Phillips catalyst, providing more room for ethylene coordination to the Cr center. The calculations showed that the initiation reactions between the $Cr(II)O_{x,surf}$ species and ethylene molecules may occur after the desorption of one or two formaldehyde molecules (on **4g-1** or **4g-2**). For **4g-2**, two formaldehyde molecules were adsorbed on the Cr(II) center from the opposite side above the chromasiloxane ring, with formation of two Cr–O bonds of 2.131 Å.

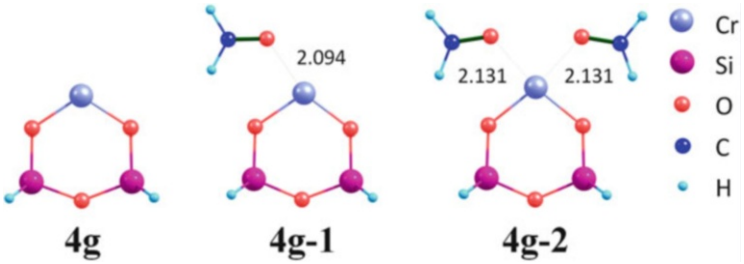

Fig. 24 Stable geometries of Cr(II) catalyst models adsorbed with different numbers of formaldehyde molecules after the reduction of chromate species by ethylene

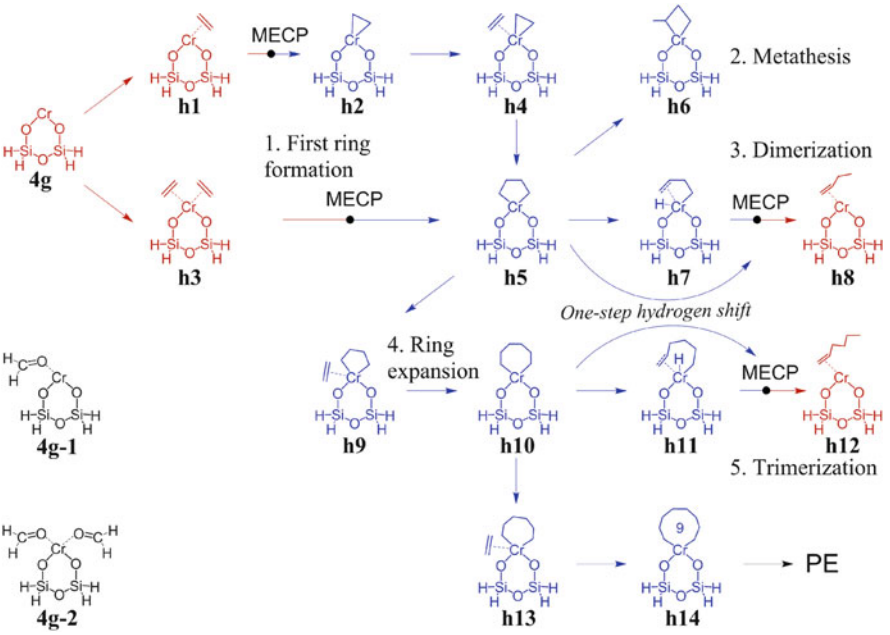

Scheme 16 Reaction pathways over the cluster model **4g** during the induction period

Scheme 16 describes all the possible reaction networks during the induction period, and the naked cluster model **4g** is taken as an example.

The electronic spin state of a transition metal species may have a dramatic effect on the catalytic reactivity. Cr-catalyzed reactions often show a two-state manner, in which the spin crossing plays a vital role in determining the behavior of the catalyst [157–159]. For the reaction initiated on **4g**, a spin crossover from quintet to triplet state occurred during the formation of chromacyclopentane from the Cr(II) complex, which dramatically lowered the activation energy barrier from 42.4 kcal mol^{-1} on a single quintet surface to 23.7 kcal mol^{-1} on a triplet surface through a spin-flipping reaction via a minimum energy crossing point

(MECP), as shown in Scheme 17, reaction 1. The following reaction may occur from the chromacyclopentane species **h5** on the triplet surface to generate a methyl-chromacyclobutane species **h6** through an intramolecular 2,1-hydrogen shift, which would lead to a metathesis reaction to produce propylene and butene molecules, as observed experimentally [79]. However, the hydrogen transfer was prohibited by a much higher energy barrier of 57.2 kcal mol^{-1} without formaldehyde adsorption, as shown in Scheme 17, reaction 2. Alternatively, the reaction from **h5** to a dimerization product 1-butene was found to be finished in a two-step manner via a Cr-hydride intermediate **h7** with an energy barrier of 39.4 kcal mol^{-1}. The reaction crossover to the quintet surface before the second triplet barrier through another MECP and 1-butene was finally released on the quintet surface, as shown in Scheme 17, reaction 3. For the ring expansion step, ethylene molecule may be directly inserted into the Cr–C bond of **h5**, generating a chromacycloheptane structure **h10** on the triplet surface with an insertion barrier of 26.9 kcal mol^{-1}, as shown in Scheme 17, reaction 4. In contrast to **h5**, the ring opening of **h10** took place in a one-step manner assisted by a direct β-H agnostic interaction. The trimerization product 1-hexene was also released on the quintet surface with a barrier of 28.0 kcal mol^{-1} and the corresponding spin crossing took place in the product channel, as shown in Scheme 17, reaction 5. The further ring expansion from chromacycloheptane **h10** was prohibited because ethylene coordination complex could not be located for **h10** due to steric hindrance.

The calculated activation barriers over models **4g**, **4g-1**, and **4g-2** for all the typical reactions (similar to reactions 1–5 in Scheme 17) during the induction period are summarized in Table 4. After a complete desorption of the formaldehyde molecules, the first initiation reaction occurred on **4g** via a MECP to generate a chromacyclopentane species on the triplet surface. The following ring expansion gave a chromacycloheptane species and a subsequent one-step reductive elimination yielded 1-hexene on the quintet surface through another MECP. On the site **4g-1**, the ring expansion step was forbidden because a third ethylene molecule could not be adsorbed on the chromacyclopentane species with one formaldehyde coordinated on the Cr center. Therefore, the reaction of ethylene trimerization on model **4g-1** was absent. Although the dimerization on model **4g-1** was likely to take place with an energy barrier of 35.5 kcal mol^{-1}, a metathesis reaction was still possible on site **4g-1** to produce short olefins. There was no reaction initiated by **4g-2** because the chromium site was completely shielded by the two coordinated formaldehyde molecules.

Table 4 also summarizes the calculated activation barriers of all the typical reactions (in Scheme 17) during the induction period over catalyst models similar to **4g**, **4g-1**, and **4g-2** except that both Si atoms within each model were fully fluorinated. Fluorination of the silica support for the F-modified Phillips catalyst showed negligible influence on ethylene dimerization to 1-butene and metathesis to propylene [160]. However, the energy barrier was increased significantly in reaction 5 of Scheme 17, in which 1-hexene was formed from the chromacycloheptane species through a one-step intramolecular hydrogen shift. Fluorination showed a positive effect on ring expansion in reaction 4 of Scheme 17.

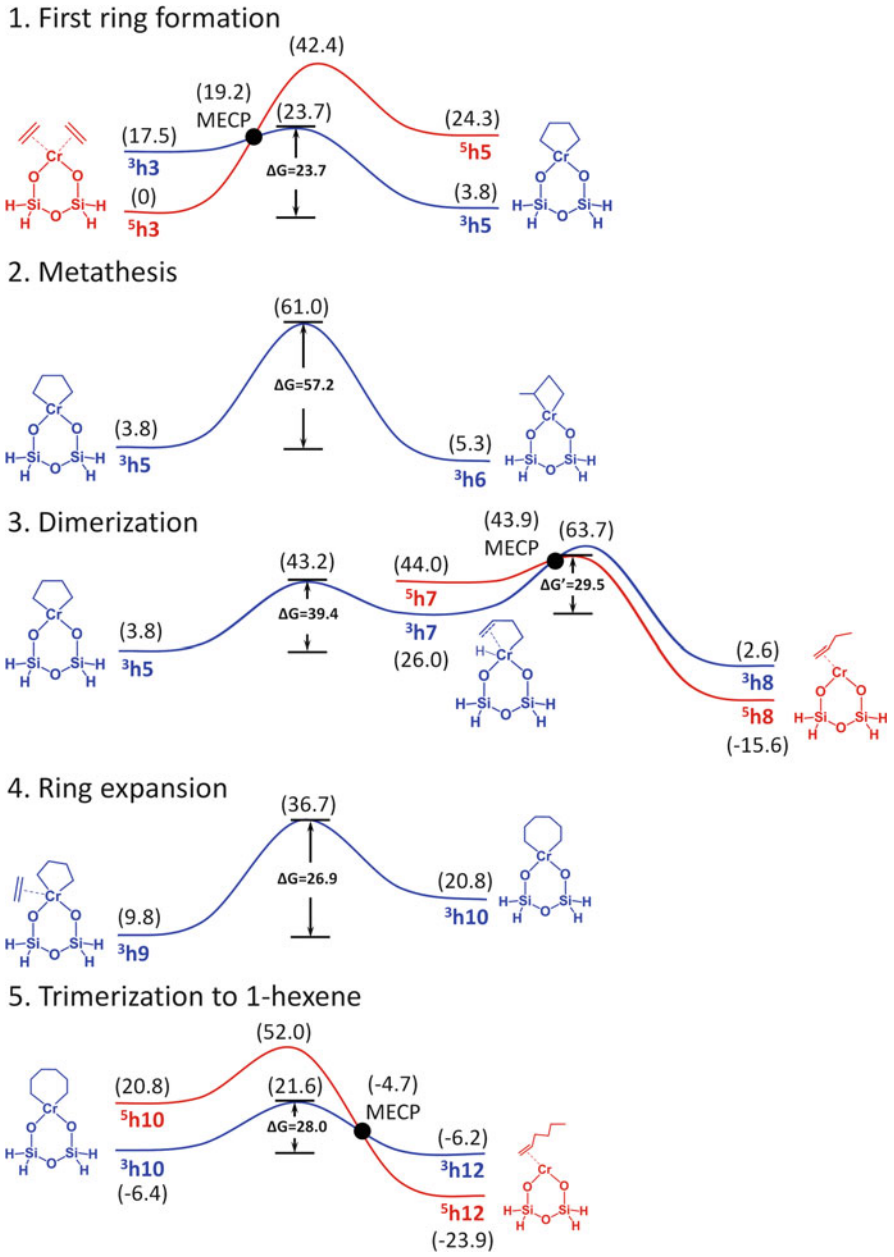

Scheme 17 Gibbs free energy profiles of reactions *1–5* over the cluster model **4g** without adsorbing formaldehyde. The triplet (^3h) and quintet (^5h) energy profiles are depicted. Energies are in kcal mol^{-1}

Table 4 Energy barriers on the proposed reaction pathways over catalyst models coordinated with different numbers of formaldehyde molecules considering spin crossing

	Energy barrier (kcal mol^{-1})					
	Without fluorination[a]			With fluorination[b]		
Reaction	$n_{HCHO} = 0$	$n_{HCHO} = 1$	$n_{HCHO} = 2$	$n_{HCHO} = 0$	$n_{HCHO} = 1$	$n_{HCHO} = 2$
First ring formation	23.7	27.4	–	27.5	29.3	–
Metathesis	57.2	46.7	–	58.4	43.0	–
Dimerization	39.4	35.5	–	46.6	34.5	–
Ring expansion	26.9	–	–	21.5	–	–
Trimerization to 1-hexene	28.0	–	–	38.2	–	–

[a]Over catalyst models **4g**, **4g-1**, and **4g-2**
[b]Over catalyst models similar to **4g**, **4g-1**, and **4g-2** except that both Si atoms within each model were fully fluorinated

6.3 *Polymerization Mechanisms and the First Cr–C Bond Formation*

Phillips catalysts initiating ethylene polymerization without using any organometallic cocatalyst brings us a long standing question: how is the first polyethylene chain initiated on the naked chromium site? That is to say, the initiation mechanism of ethylene polymerization in terms of the formation of the first polymer chain over the active site on a Phillips catalyst is the key problem awaiting elucidation. In the literature, three typical mechanisms, as previously shown in Scheme 2, have been proposed for ethylene polymerization over a Phillips catalyst: (1) the formation of an acyclic Cr–C or Cr–H bond followed by chain propagation through the classic Cossee–Arlman mechanism; (2) the formation of Cr=C (Cr-carbene) bond followed by chain propagation through the Green–Rooney mechanism; and (3) the formation of metallacycle in which both ends of the alkyl group are attached to the chromium site, followed by chain propagation through the metallacycle mechanism.

Espelid and Børve [120] first studied different routes of initiation and chain propagation mechanisms for ethylene polymerization over the Phillips catalyst using the cluster models **3g–10g**, and the six-membered chromasiloxane ring **4g** was regarded as one of the most plausible active Cr species. The potential catalytic activities of monomeric and dimeric chromium species on the silica surface were also evaluated [146, 147]. Starting from a Cr-cyclopropane, Espelid and Børve compared three different initiation mechanisms including the formation of the acyclic ethenylhydridochromium species, the ethylidenechromium species, and the cyclic chromacyclopentane species [120]. The calculations showed that initiation through a direct Cr–carbene formation could be safely excluded, while a metallacycle pathway exhibited a much lower energy barrier. Meanwhile, Schmid and Ziegler [153] found that a cationic Cr–C species could be generated by protonation of the Cr=C (Cr-carbene), which showed a lower energy barrier for chain propagation compared with that through Cr-carbene propagation. The absence of

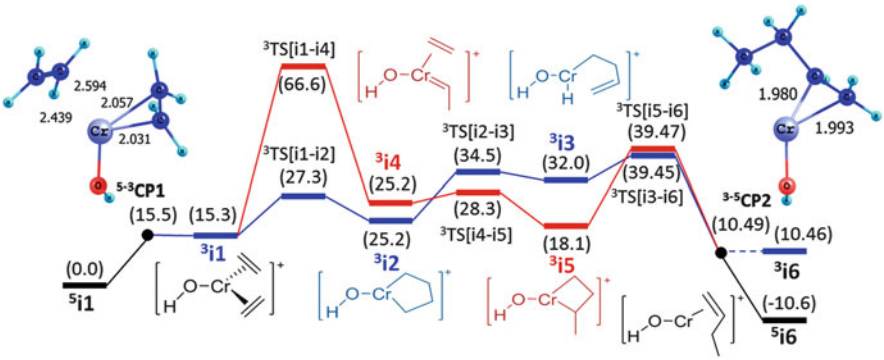

Fig. 25 Potential energy surfaces for the most feasible two-state reaction pathways for ethylene dimerization catalyzed by $Cr(II)OH^+$ (**1f**), via either a Cr-carbene mechanism or a metallacycle mechanism determined at the M06 level of theory. Also shown are the crossing points optimized at CASSCF level. The triplet metallacycle reaction pathway is depicted in *blue*, and the triplet Cr-carbene reaction pathway is shown in *dark red*. The quintet parts are in *black*. Energies are in kcal mol^{-1} and relative to ^{5}i1. Bond lengths are in angstroms. Angles are in degrees

internal C=C bonds in the copolymer produced by copolymerization of ethylene and cyclopentene over the Phillips catalyst also suggested the transformation of Cr=C into Cr–C species as polymerization active sites during the polymerization stage, as confirmed experimentally [95]. Espelid and Børve suggested that the adjacent hydroxyl group might be responsible for the formation of a Cossee-type active site. However, this proposal is questioned due to the fact that Phillips catalyst calcined at higher temperature with much less surface residual hydroxyl groups usually shows higher activity than that calcined at lower temperature. The metallacyclic mechanism through a chromacyclopentane species was supported by strong experimental evidence concerning the intermediacy of large metallacycles in polyethylene chain growth, resulting in the selective trimerization of ethylene to 1-hexene [161]. It could be concluded that the metallacycle mechanism is most probably responsible for the initiation of ethylene polymerization, especially for the formation of the first polymer chain on each active site on the Phillips catalyst.

In the above-mentioned theoretical studies of the initiation mechanism for Phillips catalysts, the spin state of the chromium center, which might play a very important role in the formation of the first chromium–carbon chain, was not considered. As discussed in Sect. 6.2, although formation of the chromacyclopentane species as the key intermediate of the metallacyclic mechanism is prohibited by the much higher energy barrier on a single quintet surface, a transition of the reaction to the adjacent triplet surface through an MECP could lower the energy barrier dramatically. Our recent work [162] proved that ethylene dimerization over **1f** model showed a two-state metallacyclic reaction pathway with the formation of chromacyclopentane as the rate-determining step. Figure 25 shows the energy surfaces for the ethylene dimerization together with two optimized geometries of the spin crossing points. In the first crossing point $^{5\text{-}3}$CP1, the Cr–C bonds are already formed between the chromium center and one of the coordinated

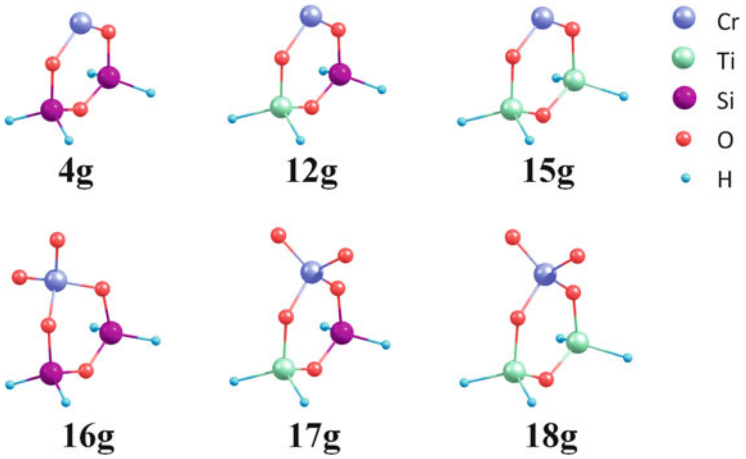

Fig. 26 Models for Cr(VI) sites (**16g**, **17g**, **18g** for Ti:Cr = 0:1, 1:1, 2:1, respectively) and Cr(II) sites (**4g**, **12g**, **15g** for Ti:Cr = 0:1, 1:1, 2:1, respectively) for the Phillips catalyst

ethylene molecules, with two Cr–C bonds of 2.057 and 2.031 Å. After the first spin-flipping to the triplet surface, the metallacycle reaction pathway was found to be more favorable than the Cr-carbene reaction pathway. 1-Butene was formed from the chromacyclopentane by a two-step reductive elimination pathway through a chromium(IV) hydride intermediate. Therefore, the initiation reaction of the ethylene polymerization could not proceed on a single quintet surface, but a spin-flipping to an adjacent triplet surface facilitated the formation of the first Cr–C bond at the crossing point of the two adjacent potential energy surfaces.

6.4 Polymerization Mechanisms for the Ti-Modified Phillips Catalyst

As an important industrial catalyst, the Ti-modified Phillips catalyst is widely used in ethylene polymerization. Recently, the mechanism of ethylene polymerization by the Ti-modified Phillips catalyst has been studied theoretically and experimentally [71]. In the DFT calculations, six mononuclear chromium cluster models including three hexavalent chromate sites (**16g**, **17g**, and **18g**) and the corresponding divalent chromium sites (**4g**, **12g**, and **15g**) were employed to mimic various Ti-modification environments on the surface of the Phillips catalyst, as shown in Fig. 26. Among these cluster models, **16g/4g** represented Cr(VI)/Cr(II) sites without Ti-modification. In **17g/12g** and **18g/15g**, the Ti/Cr atomic ratio was set to 1:1 and 2:1, respectively.

For the Ti-modified Phillips catalyst, the inclusion of small amounts of titanium on the catalyst has a promotional effect both on polymerization activity and the

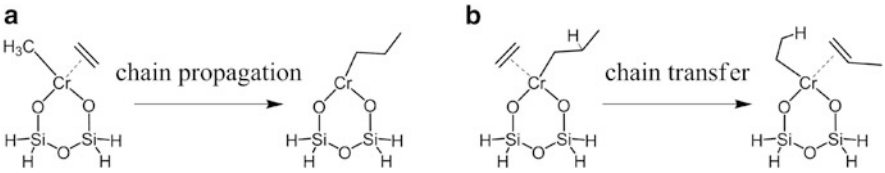

Scheme 18 (**a**) Chain propagation through classical Cossee–Arlman mechanism, (**b**) Chain transfer by β-H elimination to monomer

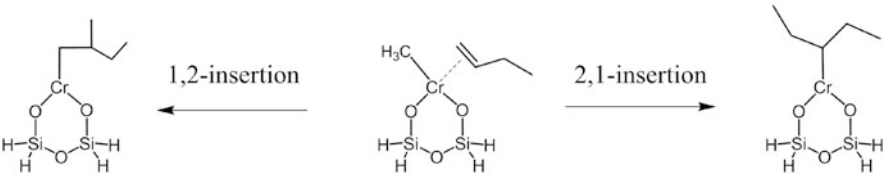

Scheme 19 Regiospecific insertion of 1-butene as comonomer in 1,2-orientation and 2,1-orientation for the Phillips catalyst

Table 5 Energy barriers[a] for chain initiation, chain propagation, and chain transfer reactions on various models of the Phillips catalyst

	Chain propagation[b]			Chain transfer[c]			Δ[d]		
Model	C_2H_4	1-C_4H_8	1-C_6H_{12}	C_2H_4	1-C_4H_8	1-C_6H_{12}	C_2H_4	1-C_4H_8	1-C_6H_{12}
Ti:Cr = 0:1	19.2	21.7	21.8	25.9	26.1	24.3	6.7	4.4	2.5
Ti:Cr = 1:1	18.4	20.2	21.2	24.7	23.5	23.3	6.3	3.3	2.1
Ti:Cr = 2:1	17.7	19.6	20.3	24.1	21.7	22.1	6.4	2.1	1.8

[a]Energy barrier is given in kcal mol^{-1}
[b]Based on primary 1,2-insertion
[c]Based on β-H elimination to monomer after 1,2-insertion of the corresponding monomer or comonomer
[d]Energy barrier differences between ethylene insertion of chain propagation and chain transfer steps, in kcal mol^{-1}

chain transfer rate. The polymerization activity is primarily determined by the feasibility of the chain propagation reaction. We considered chain propagation through the classical Cossee–Arlman mechanism through alkylated trivalent Cr(III)-alkyl active sites, as depicted in Schemes 18 and 19. The energy barriers for the chain propagation and chain transfer are listed in Table 5. The calculations showed that the Cr active sites in Ti-modified models exhibited an increased electron deficiency, and the corresponding energy barriers of the first ethylene insertion were 19.2, 18.4, and 17.7 kcal mol^{-1} for cluster models **4g**, **12g**, and **15g**, respectively. This indicated that Ti-promotional effects could enhance the polymerization activity of the Phillips catalyst. The MW and MWD of the polyethylene are known to be determined by the relative rate between chain propagation and chain transfer. β-H elimination to monomer was believed to be the predominating chain transfer mode for Phillips catalysts (reaction b in Scheme 18).

Table 6 Energy barriers[a] through different regiospecific insertion modes with comonomers in terms of regioselectivity on various models of the Phillips catalyst

Models	Insertion modes	1-Hexene	Δ^b	1-Butene	Δ^b
Ti:Cr = 0:1	1,2-insertion	21.8	1.9	21.7	2.2
	2,1-insertion	23.7		23.9	
Ti:Cr = 1:1	1,2-insertion	21.2	1.2	20.2	1.2
	2,1-insertion	22.4		21.4	
Ti:Cr = 2:1	1,2-insertion	20.3	1.8	19.6	1.8
	2,1-insertion	22.1		21.4	

[a]Energy barriers are given in kcal mol^{-1}
[b]Energy barrier difference between 2,1-insertion and 1,2-insertion, in kcal mol^{-1}

As can be seen from Table 5, the chain transfer rate was enhanced more than the chain propagation rate after Ti-modification. Consequently, Ti-modification could result in an increased in the low MW fraction of polyethylene, and thus the MWD was broadened to the lower MW region.

Copolymerization with α-olefins over a Phillips catalyst is a key method for controlling the density and microstructures of the polyethylene products in industrial processes. Table 5 also listed the energy barriers for the primary 1,2-insertion of 1-butene and 1-hexene, and the subsequent chain transfer by β-H elimination for all the three kinds of Ti-modified models. The calculated energy barriers showed that Ti-modification could also promote the activity for ethylene copolymerization with α-olefins. The energy differences between comonomer insertion and chain transfer can lead to a conclusion on the effect of Ti-modification on the distribution of the inserted comonomers in polyethylene chains. As listed in Table 5, the difference between energy barriers for chain propagation and for chain transfer decreased for model sites **4g**, **12g**, and **15g**. Therefore, it was reasonable to conclude that Ti-modified catalyst was likely to make low MW polyethylene with much less comonomer insertion because the inserted comonomer mainly led to a chain transfer reaction and left the inserted comonomer at the chain end. As a result, the increased chain termination by comonomer resulted in less SCBs in the low MW fraction and higher density of the polyethylene product for the Ti-modified Phillips catalyst.

For traditional heterogeneous olefin polymerization catalysts such as Ziegler–Natta and Phillips catalysts, the regioselectivity usually prefers 1,2-insertion (primary insertion) of α-olefins compared with 2,1-insertion (secondary insertion) due to obvious steric hindrance in the second insertion mode. The effect of Ti-modification of the Phillips catalyst on the energy barriers of 1,2-insertion and 2,1-insertion of α-olefins was calculated by a DFT method based on the three catalyst models. The regiospecific insertion of 1-butene is shown in Scheme 19. All the energy barriers of the two insertion modes for both 1-butene and 1-hexene on the three catalyst models are listed in Table 6. The calculated energy barriers for 1,2-insertion were lower than for the corresponding 2,1-insertion, indicating the dominant nature of 1,2-insertion in the copolymerization by Phillips catalyst. Ti-modification lowered the energy barriers for both

1,2-insertion and 2,1-insertion of comonomer, which was consistent with the Ti-promotional effect on activity. Moreover, the energy barriers for 2,1-insertion of comonomer decreased more than those for 1,2-insertion. The calculated results indicated that 2,1-insertion of comonomer might be enhanced by Ti-modification of the Phillips catalyst, which was consistent with McDaniel's suggestion of the plausible enhancement of the 2,1-insertion versus 1,2-insertion during ethylene copolymerization with α-olefin on Ti-modified Phillips catalyst [4].

Up to now, most of the theoretical studies on the Phillips catalyst have been conducted using cluster models built for modeling the active species on the silica surface. Through a combination of molecular modeling and experimental spectroscopy, a general agreement has been achieved on the cluster model. The reactions during the induction period, the initiation mechanisms for ethylene polymerization, and the effects of Ti-modification and fluorination of the silica surface were elucidated through DFT calculations together with comparison with the experimental results. Because the real Phillips catalyst contains an amorphous silica support with much higher heterogeneity, the cluster model may neglect the effect of the silica surface, which is believed to be very important for understanding the active sites of the Phillips catalyst. Thankfully, with the fast growth in computing power and the in-depth development of quantum packages, one can perform theoretical calculations on the Phillips catalyst using a more realistic silica-supported model, which opens a new era in modeling of the Phillips catalyst. Although the theoretical calculations using a silica-supported surface model are very limited at present, there are bright prospects for the realistic molecular modeling of the Phillips catalyst. It is always crucial to do molecular modeling with a comparison to experiments. The combination of experiments and theoretical calculations results in more interesting findings, which probably could not be obtained by means of a single technique. For the theoretical work in the study of Phillips catalysts, a more realistic mechanistic description could probably be achieved through a full ab initio quantum molecular dynamics simulation using a surface-supported model [163]. Believe it or not, molecular modeling will be playing a more and more important role in the catalytic field. Theoretical calculation is a powerful tool for interpretation of experimental results and in guidance of catalyst development through state-of-the-art catalyst design.

7 Catalyst Innovations Through Modification of the Phillips Catalyst

Parallel to the progress in the basic understanding on the nature of active sites and polymerization mechanisms, several modified Phillips catalysts with better performance and improvements in the structures and properties of PE products through surface modification of the silica support and catalyst with Ti, F, Al, or B compounds have been successfully developed and commercially applied during

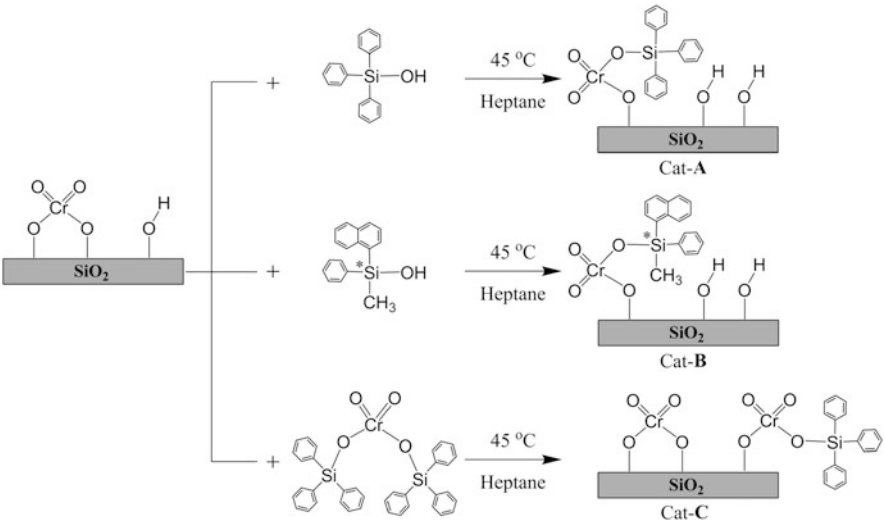

Scheme 20 Procedures for preparation of novel catalysts (Cat-**A**, Cat-**B** and Cat-**C**) by modification of the Phillips catalyst

the past 60 years [2–4, 11]. It is obvious that the catalyst innovations are very limited. During the past few years, we have successfully developed several novel Cr-based Phillips-type catalysts through simple surface modifications of the traditional Phillips catalyst, as shown in Scheme 20. Two basic procedures were taken into consideration for the innovations. One procedure was modification of surface chromate species using various types of organic silanols (to give Cat-**A** and Cat-**B**). The other procedure was modification of surface residual hydroxyl groups using various types of organometallic compounds, which could be chemically anchored on the catalyst surface and provide extra active sites for ethylene polymerization (giving Cat-**C**).

7.1 Modification of Surface Chromate Species on the Phillips Catalyst

Modification of surface chromate species on the Phillips catalyst using various types of organic silanols could be a general procedure for synthesis of various novel Cr-based polymerization catalysts. The reactions are shown in Scheme 20 for Cat-**A** and Cat-**B**. The first example of Cat-**A** was reported by Cann and coworkers through the reaction between TPS and a Phillips catalyst with the original purpose of transformation of the Phillips catalyst into UCC S-2 catalyst in order to avoid the use of toxic and expensive BC [27]. In our opinion, the Cat-**A** was similar to the UCC S-2 catalyst but differed with respect to the simultaneously formed surface

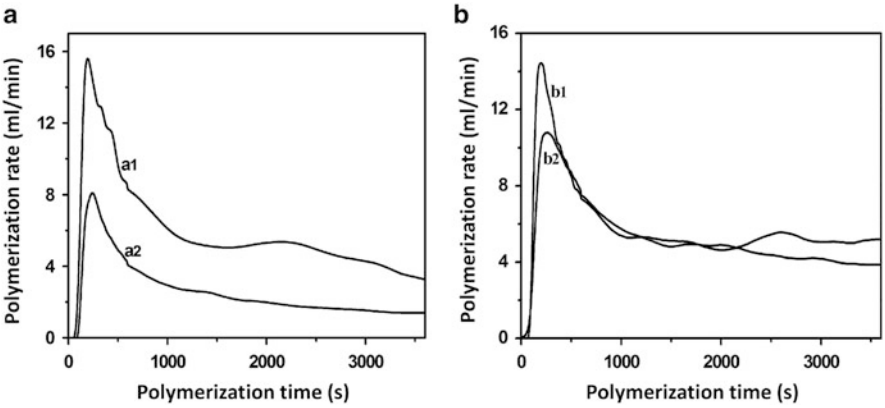

Fig. 27 Ethylene polymerization kinetic curves of catalysts activated by TEA cocatalyst during slurry polymerization: (**a**) Phillips catalyst (*a1*) and Cat-**A**/1.5 catalyst (*a2*) (Al/Cr molar ratio = 20.0); (**b**) Cat-**A**/1.5 catalyst (*b1*) and S-2 catalyst (*b2*) (Al/Cr molar ratio = 15.0). Polymerization conditions: catalyst amount, 160 mg; polymerization temperature, 90°C; ethylene pressure, 0.15 MPa; solvent, heptane, 70 mL

hydroxyl group very close to the active Cr site. Therefore, a detailed study on the synthesis of Cat-**A** was further carried out by a combination of experimental and theoretical methods [28]. The results showed that the molar ratio of TPS to Cr was important for the catalyst structure and the polymerization performance as well as the structure and properties of the PE products. An increase in TPS amount seemed to accelerate the loss of surface hexavalent chromium species from the support, suggesting that the conversion from Phillips catalyst to S-2 catalyst by the addition of TPS could not occur completely. The optimal molar ratio of TPS to Cr was 1.5 for the preparation of Cat-**A** (named Cat-**A**/1.5). Ethylene slurry polymerization kinetics activated by Al-alkyl cocatalyst during polymerization over the Phillips, Cat-**A**/1.5 and S-2 catalysts are shown in Fig. 27. All three catalysts showed hybrid-type polymerization kinetics (as shown in Fig. 10a). The polymerization activity of Cat-**A**/1.5 catalyst was much lower than that of the Phillips catalyst. For Cat-**A**/1.5 and S-2 catalysts, the kinetic curves for the two catalysts with the same cocatalyst were similar, and only a slightly higher activity of Cat-**A**/1.5 catalyst than that of S-2 catalyst was obtained, as shown in Fig. 27b. The significant decline in polymerization activity from Phillips catalyst to Cat-**A**/1.5 catalyst might be due to the different coordination environment of the Cr active site, the release of surface strain by opening of the Si–O–Cr–O–Si–O ring, and the appearance of a simultaneously formed hydroxyl group next to the Cr center after TPS modification. The theoretical studies by DFT showed that coordination of the hydroxyl to the reduced Cr site were favorable for ethylene polymerization and might be the reason for its higher polymerization activity than the S-2 catalyst. But, further modification of the hydroxyl group on the Cat-**A**/1.5 catalyst by a series of alkyl chlorosilane compounds showed that the effect of an electron-withdrawing group was limited at a certain distance away from the Cr active site.

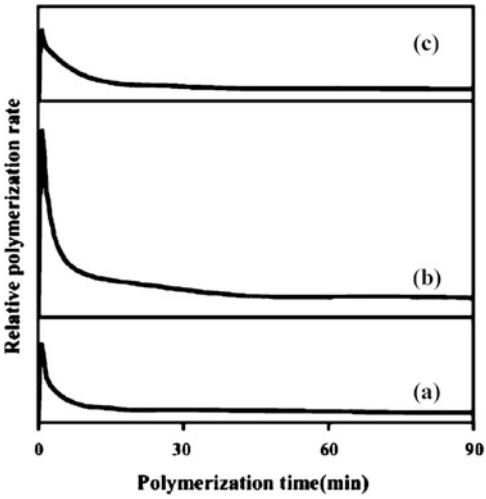

Fig. 28 Polymerization kinetic curves of catalysts activated by TEA cocatalyst during the slurry polymerization process: (**a**) Cat-**B**/600-S catalyst with 15.0 Al/Cr molar ratio; (**b**) Cat-**B**/600-S and (**c**) Cat-**B**/600-4S catalysts with 22.5 Al/Cr molar ratio. Polymerization conditions: catalyst amount, 100 mg; polymerization temperature, 60°C; ethylene pressure, 0.13 MPa; solvent, heptane, 20 mL; cocatalyst TEA in heptane, 1 M

By similar method, a new chiral organo-silanol species, methyl (1-naphthyl) phenylsilanol has been successfully introduced onto Phillips catalyst PC600 calcined at 600°C in order to synthesize a novel Phillips-type catalyst (Cat-**B**) [164]. There was a decrease in BE values of the Cr 2p core level in the XPS spectra for the catalyst samples with increasing molar ratios of chiral ligand to Cr from chiral ligand-free 1:0 (PC600), 1:1 (Cat-**B**/600-S) to 1:4 (Cat-**B**/600-4S). This could be explained by the electron donation effect of chiral organo-siloxane ligand and the formation of hydroxyl groups after anchoring of the ligand, which can release the strong surface tension on the silica support formed during high temperature calcination. The ethylene polymerization kinetic curves of Cat-**B**/600-S and Cat-**B**/600-4S activated by Al-alkyl cocatalyst with different Al/Cr molar ratios are shown in Fig. 28 and illustrate the hybrid-type kinetic behavior (as shown in Fig. 10a). At the same time, it was very interesting to find relative amounts of methyl and *n*-butyl branches in these ethylene homopolymers, which were considered to be generated from the metathesis site (as shown in Scheme 8). Therefore, this catalyst was similar to a Phillips catalyst in the transformation of ethylene metathesis sites into polymerization sites during the early stage of ethylene polymerization.

7.2 Modification of Surface Residual Hydroxyl Groups on the Phillips Catalyst

Another general procedure for synthesis of novel Cr-based ethylene polymerization catalysts could be through modification of surface residual hydroxyl groups on a Phillips catalyst using various types of organometallic compounds, which could be chemically anchored on the catalyst surface and provide extra active sites for

ethylene polymerization. Recently, a novel hybrid catalyst presented the merits of two important chromium-based catalysts, namely inorganic Phillips and organic S-2 catalysts. It was successfully prepared, and named Cat-**C**, as shown in Scheme 20 [165]. This method utilized the surface residual hydroxyl groups on a Phillips catalyst and anchored the BC complex under mild conditions. Thus, the surface residual hydroxyl group population could greatly influence the degree of supported BC, as well as the polymerization activity and the structure of the polymers. For a series of catalysts with total 0.5 wt% Cr loading prepared with increasing Cr_{BC} loading of 20% (Cat-**C1**), 50% (Cat-**C2**), and 80% (Cat-**C3**), the thermogravimetric peaks from the catalysts after the reaction of HMDS and the residual hydroxyl groups became more and more apparent, suggesting that the residual surface hydroxyl group population increases with the increasing relative addition amount of Cr_{BC}. The ethylene polymerization kinetic curves over the Cat-**C** catalysts activated by Al-alkyl cocatalyst during polymerization were insensitive to the type of cocatalyst (TEA, TiBA, and MAO) and similar to the kinetic type shown in Fig. 10a, implying the existence of two kinds of active sites. As can be seen from Table 7, Cat-**C2** catalyst with 50 wt% Cr_{BC} relative loading showed well-balanced properties of ethylene homopolymerization and ethylene/1-hexene copolymerization in terms of activities and MW of the polymers. Its copolymers had a higher average MW and broader MWD than those obtained from the Phillips catalyst, as well as higher 1-hexene incorporation than those obtained from Phillips and S-2 catalysts.

In order to investigate the SCB distribution of the ethylene/1-hexene copolymers made by Cat-**C**, TREF combined with SSA was applied according to a method established by us previously [166, 167]. The SCBs contents for each PE fraction from TREF were qualitatively obtained from the lamella thickness measured by SSA. The lamella thickness distribution of the fractions obtained by TREF for each copolymer is shown in Fig. 29. Comparison of the lamella thickness distribution of the copolymers in the highest temperature fraction (124°C fraction, corresponding to the highest MW part of the copolymer) suggested that the lamella thickness of copolymers obtained from Phillips and Cat-**C2** catalysts were similar and slightly thinner than those obtained from S-2 catalyst. This result indicated that the corresponding relative SCB content of copolymers in the highest MW part obtained from Phillips and Cat-**C2** catalysts were slightly higher than that obtained from S-2 catalyst. In the lowest temperature fraction (40°C fraction, corresponding to the lowest MW part), the copolymers obtained from the Phillips catalyst showed much thinner lamella thickness (corresponding to much higher relative SCB content) than those obtained from S-2 and Cat-**C2** catalysts. The copolymer obtained from Cat-**C2** catalyst showed thinner lamella than that obtained from S-2 catalyst. Hence, it should have the thickest lamella thickness (corresponding to the least relative SCB content) in the copolymers in the lowest MW part. Simultaneously, considering the relative SCB contents in both the lowest and highest temperature fractions of the copolymers, it was suggested that the SCB distribution of copolymers obtained from Cat-**C2** catalyst was the best: the copolymer had similar relative SCB contents in the highest MW part to those obtained from the Phillips

Table 7 Polymerization activities of different Cr-based catalysts and characterization of the polymers

Sample	1-Hexene (vol%)	Activity (kg mol^{-1} h^{-1})[a]	T_m (°C)[b]	ΔH_f (J g^{-1})[c]	M_w ($\times 10^5$)[d]	MWD	1-Hexene (mol%)[e]
Cat-**C2**	0	336	134	194.6	3.5	18.1	nd
Cat-**C2**	1	201	134	189.5	nd	nd	nd
Cat-**C2**	3	160	133	188.8	3.4	17.9	1.2
Cat-**C2**	5	110	131	179.1	4.8	25.4	nd
Cat-**C2**	7	139	131	175.6	4.0	22.1	2.7
Phillips	0	1,635	135	nd	2.5	14.5	nd
Phillips	3	405	131	175.3	2.1	11.3	0.8
Cat-**C1**	0	1,360	134	nd	3.1	21.2	nd
Cat-**C1**	3	162	131	183.4	2.2	14.2	nd
Cat-**C3**	0	242	134	nd	4.1	17.9	nd
Cat-**C3**	3	127	132	190.4	5.0	18.1	nd
S-2	0	221	134	nd	4.7	19.6	nd
S-2	3	76	133	194.2	5.0	20.8	0.7

Polymerization conditions: catalyst amount, 100 mg; polymerization temperature, 90°C; ethylene pressure, 0.3 MPa; solvent, heptane, 200 mL; cocatalyst TEA in heptane, Al/Cr molar ratio = 15
nd not detected
[a]Activities in kg_{PE} $(mol_{Cr})^{-1}$ h^{-1}
[b]By DSC thermograms
[c]Enthalpy of fusion by DSC thermograms
[d]By GPC in TCB versus polystyrene standards
[e]1-Hexene incorporation estimated by ^{13}C NMR in DCB-d_4 at 130°C and 75 MHz with delay index of 3 s for at least 4,000 times (sample concentration: ca. 100 mg mL^{-1})

catalyst, and slightly higher SCBs in the highest MW part than those of the S-2 catalyst. In contrast, it had the least relative SCB content in the lowest MW part. Therefore, the SCB distribution for the copolymers from Cat-**C2** should be much more beneficial for improvement of the long-term mechanical properties and gives these copolymers great potential for application as high grade HDPE pipe materials.

In summary, it has been demonstrated that various novel Cr-based polyethylene catalysts with better performance and with improved structures and properties of the PE products can be expected through successive surface modifications of either the chromate species or the silica support through the reaction with the surface residual hydroxyl groups on the traditional Phillips catalyst. Furthermore, by combination of the performance of two metal active sites in the ethylene polymerization, silica-supported bimetallic catalysts are expected to be able to yield PE products with bimodal MWD, which would attract more and more attention from the polyolefin field. One kind of catalyst utilized group 4 metals supporting Cp_2ZrCl_2 or $(n\text{-BuCp})_2HfCl_2$ metallocene catalysts on Cr-montmorillonite and was studied as a binuclear catalyst system to produce HDPEs with bimodal molecular weight distribution [168]. Chromium oxide and $(n\text{-BuCp})_2ZrCl_2$/MAO species supported onto several inorganic supports could produce PE with bimodal MWD [169]. Another group of catalysts based on chromium and vanadium would be more promising catalysts for commercial application in the near future. Examples are the

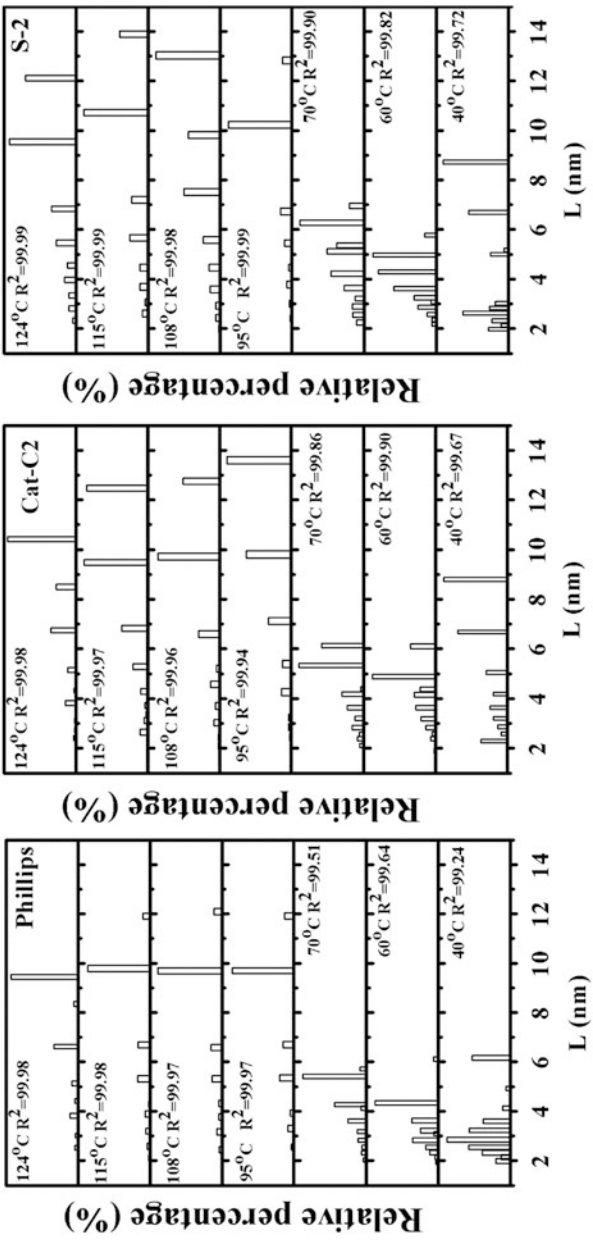

Fig. 29 Lamella thickness distribution of different TREF fractions of copolymers obtained from different catalysts (Phillips, Cat-**C2**, and S-2 catalysts)

recently reported silica-supported inorganic Cr-V bimetallic catalysts [30, 170] and silica-supported organic Cr-V bimetallic catalysts [171] have been successfully synthesized. Much improved SCB distribution of the PE products with better properties and performance made from such bimetallic catalysts within single polymerization reactor could be expected commercially in the near future.

8 Conclusions and Outlook

Since the discovery of the Phillips Cr/silica catalyst by Hogan and Banks in the early 1950s, it has achieved great success as one of the most important industrial catalysts for production of more than ten million tons of HDPE per year. However, academic progress regarding basic understanding of the nature of active sites and polymerization mechanisms is lagging far behind due to the complexity of this heterogeneous catalyst system and the limitation of current technologies. The complexity of Phillips-type catalysts mainly originates from the low percentage of active Cr species in the total Cr loading, the multiple valence states of Cr including +1, +2, +3, +4, +5, and +6, the high surface heterogeneity of the amorphous silica support, the concealment of over 99% of the active sites on the inner surface within the micro- and mesopores of the silica support, the instant encapsulation of active sites by produced polymer and the very short lifetime of the growing polymer chains due to the ultrafast polymerization rate, as well as the coexistence of many side reactions in the polymerization system during the whole process, such as catalyst deactivation and various chain transfer reactions.

During the last decade, increasing research efforts have focused on Phillips-type catalysts through various approaches, including spectroscopic methods, polymerization kinetics, heterogeneous model catalysts, homogeneous model catalysts, and molecular modeling, accompanied by successive catalyst innovations through modification of the traditional Phillips catalyst. Much deeper and better understanding of the nature of active sites and polymerization mechanisms has been achieved by various explorations concerning the activation by high temperature calcination, CO, or Al-alkyl cocatalysts during catalyst preparation; activation by ethylene monomer and Al-alkyl cocatalysts during polymerization; promotional effects of modification of the catalyst by Ti; spin-crossover phenomenon and its effects on the reactivity; and analysis of the microstructures of the produced PE chains, etc. Combined experimental and computational methodologies have been used. Investigations of polymerization kinetics over Phillips-type catalysts combined with different Al-alkyl cocatalysts have provided deeper understanding on formation and transformation of plausible active sites as well as strategies of cocatalyst introduction for design and optimization of commercial polymerization processes. It was also made clear that coordination of divalent active site precursor with siloxane ligands on the silica surface in terms of catalyst calcination temperature was crucial for determination of the precise microstructure and coordination environment of the active Cr species and thus for the performance of the catalyst.

The strategies for catalyst innovations are also shown to be greatly dependent on the progress in surface science of Phillips-type catalysts. More and more novel Cr-based polyethylene catalysts with better performance and products of improved structure and properties can be expected through successive surface modifications of either the chromate species or the silica support on the traditional Phillips catalyst.

In spite of the progress achieved so far, the long-standing key question concerning the precise structure of the active sites and the initiation mechanism in terms of the formation of the Cr–C bond and the first polyethylene chain on the Phillips catalyst have not yet been completely elucidated. A step forward in interpretation of these basic questions requires the combination of heterogeneous and homogeneous model catalyst systems with more advanced and multiple characterization techniques, especially in-situ or operando techniques as well as theoretical molecular modeling. The rational design and utilization of novel heterogeneous and homogeneous model catalysts resembling the traditional Phillips catalyst will greatly facilitate research on the real and complex catalyst system. The ever-growing computational power will enable us to handle more and more complex catalyst systems. A state-of-the-art catalyst design with greatly improved efficiency based on computational high-throughput screening techniques is expected in the polyolefin field in the near future. All in all, further progress in this important field still greatly depends on a combination of multiple techniques for basic research on both catalyst and polymer, as well as on persistent efforts and collaboration of scientists with different expertise from all over the world.

Acknowledgements We are gratefully thankful for the financial support by the National Natural Science Foundation of China (No. 21104019 and 21274040), the National High Technology Research and Development Program 863 (2012AA040306), and the Shanghai Science and Technology Commission (Key Project for Basic Research 10JC1403700). This work is also financially supported by the Fundamental Research Funds for the Central Universities, Research Program of Introducing Talents of Discipline of University (B08021).

References

1. Hogan JP, Banks RL (1954) Patent US 2825721
2. McDaniel MP (1985) Adv Catal 33:47
3. McDaniel MP (2008) Polymerization reactions. In: Ertl G, Knozinger H, Schüth F, Weitkamp J (eds) Handbook of heterogeneous catalysis. Wiley-VCH, Weinheim
4. McDaniel MP (2010) Adv Catal 53:123
5. McDaniel MP (1981) J Catal 67:71
6. Merryfield R, McDaniel MP, Parks G (1982) J Catal 77:348
7. McDaniel MP (1982) J Catal 76:37
8. Liu B, Terano M (2001) J Mol Catal A Chem 172:227
9. Qiu P, Li X, Zhang S, Cheng R, Dong Q, Liu B, Li L, Yu Y, Tang Y, Xie J, Wang W (2009) Asia Pac J Chem Eng 4:660
10. Clark A (1970) Catal Rev 3:145
11. Groppo E, Lamberti C, Bordiga S, Spoto G, Zecchina A (2005) Chem Rev 105:115

12. Kantcheva M, Lana IGD, Szymura JA (1995) J Catal 154:329
13. Nishimura M, Thomas JM (1993) Catal Lett 19:33
14. Ghiotti G, Garrone E, Coluccia S, Morterra C, Zecchina A (1979) J Chem Soc Chem Comm 1032
15. Al-Mashta F, Davanzo CU, Sheppard N (1983) J Chem Soc Chem Comm 1258
16. Ghiotti G, Garrone E, Zecchina A (1988) J Mol Catal 46:61
17. Zielinski P, Lana IGD (1992) J Catal 137:368
18. Ruddick VJ, Badyal JPS (1998) J Phys Chem B 102:2991
19. Vikulov K, Spoto G, Coluccia S, Zecchina A (1992) Catal Lett 16:117
20. Krauss HL (1988) J Mol Catal 46:97
21. Scarano D, Spoto G, Bordiga S, Carnelli L, Ricchiardi G, Zecchina A (1994) Langmuir 10:3094
22. Rebenstorf B, Larsson R (1981) J Mol Catal 11:247
23. Groppo E, Lamberti C, Bordiga S, Spoto G, Zecchina A (2006) J Catal 240:172
24. Hogan JP (1970) J Polym Sci Part A Polym Chem 8:2637
25. Cossee P (1964) J Catal 3:80
26. Cann K (2010) Silica-supported silyl chromate-based ethylene polymerization catalysts. In: Hoff R, Mathers RT (eds) Handbook of transition metal polymerization catalysts. Wiley, Blackwell
27. Cann K, Apecetche M, Zhang MH (2004) Macromol Symp 213:29
28. Li X, Cheng R, Luo J, Dong Q, He X, Li L, Yu Y, Da J, Liu B (2010) J Mol Catal A Chem 330:56
29. Karol FJ, Karapinka GL, Wu C, Dow AW, Johnson RN, Carrick WL (1972) J Polym Sci Part A Polym Chem 10:2621
30. Matta A, Zeng Y, Taniike T, Terano M (2012) Macromol React Eng 6:346
31. Weckhuysen BM, Wachs IE, Schoonheydt RA (1996) Chem Rev 96:3327
32. Vuillaume G, Spitz R, Revillon A, Charcosset H, Turlier P, Guyot A (1971) J Catal 21:159
33. Groeneveld C, Wittgen PPMM, van Kersbergen AM, Mestrom PLM, Nuijten CE, Schuit GCA (1979) J Catal 59:153
34. Wang SB, Murata K, Hayakawa T, Hamakawa S, Suzuki K (2000) Appl Catal A Gen 196:1
35. Vuurman MA, Hardcastle FD, Wachs IE (1993) J Mol Catal 84:193
36. Jozwiak WK, Lana IGD (1997) J Chem Soc Faraday Trans 93:2583
37. Cimino A, Cordischi D, De Rossi S, Ferraris G, Gazzoli D, Indovina V, Occhiuzzi M, Valigi M (1991) J Catal 127:761
38. Ellison A, Overton TL, Bencze L (1993) J Chem Soc Faraday Trans 89:843
39. Bensalem A, Weckhuysen BM, Schoonheydt RA (1997) J Chem Soc Faraday Trans 93:4065
40. Qiu P, Cheng R, Liu B, Tumanskii B, Batrice RJ, Botoshansky M, Eisen MS (2011) Organometallics 30:2144
41. Qiu P, Cheng R, Liu Z, Liu B, Tumanskii B, Eisen MS (2012) J Organomet Chem 699:48
42. Ellison A, Overton TL (1993) J Chem Soc Faraday Trans 89:4393
43. Zaki MI, Fouad NE, Leyrer J, Knoezinger H (1986) Appl Catal 21:359
44. Hardcastle FD, Wachs IE (1988) J Mol Catal 46:173
45. Richter M, Reich P, Oehlmann G (1988) J Mol Catal 46:79
46. Dines TJ, Inglis S (2003) Phys Chem Chem Phys 5:1320
47. Groppo E, Damin A, Bonino F, Zecchina A, Bordiga S, Lamberti C (2005) Chem Mater 17:2019
48. Moisii C, Deguns EW, Lita A, Callahan SD, van de Burgt LJ, Magana D, Stiegman AE (2006) Chem Mater 18:3965
49. Damin A, Bonino F, Bordiga S, Groppo E, Lamberti C, Zecchina A (2006) Chemphyschem 7:342
50. Groppo E, Damin A, Arean CO, Zecchina A (2011) Chem Eur J 17:11110
51. Ellison A, Diakun G, Worthington P (1988) J Mol Catal 46:131

52. Groppo E, Prestipino C, Cesano F, Bonino F, Bordiga S, Lamberti C, Thüne PC, Niemantsverdriet JW, Zecchina A (2005) J Catal 230:98
53. Agostini G, Groppo E, Bordiga S, Zecchina A, Prestipino C, D'Acapito F, van Kimmenade E, Thüne PC, Niemantsverdriet JW, Lamberti C (2007) J Phys Chem C 111:16437
54. Demmelmaier CA, White RE, van Bokhoven JA, Scott SL (2009) J Catal 262:44
55. Zhong L, Lee MY, Liu Z, Wanglee YJ, Liu B, Scott SL (2012) J Catal 293:1
56. Rahman A, Mohamed MH, Ahmed M, Aitani AM (1995) Appl Catal A Gen 121:203
57. Schmidt H, Riederer W, Krauss HL (1996) J Prakt Chem 338:627
58. Nishimura M, Thomas JM (1993) Catal Lett 21:149
59. Groppo E, Lamberti C, Bordiga S, Spoto G, Damin A, Zecchina A (2005) J Phys Chem B 109:15024
60. Groppo E, Lamberti C, Spoto G, Bordiga S, Magnacca G, Zecchina A (2005) J Catal 236:233
61. Groppo E, Lamberti C, Cesano F, Zecchina A (2006) Phys Chem Chem Phys 8:2453
62. Groppo E, Estephane J, Lamberti C, Spoto G, Zecchina A (2007) Catal Today 126:228
63. Barzan C, Groppo E, Quadrelli EA, Monteil V, Bordiga S (2012) Phys Chem Chem Phys 14:2239
64. Cimino A, De Angelis BA, Luchetti A, Minelli G (1976) J Catal 45:316
65. Okamoto Y, Fujii M, Imanaka T, Teranishi S (1976) Bull Chem Soc Jpn 49:859
66. Best SA, Squires RG, Walton RA (1977) J Catal 47:292
67. Liu B, Nakatani H, Terano M (2002) J Mol Catal A Chem 184:387
68. Liu B, Fang Y, Terano M (2004) J Mol Catal A Chem 219:165
69. Liu B, Sindelar P, Fang Y, Hasebe K, Terano M (2005) J Mol Catal A Chem 238:142
70. Fang Y, Liu B, Terano M (2005) Appl Catal A Gen 279:131
71. Cheng R, Xu C, Liu Z, Dong Q, He X, Fang Y, Terano M, Hu Y, Pullukat TJ, Liu B (2010) J Catal 273:103
72. Xia W, Liu B, Fang Y, Fujitani T, Taniike T, Terano M (2010) Appl Catal A Gen 389:186
73. Thüne PC, Loos J, Chen X, van Kimmenade EME, Kong B, Niemantsverdriet JW (2007) Top Catal 46:239
74. van Kimmenade EME, Kuiper AET, Tamminga K, Thüne PC, Niemantsverdriet JW (2004) J Catal 223:134
75. Aubriet F, Muller JF, Poleunis C, Bertrand P, Di Croce PG, Grange P (2006) J Am Soc Mass Spectrom 17:406
76. Groppo E, Seenivasan K, Barzan C (2013) Catal Sci Technol 3:858
77. Lamberti C, Zecchina A, Groppo E, Bordiga S (2010) Chem Soc Rev 39:4951
78. Panchenko VN, Zakharov VA, Paukshtis EA (2006) Appl Catal A Gen 313:130
79. Liu B, Nakatani H, Terano M (2003) J Mol Catal A Chem 201:189
80. Liu B, Fang Y, Nakatani H, Terano M (2004) Macromol Symp 213:37
81. Weckhuysen BM, Wachs IE (1997) J Phys Chem B 101:2793
82. Cimino A, Cordischi D, De Rossi S, Ferraris G, Gazzoli D, Indovina V, Minelli G, Occhiuzzi M, Valigi M (1991) J Catal 127:744
83. Weckhuysen BM, De Ridder LM, Schoonheydt RA (1993) J Phys Chem 97:4756
84. Xia W, Liu B, Fang Y, Hasebe K, Terano M (2006) J Mol Catal A Chem 256:301
85. Terano M, Fang Y, Liu B (2003) Polymer Preprints 44:22
86. O'Neill PP, Rooney JJ (1972) J Am Chem Soc 94:4383
87. Ivin KJ, Mol JC (1997) Olefin metathesis and metathesis polymerization. Academic Press, San Diego
88. Krauss HL, Hums E (1979) Naturforsch 34B:1628
89. Hugues F, Besson B, Basset JM (1980) J Chem Soc Chem Comm 719
90. Ajjou JAN, Scott SL (1997) Organometallics 16:86
91. Ajjou JAN, Scott SL, Paquet V (1998) J Am Chem Soc 120:415
92. Ajjou JAN, Rice GL, Scott SL (1998) J Am Chem Soc 120:13436
93. Ajjou JAN, Scott SL (2000) J Am Chem Soc 122:8968
94. Scott SL, Ajjou JAN (2001) Chem Eng Sci 56:4155

95. Xia W, Tonosaki K, Taniike T, Terano M, Fujitani T, Liu B (2009) J Appl Polym Sci 111:1869
96. McGuinness DS, Davies NW, Horne J, Ivanov I (2010) Organometallics 29:6111
97. Grubbs RH, Tumas WS (1989) Science 243:907
98. Natta G, Dall'Asta G, Mazzanti G (1964) Angew Chem Int Ed 3:723
99. Bordiga S, Groppo E, Agostini G, van Bokhoven JA, Lamberti C (2013) Chem Rev 113:1736
100. Choi KY, Tang S, Yoon WJ (2004) Macromol Theory Simul 13:169
101. Choi KY, Tang S (2004) J Appl Polym Sci 91:2923
102. Matos I, Zhang Y, Lemos M, Freire F, Fonseca IF, Marques MM, Lemos F (2004) J Polym Sci Part A Polym Chem 42:3464
103. Kissin YV, Brandolini AJ, Garlick JL (2008) J Polym Sci A Polym Chem 46:5315
104. Spitz R, Florin B, Guyot A (1979) Eur Polym J 15:441
105. McDaniel MP, Johnson MM (1986) J Catal 101:446
106. McDaniel MP, Johnson MM (1987) Macromolecules 20:773
107. Wang S, Tait PJT, Marsden CE (1991) J Mol Catal 65:237
108. Fang Y, Liu B, Terano M (2006) Kinet Catal 47:295
109. Li L, Wu Y, Dong Q, Hao A, Cheng R, Zhong L, Liu B (2012) Asia Pac J Chem Eng. doi:10.1002/apj.1692
110. Fang Y, Liu B, Hasebe K, Terano M (2005) J Poly Sci A Poly Chem 43:4632
111. Baker LM, Carrick WL (1970) J Org Chem 35:774
112. Carrick WL, Turbett RJ, Karol FJ, Karapinka GL, Fox AS, Johnson RN (1972) J Polym Sci A Polym Chem 10:2609
113. McDaniel MP (1982) J Catal 76:17
114. Demmelmaier CA, White RE, van Bokhoven JA, Scott SL (2008) J Phys Chem C 112:6439
115. Thüne PC, Verhagen CPJ, van den Boer MJG, Niemantsverdriet JW (1997) J Phys Chem B 101:8559
116. Tonosaki K, Taniike T, Terano M (2011) Macromol React Eng 5:332
117. Scott SL, Fu A, MacAdams LA (2008) Inorg Chim Acta 361:3315
118. Ikeda H, Monoi T, Sasaki Y (2003) J Polym Sci A Polym Chem 41:413
119. Monoi T, Ikeda H, Sasaki Y, Matsumoto Y (2003) Polym J 35:608
120. Espelid Ø, Børve KJ (2000) J Catal 195:125
121. Theopold KH (1998) Eur J Inorg Chem 1998(1):15
122. Hanmura T, Ichihashi M, Monoi T, Matsuura K, Kondow T (2004) J Polym Sci A Polym Chem 108:10434
123. Hanmura T, Ichihashi M, Monoi T, Matsuura K, Kondow T (2005) J Polym Sci A Polym Chem 109:6465
124. Feher FJ, Blanski RL (1990) J Chem Soc Chem Comm 1614
125. Feher FJ, Blanski RL (1993) Macromol Sym 66:95
126. Abbenhuis HCL, Vorstenbosch MLW, van Santen RA, Smeets WJJ, Spek AL (1997) Inorg Chem 36:6431
127. Motevalli M, Sanganee M, Savage PD, Shah S, Sullivan AC (1993) J Chem Soc Chem Comm 1132
128. Köhn RD, Haufe M, Mihan S, Lilge D (2000) Chem Comm 1927
129. MacAdams LA, Kim WK, Liable-Sands LM, Guzei IA, Rheingold AL, Theopold KH (2002) Organometallics 21:952
130. Thomas BJ, Noh SK, Schulte GK, Sendlinger SC, Theopold KH (1991) J Am Chem Soc 113:893
131. Bhandari G, Kersten JL, Kucharczyk RR, White PA, Liang Y, Theopold KH (1996) Stud Surf Sci Catal 101:153
132. Britovsek GJP, Gibson VC, Wass DF (1999) Angew Chem Int Ed 38:428
133. Budagumpi S, Kim KH, Kim I (2011) Coord Chem Rev 255:2785
134. Coles MP, Gibson VC (1994) Polym Bull 33:529

135. Coles MP, Dalby CI, Gibson VC, Little IR, Marshall EL, da Costa MHR, Mastroianni S (1999) J Org Chem 591:78
136. Al Thagfi J, Lavoie GG (2012) Organometallics 31:2463
137. Chen F, Lu X, Chen X, Li H, Hu Y (2012) Inorg Chim Acta 387:407
138. Haftbaradaran F, Mund G., Batchelor RJ, Britten JF, Leznoff DB (2005) Dalton Trans 2343
139. Albahily K, Al-Baldawi D, Gambarotta S, Duchateau R, Koc E, Burchell TJ (2008) Organometallics 27:5708
140. Boor J (1979) Ziegler–Natta catalysts and polymerizations. Academic Press, New York
141. Jabri A, Crewdson P, Gambarotta S, Korobkov I, Duchateau R (2006) Organometallics 25:715
142. Liu B, Fang Y, Terano M (2004) Mol Simulat 30:963
143. Liu B, Fang Y, Xia W, Terano M (2006) Kinet Catal 47:234
144. Cheng R, Liu Z, Qiu P, Zhang S, Liu B (2008) Chin J Polym Sci 26:579
145. Espelid Ø, Børve KJ (2001) Catal Lett 75:49
146. Espelid Ø, Børve KJ (2002) J Catal 206:331
147. Espelid Ø, Børve KJ (2002) J Catal 205:366
148. Espelid Ø, Børve KJ (2002) J Catal 205:177
149. Børve KJ, Espelid Ø (2003) Theoretical models of active sites: general considerations and application to the study of Phillips-type Cr/silica catalysts for ethylene polymerization. In: Scott SL, Crudden CM, Jones CW (eds) Nanostructured Catalysts. Springer, Berlin
150. Weckhuysen BM, Wachs IE (1996) J Chem Soc Faraday Trans 92:1969
151. Damin A, Vitillo JG, Ricchiardi G, Bordiga S, Lamberti C, Groppo E, Zecchina A (2009) J Phys Chem A 113:14261
152. Tonosaki K, Taniike T, Terano M (2011) J Mol Catal A Chem 340:33
153. Schmid R, Ziegler T (2000) Can J Chem 78:265
154. Zhong L, Liu Z, Cheng R, Tang S, Qiu P, He X, Terano M, Liu B (2012) ChemCatChem 4:872
155. Sautet P, Delbecq F (2010) Chem Rev 110:1788
156. Guesmi H, Tielens F (2012) J Phys Chem C 116:994
157. Liu Z, Cheng R, He X, Wu X, Liu B (2012) J Phys Chem A 116:7538
158. Hess JS, Leelasubcharoen S, Rheingold AL, Doren DJ, Theopold KH (2002) J Am Chem Soc 124:2454
159. Estephane J, Groppo E, Vitillo JG, Damin A, Gianolio D, Lamberti C, Bordiga S, Quadrelli EA, Basset JM, Kervern G, Emsley L, Pintacuda G, Zecchina A (2010) J Phys Chem C 114:4451
160. Zhong L, Liu Z, Cheng R, He X, Liu B (2013) Chin J Chem Eng 64:539
161. Tomov AK, Chirinos JJ, Jones DJ, Long RJ, Gibson VC (2005) J Am Chem Soc 127:10166
162. Liu Z, Zhong L, Yang Y, Cheng R, Liu B (2011) J Phys Chem A 115:8131
163. Xu R, Klatt G, Enders M, Koppel H (2012) J Phys Chem A 116:1077
164. Fang Y, Xia W, He M, Liu B, Hasebe K, Terano M (2006) J Mol Catal A Chem 247:240
165. Zhang S, Dong Q, Cheng R, He X, Wang Q, Tang Y, Yu Y, Xie K, Da J, Liu B (2012) J Mol Catal A Chem 358:10
166. Zhang S, Zhao N, Wu Y, Dong Q, Wang Q, Tang Y, Yu Y, Da J, He X, Cheng R, Liu B (2012) Macromol Symp 312:63
167. Zhang S, Cheng R, Dong Q, He X, Wang Q, Tang Y, Yu Y, Xie K, Da J, Terano M, Liu B (2013) Macromol React Eng 7:254
168. Yamamoto K, Ishihama Y, Sakata K (2010) J Polym Sci Polym Chem 48:3722
169. Moreno J, van Grieken R, Carrero A, Paredes B (2011) Polymer 52:1891
170. Xue X (2010) Study on novel and highly efficient hybrid CrO_x-VO_x/SiO_2 catalyst for ethylene polymerization. Master Dissertation. East China University of Science and Technology, Shanghai, China
171. Zhao N, Cheng R, He X, Liu Z, Liu B (2012) Patent CN 102627710A